GFZ
Helmholtz-Zentrum
POTSDAM

HELMHOLTZ-ZENTRUM POTSDAM
DEUTSCHES
GEOFORSCHUNGSZENTRUM

Dissertation

NUMERICAL ANALYSIS OF THERMAL, HYDRAULIC AND MECHANICAL PROCESSES IN THE NEAR- AND FAR-FIELD OF UNDERGROUND COAL GASIFICATION REACTORS

Christopher Otto

Potsdam, 2017

Institut für Erd- und Umweltwissenschaften
Mathematisch-Naturwissenschaftliche Fakultät
Universität Potsdam

NUMERICAL ANALYSIS OF THERMAL, HYDRAULIC AND MECHANICAL PROCESSES IN THE NEAR- AND FAR-FIELD OF UNDERGROUND COAL GASIFICATION REACTORS

KUMULATIVE DISSERTATION

zur Erlangung des akademischen Grades

"doctor rerum naturalium"

(Dr. rer. nat.)

In der Wissenschaftsdisziplin „Hydrogeologie“

Eingereicht an der Mathematisch-Naturwissenschaftlichen Fakultät
der Universität Potsdam

vorgelegt von

DIPL.-GEOL. CHRISTOPHER OTTO

Potsdam, 2017

Published online at the
Institutional Repository of the University of Potsdam:
URN urn:nbn:de:kobv:517-opus4-404625
http://nbn-resolving.de/urn:nbn:de:kobv:517-opus4-404625

1. Gutachter:	Prof. Dr. Dr.-Ing. habil. Michael Kühn Deutsches GeoForschungsZentrum Potsdam GFZ Department 3: Geochemie Sektion 3.4: Fluidsystemmodellierung und Universität Potsdam Mathematisch-Naturwissenschaftliche Fakultät Institut für Erd- und Umweltwissenschaften
2. Gutachter:	Prof. Dr. rer. nat. Tomás Manuel Fernandez-Steeger Technische Universität Berlin Fakultät VI Planen Bauen Umwelt Angewandte Geowissenschaften Fachgebiet Ingenieurgeologie
3. Gutachter:	PD Dr. rer. nat. habil. Oliver Heidbach Deutsches GeoForschungsZentrum Potsdam GFZ Department 2: Geophysik Sektion 2.6: Erdbebengefährdung und Spannungsfeld und Technische Universität Karlsruhe und Karlsruher Institut für Technologie (KIT) Fakultät für Physik Geophysikalisches Institut (GPI)
Tag der Disputation:	27. November 2017

ABSTRACT

Underground coal gasification (UCG) has the potential to increase worldwide coal reserves by developing coal resources, currently not economically extractable by conventional mining methods. For that purpose, coal is combusted *in situ* to produce a high-calorific synthesis gas with different end-use options, including electricity generation as well as production of fuels and chemical feedstock. Apart from the high economic potentials, UCG may induce site-specific environmental impacts, including ground surface subsidence and pollutant migration of UCG by-products into shallow freshwater aquifers. Sustainable and efficient UCG operation requires a thorough understanding of the coupled thermal, hydraulic and mechanical processes, occurring in the UCG reactor vicinity. The development and infrastructure costs of UCG trials are very high; therefore, numerical simulations of coupled processes in UCG are essential for the assessment of potential environmental impacts. Therefore, the aim of the present study is to assess UCG-induced permeability changes, potential hydraulic short circuit formation and non-isothermal multiphase fluid flow dynamics by means of coupled numerical simulations. Simulation results on permeability changes in the UCG reactor vicinity demonstrate that temperature-dependent thermo-mechanical parameters have to be considered in near-field assessments, only. Hence, far-field simulations do not become inaccurate, but benefit from increased computational efficiency when thermo-mechanical parameters are maintained constant. Simulations on potential hydraulic short circuit formation between single UCG reactors at regional-scale emphasize that geologic faults may induce hydraulic connections, and thus compromise efficient UCG operation. In this context, the steam jacket surrounding high-temperature UCG reactors plays a vital role in avoiding UCG by-products escaping into freshwater aquifers and in minimizing energy consumption by formation fluid evaporation. A steam jacket emerges in the close reactor vicinity due to phase transition of formation water and is a non-isothermal flow phenomenon. Considering this complex multiphase flow behavior, an innovative conceptual modeling approach, validated against field data, enables the quantification and prediction of UCG reactor water balances. The findings of this doctoral thesis provide an important basis for integration of thermo-hydro-mechanical simulations in UCG, required for the assessment and mitigation of its potential environmental impacts as well as optimization of its efficiency.

ZUSAMMENFASSUNG

Die Untertagevergasung von Kohle (UTV) ermöglicht die Erschließung konventionell nicht förderbarer Kohleressourcen und bietet dadurch Potenzial zur Erhöhung der weltweiten Kohlereserven. Bei der in-situ Kohleumwandlung entsteht ein hochkalorisches Synthesegas, das elektrifiziert oder zur Gewinnung chemischer Rohstoffe und synthetischer Kraftstoffe eingesetzt werden kann. Neben den wirtschaftlichen Möglichkeiten, bestehen jedoch auch standort-spezifische Umweltgefährdungspotentiale durch Subsidenz und Schadstoffmigration von UTV-Rückständen in nutzbare Grundwasserleiter. Eine nachhaltige und effiziente UTV erfordert ein umfangreiches Verständnis der thermisch, hydraulisch und mechanisch gekoppelten Prozesse im UTV-Reaktornahbereich. Aufgrund der hohen Investitionskosten von UTV-Pilotanlagen, sind numerische Simulationen gekoppelter Prozesse von entscheidender Bedeutung für die Bewertung möglicher UTV-Umweltauswirkungen. Im Rahmen dieser Arbeit wird die UTV-induzierte Permeabilitätsveränderung, Erzeugung möglicher hydraulischer Kurzschlüsse benachbarter Reaktoren und Dynamik nicht-isothermer Multiphasenflüsse mit gekoppelten Simulationen analysiert. Die Simulationsergebnisse zeigen, dass eine Implementierung temperaturabhängiger thermo-mechanischer Gesteinsparameter nur für Untersuchungen von Permeabilitäts-änderungen im Reaktornachbereich notwendig ist. Die Ergebnisse erlauben somit eine recheneffiziente Realisierung von komplexen thermo-mechanisch gekoppelten Simulations-studien regionalskaliger Modelle mit konstanten Gesteinsparametern, bei nahezu gleichbleibender Ergebnisgenauigkeit, die zur Bewertung von UTV-Umweltgefährdungs-potenzialen beitragen. Simulationen zur Ausbildung hydraulischer Kurzschlüsse zwischen einzelnen UTV-Reaktoren auf regionaler Skala, verdeutlichen die Relevanz von geologischen Störungen an einem UTV-Standort, da diese durch Reaktivierung hydraulische Verbindungen induzieren und somit einen effizienten und nachhaltigen UTV-Betrieb negativ beeinträchtigen können. In diesem Zusammenhang kommt der Ausbildung einer Wasserdampfphase, der sogenannte „steam jacket“, im Hochtemperaturnahbereich von UTV-Reaktoren, als potenzielle Barriere zur Vermeidung von UTV-Schadstoffaustritten und zur potenziellen Minimierung von Energieverlusten eine entscheidende Bedeutung zu. Diese steam jackets entstehen durch evaporiertes Formationswasser und sind komplexe nicht-isotherme Multiphasenfluss-Phänomene. Für ein verbessertes Prozessverständnis dieser Multiphasenflüsse, wurde ein neuartiges Modellkonzept entwickelt, welches, validiert gegen Feldversuchsdaten, erstmals sowohl eine Quantifizierung als auch Prognose von Wasserflussraten in und aus einem UTV-Reaktor erlaubt. Die Ergebnisse der vorgelegten Doktorarbeit bilden eine wichtige Grundlage für eine erfolgreiche Integration gekoppelter thermo-hydro-mechanischer Simulationen in weiterführende Studien. Vor dem Hintergrund hoher UTV-Umweltgefährdungspotentiale, können diese zur verbesserten Bewertung und Minderung von UTV-Umweltauswirkungen beitragen, sowie die UTV-Effizienz nachhaltig optimieren.

ACKNOWLEDGMENTS

The present thesis was partly carried out within the TOPS project funded by the European Union Seventh Framework Programme (EU-FP7) under grant agreement no. 608517. The financial support is very much appreciated.

Producing such a thesis would not be possible without the support and help of many people and thus the following paragraphs are “probably” the most important parts of the thesis. I would like to thank everyone who was in someway involved in my PhD-thesis.

I am very grateful to my first supervisor, Prof. Michael Kühn, for his support on any level and providing an inspiring working atmosphere in the section. His continuous assistance, encouragement and valuable suggestions have hugely contributed to the realization of this work.

My thanks go to Prof. Tomás Manuel Fernandez-Steeger and PD. Oliver Heidbach for accepting to be the second and third supervisor of this work.

I would like to acknowledge Dr.-Ing. Thomas Kempka for the precise and immense support, ideas and expertise, imparting hard and soft skills required to accomplish this thesis. There is no doubt that without his contribution and lesson as well as his patience; this thesis would not have been possible at all. Thank you Thomas!

Thanks to Prof. Jens Tronicke (University of Potsdam) for mentoring my doctoral study, providing lots of helpful suggestions and ideas.

Thanks also to Dr. David Camp (Lawrence Livermore National Laboratory, USA) for data provision as well as many valuable discussions on the U.S. field trial data and related modeling activities.

I would like to express my sincere appreciation to the team of section Fluid Systems Modelling for the friendly atmosphere, which greatly embellished the everyday work life and after work life as well. Here, special thanks go to Jenny, Sonja, Maria, Natalie, Benjamin, Marco, Peter and Elena.

Furthermore, I thank my proofreaders Dr. Thomas Kempka, Dr. Marco De Lucia, Dr. Bernd Wiese, Hagen and Emma.

Over the last 8 years at the GFZ I shared a great deal of time and had inspiring discussions with many colleagues at GFZ, which I do not have the space to enumerate here. My thanks to all of you.

Finally, I wish to express my deepest gratitude to my family, friends, former fellow students, roommates and of course my girlfriend for their support and encouragement during the past years.

CONTENTS

LIST OF FIGURES

LIST OF TABLES

LIST OF ACRONYMS AND SYMBOLS

ABBREVIATIONS	MEANING
CCS	Carbon Capture and Storage
CH_4	Methane
CO	Carbon monoxide
CO_2	Carbon dioxide
CRIP	Controlled Retracting Injection Point
CV	Calorific Value
EU	European Union
FLAC	Fast Lagrangian Analysis of Continua
GFZ	GeoForschungsZentrum Potsdam
GJ	Gigajoules
Gt	Gigaton
Gtoe	Gigatons of oil equivalent (1 toe = 41.868 GJ)
H_2	Hydrogen
IPCC	Intergovernmental Panel on Climate Change
LERC	Laramie Energy Technology Center
LLNL	Livermore National Laboratory
LVW	Linked Vertical Wells
Mt	Megaton
N_2	Nitrogen
N	North
O_2	Oxygen
ROW	Rest of the World
S	South
S_{Hmax}	Maximum horizontal stress orientation
S_{hmin}	Minimum horizontal stress orientation
S_v	Vertical stress
SDB	Steeply Dipping Bed
UCG	Underground Coal Gasification
3D	Three-dimensional
2D	Two-dimensional

SYMBOLS	MEANING	DIMENSION
C_P	Specific heat capacity	J/kg/K
c	Cohesion	MPa
E	Elastic modulus	GPa
e	Internal energy	MW day
$\boldsymbol{g}$	Gravitational acceleration	m/s^2
h	Total enthalpy	MJ/kg

SYMBOLS	MEANING	DIMENSION
$\tilde{h}$	Mass enthalpy	MJ/kg
K	Permeability	mD
k_r	Relative permeability	-
m	Mass fraction	-
P	Pressure	MPa
Q	Energy flux	MW
S_H	Maximal horizontal stress	MPa
S_h	Minimum horizontal stress	MPa
S_v	Vertical stress	MPa
s	Saturation	-
T	Temperature	°C, K
V	Phase molar fraction	-
$\boldsymbol{w}$	Darcy velocity	m/s
$\boldsymbol{x}$	Mixture molar composition	mol
α	Linear thermal expansion coefficient	K^{-1}
ε_v	Volumetric strain	-
Λ	Molar entropy	MJ/mol/K
λ	Thermal conductivity	W/m/K
μ	Viscosity	Pa·s
ν	Poisson ratio	-
ρ	Density	kg/m^3
σ_n	Normal stress	MPa
σ_t	Tensile strength	MPa
σ_v	Vertical stress	MPa
σ_H	Horizontal stress	MPa
σ_1	Maximum principle stress	MPa
σ_3	Minimum principle stress	MPa
τ	Shear stress	MPa
ϕ	Porosity	-
φ	Friction angle	°

INDICES	MEANING
0	Initial value
g	Gas phase
i	i = 1-, 2-, 3-phase (1 = liquid, 2 = gas, 3= super-critical)
j	Component
l	Liquid phase
n	Porosity sensitivity exponent
s	Refers to the host rock parameters
t	Total parameters of the mixture

1 INTRODUCTION

The worldwide energy system is facing great change and major challenges in the present century. Oil, coal and natural gas have dominated the world's energy supply since the 20th century and still account for more than 80% of primary energy demand (IEA, 2016). Fossil fuels are abundant for the moment but limited, becoming ever-scarcer resources in the future and are jointly responsible for the global climate change (Edenhofer et al., 2011). The consumption of fossil fuels is the main source of anthropogenic greenhouse gas emissions, whereby particularly coal is the most carbon-intensive of the three main fossil fuels (Edenhofer et al., 2011; Self et al., 2012). The reduction of anthropogenic greenhouse gas emissions is of global interest to reach national and international climate targets. Therefore, the decarbonization of the energy system is one of a number of energy-related policy priorities being pursued by governments around the world (IEA, 2016). However, there is still a long way to go until then, because renewables are still too intermittent and costly (Verbruggen and Yurchenko, 2017), and nuclear has yet to satisfactorily solve its waste disposal and proliferation issues (Alexander et al., 2015). Even if all nations abide by Paris Agreement pledges (UNFCCC, 2015), only 37% of power generation of the global energy sector is produced from renewables, especially wind power and solar power in 2040 (IEA, 2016). Until these issues are solved, the near- to mid-term sources of primary energy are likely to be fossil fuels (IEA, 2016). In this context, natural gas continues to expand in the next 25 years, while the shares of coal and oil fall back; nevertheless, coal is the most abundant wide-spread source for energy and chemicals around the world (IEA, 2015; World Energy Council, 2013). As proven oil and gas reserves are depleted more rapidly, coal is still expected to play an important role in the following decades, at least until more sophisticated economical renewable energy sources are further developed (IEA, 2016; Shafirovich and Varma, 2009). In this context, underground coal gasification (UCG) is an option that allows for utilization of deep-seated coal deposits not economically exploitable by conventional coal mining, and has therefore the potential to increase the worldwide coal reserves (Couch, 2009).

1.1 COAL AND ITS CURRENT RELEVANCE FOR THE GLOBAL ENERGY SYSTEM

The reach of the world`s onshore and offshore hard coal (593 Gtoe = Gigatons of oil equivalent) and lignite (112 Gtoe) reserves are significant (about 55% of major fossil fuels), and play a central role in the worldwide supply of the energy system (BGR, 2015; Schiffer and Thielemann, 2012). These reserves have the potential to provide security of future energy supply long after oil and natural gas reserves are exhausted (IEA, 2015; World Energy Council, 2013). Coal is still the second most important source of primary energy (about 30%) and is mostly used for power generation - over 40% of worldwide electricity is produced from coal (IEA, 2016). In addition, coal is affordable, easy to transport, store and use, free of geopolitical tensions and used to produce virtually all non-recycled iron (IEA, 2015). For this purpose, there are currently numerous coal-fired power stations around the world at different stages of construction and planning, which could be completed in the next decade (see Figure 1), in spite of the goal set by the international community in the Paris agreement (González-Eguino et al., 2017). In the years between 2010 and 2015 around

500 coal-fired plants were built globally, especially countries such as China and India greatly increased their stock (González-Eguino et al., 2017).

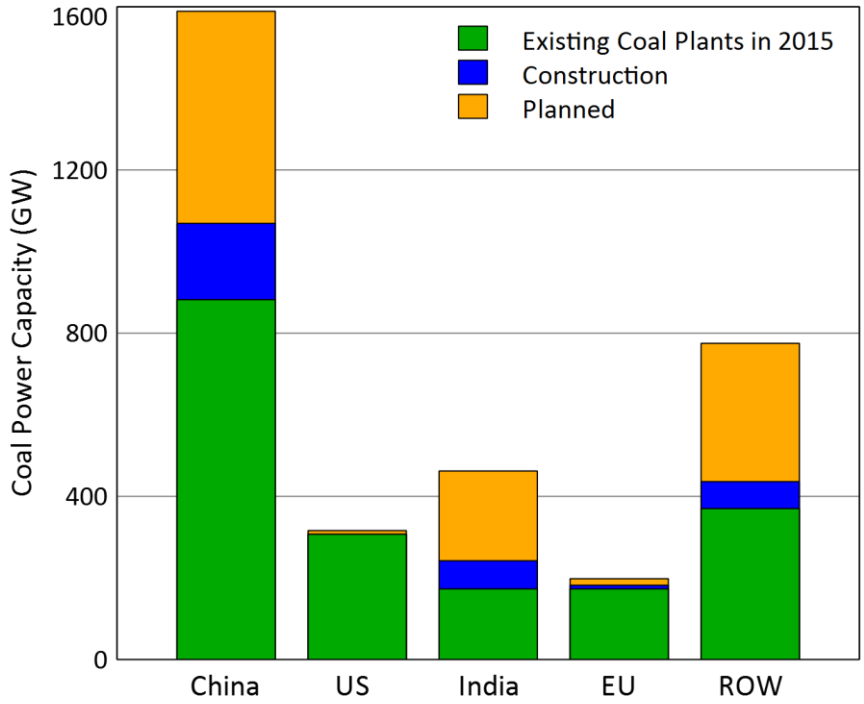

Figure 1: Existing coal power plant capacity in 2015 (green), under construction in 2016 (blue) and planned (orange) after González-Eguino et al. (2017) (EU = European Union; ROW = Rest of the World).

However, the traditional extraction of coal reserves (e.g., open pit mining, longwall mining as well as room- and -pillar mining) is problematic not only due to the high amount of carbon dioxide and methane releases (Boger et al., 2014; Karacan et al., 2011). It is known that both conventional methods (open pit and underground mining) are problematic, since they leave a massive environmental footprint due to high potential ground surface subsidence, localized flooding and water pollution (Eftekhari et al., 2012; Self et al., 2012). Especially water resources are affected by discharging huge amounts of acid mine water (Tiwary, 2001). Moreover, the depth of coal exploitation will increase, when shallow coal resources are exhausted, e.g., with coal-mining faces in China reaching depth of up to 1500 m (Haifeng et al., 2012) and in Germany up to more than 1600 m (RAG, 2017; Wolters et al., 2015), which relates to very cost-intensive mining. In addition, conventional mining methods are generally not suited to offshore working, while the development and infrastructure costs of new onshore mines can render exploitation of reserves uneconomic (Sury et al., 2004). Currently, more than 95% of the world's known coal is technically or economically not accessible (BGR, 2015).

1.2 UNDERGROUND COAL GASIFICATION (UCG)

The technology of underground coal gasification aims at *in situ* conversion of coal deposits and production of a high-calorific synthesis gas, which is, e.g., applicable for power generation, natural gas substitution as well as fuel, hydrogen, fertilizer and chemical feedstock production (Bhutto et al., 2013; Blinderman et al., 2008; Burton et al., 2006; Friedmann et al., 2009; Hewing et al., 1978; Kempka et al., 2011b; Klimenko, 2009; Nakaten et al., 2013; Prabu and Jayanti, 2011). Nowadays,

the target seam is developed by directional drilling to make the coal accessible for *in situ* combustion (Couch, 2009). It facilitates the possibility of exploiting coal seams, currently not mineable by conventional methods due to geologically complex settings, high deposit depths, low coal seam thickness or quality, in an economical, safe and more environmental-friendly manner compared to conventional coal mining (Burton et al., 2006). Furthermore, UCG has a higher resource utilization efficiency (Burton et al., 2006; Friedmann et al., 2009). Hence, UCG has the potential to increase the global ratio between economically recoverable coal reserves and geological coal resources. The World Energy Council states that early studies suggest a potential increase of the world's coal reserves by as much as 600 billion tons, which represents a 70% increase by the use of UCG (Couch, 2009; World Energy Council, 2007). UCG also offers a high potential for integration with Carbon Capture and Storage (CCS), using the pipe infrastructure aboveground as well as the voids created by *in situ* combustion and the fractured surrounding rocks in the subsurface to store CO_2 and to realize lower greenhouse gas emissions (Kempka et al., 2011a; Ramasamy et al., 2014; Roddy and Younger, 2010; Younger, 2011). The potential of economically storing greenhouse gas emissions gives UCG an especially important added value compared to other clean coal technologies (Burton et al., 2006). In addition, compared to conventional coal mining, UCG has advantages such as lower operating costs and surface subsidence, and no mine safety issues (e.g., mine collapse, methane outbursts, asphyxiation; Burton et al., 2006).

1.2.1 PRINCIPLE OF UCG

The concept of UCG, schematically illustrated in Figure 2, is based on borehole mining, whereby the target coal deposits are developed by directional drilling and then converted into a synthesis gas by sub-stoichiometric combustion, using gasification agents based on oxygen-enriched air and/or steam (Burton et al., 2006; Couch, 2009; Sury et al., 2004).

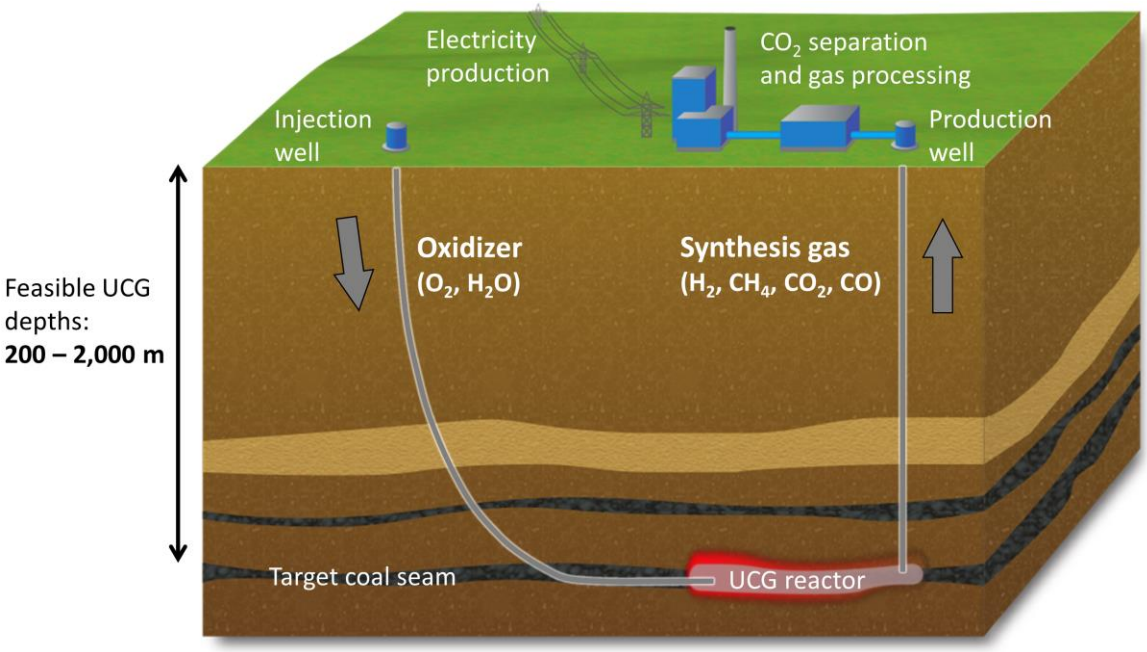

Figure 2: Schematic view of the *in situ* underground coal gasification principle based on the CRIP (Controlled Retracting Injection Point) method, modified after Kempka et al. (2009).

The subsurface preparation of the seam and gasification needs a minimum of two boreholes. The wells are linked to form a highly permeable path between injection and production wells to allow for injection of an oxidizer, UCG reactor growth, synthesis gas flow and extraction of the synthesis gas. The rate of reactor growth is controllable via the rate of air enriched with steam injection (Najafi et al., 2015). Earlier, Linked Vertical Wells (LVW) and Steeply Dipping Bed (SDB) were the most popular drilling configurations for horizontal and steeply dipping coal seams (> 60°), respectively (Khan et al., 2015; Mostade, 2014). The LVW method requires drilling of injection and production wells and a linkage between them. The SDB configuration comprises two slanted boreholes, whereby the production well is drilled in-seam to a predetermined distance above the base of the injection well, which is drilled initially beneath the coal seam until it intersects the coal seam (Mostade, 2014). Recently, the Controlled Retracting Injection Point (CRIP), invented in the 1980s Centralia series of UCG trials in Washington (Oliver et al., 1989), has gained considerable attraction due to its enhanced control and improved overall efficiency (Bhutto et al., 2013). The simplest CRIP configuration needs one vertical production well and a deviated in-seam horizontal injection well (Figure 2). The coal seam is ignited subsequently around the injection point and near the production well by the injection of gases or fluids (O_2, inflammable gas, steam). After sufficient amount of coal has been gasified, the injection point is retracted in the upstream direction (Oliver et al., 1989). Therefore, the CRIP method allows for greater volumes of coal to be gasified by the creation of multiple UCG reactors along the in-seam length of the injection well of up to 1500 m (Mostade, 2014). Surface equipment will be required to store, monitor, control and to provide N_2 to extinguish gasification if required (Staúczyk et al., 2012).

UCG is a complex, coupled thermo-hydro-chemical-mechanical process. During the gasification process, coal is converted into a high-calorific synthesis gas and temperatures in the order of more than 1000 °C are generated (Burton et al., 2006). Hence, turning initial solid coal to char and ash, creates a cavity (in the following called UCG reactor), and induces water phase transitions from liquid to steam (steam jacket) with non-isothermal multiphase flow (Blinderman and Jones, 2002). Figure 3 schematically shows the most relevant processes occurring between the gasification reactor and its cooler surroundings. Perkins and Love (2010) emphasize that sustainable operation of UCG reactors aims to maintain a small, but nonetheless positive flow of formation fluids into the reactor to reduce gas losses and the escapes of organics which may have environmental impacts on the groundwater resources. In this context, the water balance (water in- and outflow into and out of the reactor) can be managed by varying the reactor operating pressure. Due to the high temperature, the water flow is subject to multiphase interactions at the reactor boundary, including the generation of steam due to the phase change from liquid water to vapor (Pakala, 2012; Plumb and Klimenko, 2010).

Furthermore, reactor growth develops thermally and mechanically induced stress changes in the coal seam and its surrounding rock layers (Couch, 2009; Vorobiev et al., 2008). Field and laboratory tests have shown that as gasification proceeds, an underground reactor is formed radial-symmetric around the injection well (Daggupati et al., 2010; Mortazavi, 1989). The growth and mechanical stability of the reactor are of fundamental importance to the UCG process, since both have a major impact on the coal resource recovery and energy efficiency, and therefore economic feasibility (Britten and Thorsness, 1989; Sarraf et al., 2011; Yang et al., 2014).

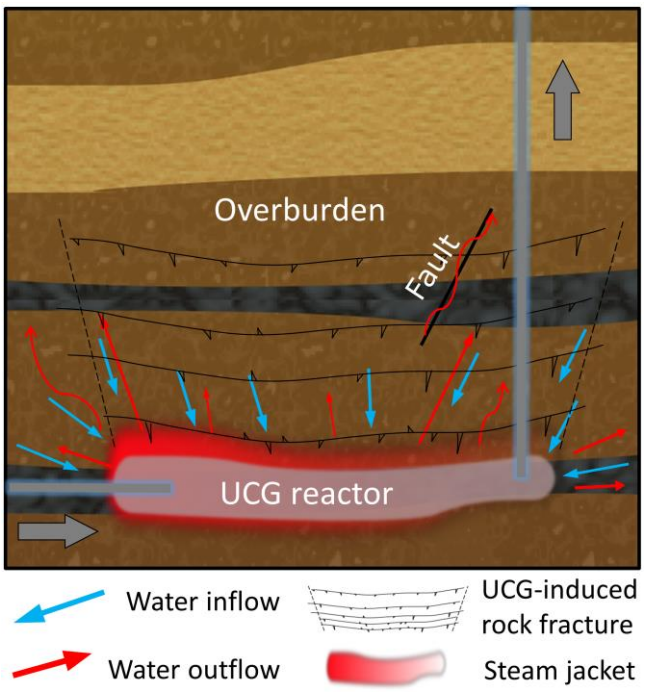

Figure 3: Schematic of multiphase flow processes and potential geomechanical impacts in the UCG reactor near-field. Faults may act as potential pathways for pollutant migration after Sarhosis et al. (2016).

Within the reactor overburden, dilation of pre-existing and development of new fractures may occur (Figure 3) and result in permeability changes and potential pathways that may allow UCG fluids to escape (Younger, 2011). Reactor growth is also related to potential design considerations, including mitigating ground subsidence and avoiding groundwater contamination (Luo et al., 2009). Lateral dimensions between reactors (safety pillar width to avoid hydraulic short circuits and minimize subsidence) also influence coal resource recovery and energy efficiency, and the overall dimensions affect the hydrogeological as well as surface subsidence responses of the overburden (Elahi and Chen, 2016; Mortazavi, 1989; Mostade, 2014; Tian, 2013). However, the exact geomechanical response of overburden to the development of a UCG reactor is highly complex and strongly influenced by site-specific conditions, e.g., the thickness and strength of overlying rock layers, coal seam depth, dip angles and the presence of faults; Sarhosis et al. (2016).

The coal conversion process is composed of three chemical regions of drying, pyrolysis, as well as combustion and gasification of solid char (Thorsness and Rozsa, 1978). The high-calorific synthesis gas constituents are mainly a mixture of hydrogen, carbon monoxide, carbon dioxide and methane in addition to nitrogen and minor components such as sulfuric acid (Friedmann et al., 2009; Kempka et al., 2011b). Apart from its high energetic and economic potential (Budzianowski, 2012; Eftekhari et al., 2012; Nakaten et al., 2014a, 2014b, 2014c), environmental hazards exist also in the UCG context due to aforementioned complex chemical and physical processes accompanying the gasification process. The main potential environmental impacts of UCG are contamination of groundwater aquifers and ground subsidence (Blinderman and Jones, 2002; Couch, 2009; DTI, 2004; Imran et al., 2014; Kapusta and Stańczyk, 2011). Nevertheless, compared to conventional methods, UCG offers many advantages, such as increased work safety, no surface disposal of ash as well as lower dust pollution, water consumption and methane emissions to the atmosphere (Burton et al., 2006; Khadse et al., 2007).

1.2.2 HISTORY OF UCG

The original concept of UCG has a history of over a hundred thirty years. The earliest recorded mentioning of gasifying coal *in situ* belongs to Sir William Siemens, a German-born scientist and engineer, who suggested it in his address in 1868 to the British Chemical Society (Siemens, 1868). At about the same time, the idea was consolidated independently by the Russian chemist Dmitri Mendeleev, who also pointed out the economic benefits over conventional mining (Klimenko, 2009). At the beginning of the 20th century, many industrial cities were covered by heavy smoke — an unpleasant side-effect of the coal-fueled industrial revolution (Klimenko, 2009). At that time, the British scientist Sir William Ramsay prepared the first UCG trial at Hett Hill near Durham (UK), but due to the outbreak of the First World War and Ramsay's death in 1916, the experiment stopped before it was actually started. In the following 1920s and 1930s, the basic UCG technology was developed in the former Union of Soviet Socialist Republics (USSR), whereby extensive knowledge on the UCG process was gained (Klimenko, 2009). The program continued at a high level for nearly 50 years, including successful commercial production (Burton et al., 2006). However, most of the information on USSR field tests was not well documented. As a result, most of the field trials conducted by other countries before the 1960s did not benefit from detailed data on these developments (Khan et al., 2015). Today only the 100 MW UCG Yerostigaz power plant in Angren, Uzbekistan, remains. It is still the world's only commercial UCG site, in operation since 1961. Each day it is continuously producing about one million cubic meters of synthesis gas at a coal seam depth of about 110 m, which is co-combusted in a lignite-fired power plant (Akbarzadeh and Chalaturnyk, 2014a; Younger, 2011). Numerous UCG pilot operations have taken place in the USA. The efforts began with field tests in the early 1960s and were terminated in the mid-1980s due to large natural gas discoveries, which rendered UCG uneconomic. According to Klimenko (2009), especially due to efforts at the Hanna, Hoe Creek and Rocky Mountain sites, the U.S. significantly improved the Soviet technologies during that period. In Europe, the UCG efforts started in the 1980s with deep field trials at Thulin, Belgium, at 850 m depth followed by El Tremedal, Spain, at 580 m depth, but was not pursued further (Burton et al., 2006). In China, UCG efforts began in the 1980s and it is believed that China has the largest UCG program currently underway. This is confirmed by the relatively large number of patents in UCG that have been obtained by Chinese engineers (Shafirovich and Varma, 2009). Further, UCG is a promising technology for India, which has vast coal resources, primarily of low grade (Khadse et al., 2007). India looks to utilize its coal reserves, which are the fourth-largest in the world, to reduce dependency on oil and gas imports (Shafirovich and Varma, 2009).

Up to now, feasibility of UCG was investigated at more than 50 pilot sites worldwide (Burton et al., 2006; Couch, 2009). Earlier, the field tests were limited to shallow depths, but over time and with improvements in drilling technology, the depth of UCG operations has increased markedly as can be observed in the European field trials (Burton et al., 2006; Yang et al., 2016). All these activities contributed to the development of the basis for the modern UCG technology. However, despite of the Yerostigaz site, the UCG process is still not in worldwide commercial operation due to remaining technical and environmental concerns (Burton et al., 2006; Couch, 2009; Sarhosis et al., 2016; Sury et al., 2004).

1.3 MOTIVATION AND OBJECTIVES

The UCG technique itself is a rather simple concept in theory. However, experience from major global field trials in the last decades indicates that an efficient and sustainable operation in practice is much more complicated (Imran et al., 2014; Sury et al., 2004; Yang et al., 2016). Each UCG site will be unique and site-specific coupled thermo-hydro-chemical-mechanical processes occurring in rocks adjacent to a UCG reactor are generally not well known in the field, because of the difficulty to quantify all occurring reactions during the UCG process and their effects on UCG reactor size and shape (Najafi et al., 2014, 2015; Sirdesai et al., 2015). Especially the temperatures above 1000 °C in the close vicinity of the UCG reactor result in complex thermo-mechanical rock behavior and multiphase fluid flow. For a sustainable and efficient UCG operation, it is of uttermost importance to quantify impacts of UCG-related geomechanical responses, such as permeability changes, rock failure as well as fault reactivation (Akbarzadeh and Chalaturnyk, 2014a; Buscheck et al., 2009; Prabu and Jayanti, 2014). The UCG-related environmental concerns such as ground subsidence and groundwater contamination result from the interaction of these coupled processes.

In order to minimize groundwater pollution, the UCG reactor should generally be operated below hydrostatic pressure to avoid the outflow of UCG process fluids into adjacent aquifers (Burton et al., 2006; Seifi et al., 2014). Similar to longwall mining safety pillars between UCG reactors are required. The pillar design significantly impact the evolution of the stress distribution, yielding and subsidence within the strata (Corkum and Board, 2016). In UCG the pillars act additionally as a barrier to avoid hydraulic short circuits. Any hydraulic connection between UCG reactors renders the gasification process uncontrollable in view of pressure and fluid mass balance monitoring and maintenance (Burton et al., 2006). Therefore, the pillar width determines the ground surface subsidence and coal yield at the same time (Li et al., 2015).

The knowledge about the coupled thermo-hydro-chemical-mechanical processes is mainly based on laboratory experiments (e.g., Hettema et al., 1993; Prabu and Jayanti, 2014; Stańczyk et al., 2010; Tian, 2013; Tian et al., 2015; Wolf et al., 1992) and UCG field trials (e.g., Bartke et al., 1985a; Blinderman and Jones, 2002; Chandelle et al., 1993; Liberatore and Wilson, 1983; Nordin, 1992). Due to the high financial efforts associated with UCG field trials, numerical modeling has become a vital methodology to study these processes influencing the UCG performance (Khan et al., 2015). Developing a useful UCG model requires a sound understanding of physical theory as well as knowledge of details to interpret laboratory experimental results in order to successfully predict field data and performance of a new site before proceeding with gasification (Khan et al., 2015). A detailed knowledge on the geological boundary conditions and design parameters (e.g., coal seam depth, thickness, inclination, coal and rock properties, pillar width, water inflow) is rarely the case in practice. However, various simulation models have been developed in order to improve the understanding of processes in UCG (e.g., Akbarzadeh Kasani, 2016; Buscheck et al., 2009; Eftekhari et al., 2015; Nitao et al., 2011; Nourozieh et al., 2010; Sarhosis et al., 2013; Sirdesai et al., 2015; Yang et al., 2014). The complexity of simultaneously occurring physical and chemical processes, such as chemical reactions and their kinetics, transport phenomena, turbulent flow patterns in the reactor and water inflow from the surrounding rock mass and thermo-mechanical processes related to stress changes, is remarkably high (Adhikary et al., 2016; Nitao et al., 2011;

Nourozieh et al., 2010). Therefore, various simplifying physical and chemical assumptions in models (e.g., non-regular reactor shape, heat transfer included for solids only), according to the problem formulations are necessary to isolate and understand important effects, ensure numerical convergence issues and/or achieve faster computational runtimes (Khan et al., 2015).

Various mechanisms such as chemical reactions, thermo-mechanical rock failure as well as sidewall and roof collapse contribute to reactor growth in UCG (Elahi and Chen, 2016; Xi et al., 2015; Xin et al., 2014). Hence, mechanically- and thermally-induced stress changes cause strains in the surroundings as well as shear and tensile rock failure (Yin et al., 2011). Generation of fractures and changes in permeability as a result of UCG may also introduce potential migration pathways for contaminants from the reactor into overburden aquifers (Kapusta and Stańczyk, 2011; Liu et al., 2007). How permeability is influenced by high temperatures around a gasification reactor has so far only been discussed by Akbarzadeh and Chalaturnyk (2014b). Until now no thermo-mechanical simulation studies exist, taking into account temperature-dependent rock properties in view of induced stress changes.

Previous UCG modeling studies applied often 1D or 2D models to account for selected coupled processes (Sirdesai et al., 2015). However, these models have only a limited validity in predicting the performance of UCG field trial operations due to neglecting 3D effects of stress changes and stress redistribution. According to Adhikary et al. (2016), it is known that 2D models generally overestimate the magnitude of stresses in pillars and ground surface subsidence. For investigations on the effect of the presence of faults in a potential gasification area, this can be crucial. In this context, thermo-mechanical effects may introduce fault reactivation of major and/or undetected faults, which can result in formation of potential migration pathways for UCG fluids and hydraulic short circuits between single UCG reactors. The absence of faults in deep coal deposits is highly unlikely. Thus, in conventional coal mining, the extent of faulting in a coal field is described by the terms undisturbed, minor disturbed (distance between faults > 150 m), medium disturbed (distance between faults 100 - 150 m), strongly disturbed (distance between faults 50 - 100 m) and very strongly disturbed (distance between faults < 50 m) (Balley et al., 1989). Consequently, 3D numerical models are required for reliable assessment and prediction of site-specific thermo-mechanical UCG performance impacts (Khan et al., 2015). This additionally requires consideration of different fault orientations with respect to the present stress regime and/or different stress ratios; otherwise, safety pillar width may be easily underestimated.

The steam jacket surrounding a hot UCG reactor results from vaporization of formation fluids. The term steam jacket and the concept was first introduced by Blinderman and Jones (2002), and further discussed in several publications related to UCG (Burton et al., 2006; DTI, 2004; Imran et al., 2014; Moorhouse et al., 2010; Pakala, 2012; Pana, 2009; Saulov et al., 2010; Staúczyk et al., 2012). The steam jacket can effectively affect flow of water into the reactor and reduce the heat consumed for inflowing formation fluid vaporization, which is also required by the endothermic steam-char reaction. On the other hand, due to the changed relative permeabilities the steam jacket can limit gas and contaminant migration out of the reactor (Blinderman and Jones, 2002; Perkins and Love, 2010). Optimal water balances contribute significantly to the calorific value of the synthesis gas, since water is a source of hydrogen for the steam-char and methanation reactions (Camp and White, 2015). In spite of the significance for a sustainable UCG performance and with regard to environmental concerns, neither the formation, dynamics nor the presence of

a steam jacket have been addressed in detail so far (Akbarzadeh Kasani, 2016; Buscheck et al., 2009; Khan et al., 2015).

Based on the previous discussion, three research objectives are formulated for this thesis in order to achieve new insights and a deeper understanding of coupled processes in the near- and far-field of UCG reactors:

The **first objective** is to investigate how thermo-mechanical rock behavior impacts far-field permeability and whether temperature-dependent rock parameters need to be implemented in simulations with regard to upscaling from 2D near-field to large-scale 3D UCG models (Chapter 2). Based on the previous finding, the **second objective** is to analyze the effect of the presence of a regional-scale fault on potential formation of hydraulic short circuits and to quantify resulting ground surface subsidence in a coupled thermo-mechanical 3D model of a hypothetical UCG site (Chapter 3). The **third objective** is to improve the understanding of the hitherto neglected steam jacket dynamics in the UCG reactor vicinity to allow for a more detailed assessment of hydraulic short circuits in future studies. Coupled thermo-hydraulic simulations are employed to validate the modeling approach by means of operational data (Chapter 4).

Two software packages are used to approach the defined research objectives. In this thesis, FLAC^{3D} (Itasca, 2014) was applied for the coupled thermo-mechanical simulations. FLAC^{3D} is a three-dimensional explicit finite-difference program for advanced geotechnical and geomechanical analyses of rock media to calculate stress and deformation as well as heat conduction, using several built-in material models. For analyzing the non-isothermal multiphase flow in porous media, the numerical reservoir Multiphase Filtration Transport Simulator (MUFITS) was applied (Afanasyev, 2015a).

1.4 ORGANIZATION OF THE THESIS AND AUTHOR CONTRIBUTIONS

The goal of the present thesis is the quantification of UCG-related impacts and assessment of UCG-related rock behavior and multiphase flows by coupled thermo-mechanical and thermo-hydraulic 2D and 3D simulations. The cumulative doctoral thesis consists of three peer-reviewed articles published in international scientific journals. Author and co-author contributions to each publication are listed below and the publications are presented in detail in Chapters 2 to 4. In Chapter 5, all results and findings are discussed, a conclusion is given with respect to the thesis' objectives and an outlook for future research is introduced.

Chapter 2, titled “Thermo-Mechanical Simulations of Rock Behavior in Underground Coal Gasification Show Negligible Impact of Temperature-Dependent Parameters on Permeability Changes”, was prepared by Christopher Otto and Thomas Kempka and published in *Energies*, 8, 6, 5800–5827. The study determines the near-field impact of temperature-dependent sandstone and coal properties and resulting permeability changes in the close vicinity of UCG reactors by means of a coupled thermo-mechanical 2D modeling approach. My contribution to this study, as the first author, was designing and performing the research. I was further responsible for analyzing the data and illustrating simulation results as well as the preparation, illustration and revision of the manuscript. Thomas Kempka co-designed the research and supported data analysis. I and Thomas Kempka wrote the manuscript. It is cited in the following as Otto and Kempka (2015a).

Chapter 3, titled “Fault Reactivation Can Generate Hydraulic Short Circuits in Underground Coal Gasification − New Insights from Regional Scale Thermo Mechanical 3D Modeling”, was prepared by Christopher Otto, Thomas Kempka, Krzysztof Kapusta and Krzysztof Stańczyk and published in *Minerals*, 6, 101, 1–23. Within this study, we analyzed the presence of regional-scale faults on the required safety pillar width of a hypothetical UCG operation in the Silesian Basin by coupled thermo-mechanical 3D simulations. Furthermore, regional-scale geomechanical impacts and related permeability changes, hydraulic short circuits and ground subsidence were investigated by applying isothermal and non-isothermal simulation scenarios. My contribution to this study, as the first author, was designing and performing the research. I was responsible for analyzing the data and illustrating the simulation results as well as the preparation and revision of the manuscript. Krzysztof Kapusta and Krzysztof Stańczyk provided unpublished geological and coal-related data for the study area. Thomas Kempka co-designed the research and supported data analysis. I and Thomas Kempka wrote the manuscript. It is cited below as Otto et al. (2016).

Chapter 4, titled “Prediction of Steam Jacket Dynamics and Water Balances in Underground Coal Gasification”, was prepared by Christopher Otto and Thomas Kempka and published in *Energies, 10,* 739, 1-17. Within this study, we investigated steam jacket formation and dynamics as well water balances in the close UCG reactor vicinity by applying a new and validated coupled thermo-hydraulic modeling approach in 2D and 3D simulations. My contribution to this study, as the first author, was designing and performing the research. I was further responsible for analyzing the data and illustrating the simulation results as well as the preparation and revision of the manuscript. Thomas Kempka co-designed the research and supported data analysis. I wrote the manuscript in close collaboration with Thomas Kempka. It is cited below as Otto and Kempka (2017).

In addition, a study extending the findings of the manuscript presented in Chapter 2, has been published within the time of the preparation of this doctoral thesis. This study is not part of this thesis, but listed in Appendix A in favor of completeness. “Thermo-mechanical Simulations Confirm: Temperature-dependent Mudrock Properties are Nice to have in Far-field Environmental Assessments of Underground Coal Gasification.” was prepared by Christopher Otto and Thomas Kempka and published in *Energy Procedia*, 76, 582–591. My contribution to this study, as the first author, was designing and performing the research. I was further responsible for analyzing the data and illustrating simulation results as well as the preparation, illustration and revision of the manuscript. Thomas Kempka co-designed the research and supported data analysis. I and Thomas Kempka wrote the manuscript. It is cited in the following as Otto and Kempka (2015b).

2 Thermo-Mechanical Simulations of Rock Behavior in Underground Coal Gasification Show Negligible Impact of Temperature-Dependent Parameters on Permeability Changes

Abstract

A coupled thermo-mechanical model has been developed to assess permeability changes in the vicinity of an underground coal gasification (UCG) reactor resulting from excavation and thermo-mechanical effects. Thereto, we consider a stepwise UCG reactor excavation based on a pre-defined coal consumption rate and dynamic thermal boundary conditions. Simulation results demonstrate that thermo-mechanical rock behavior is mainly driven by the thermal expansion coefficient, thermal conductivity, tensile strength and elastic modulus of the surrounding rock. A comparison between temperature-dependent and temperature-independent parameters applied in the simulations indicates notable variations in the distribution of total displacements in the UCG reactor vicinity related to thermal stress, but only negligible differences in permeability changes. Hence, temperature-dependent thermo-mechanical parameters have to be considered in the assessment of near-field UCG impacts only, while far-field models can achieve a higher computational efficiency by using temperature-independent thermo-mechanical parameters. Considering the findings of the present study in the large-scale assessment of potential environmental impacts of underground coal gasification, representative coupled simulations based on complex 3D large-scale models become computationally feasible.

2.1 INTRODUCTION

Underground coal gasification (UCG) has the potential to increase the worldwide coal reserves by utilization of coal deposits that are currently not mineable by conventional methods. The original idea of UCG is not new, but rather has a long history. A detailed description of the early ideas and their evolution is given by Klimenko (2009). Nowadays, a target coal seam is developed by directional drilling to make the coal accessible for *in situ* coal combustion (Blinderman et al., 2008). The resulting high-calorific synthesis gas can be applied for fuel production, electricity generation or chemical feedstock production (Bhutto et al., 2013; Blinderman et al., 2008; Burton et al., 2006; Friedmann et al., 2009; Hewing et al., 1978; Kempka et al., 2011b; Klimenko, 2009; Nakaten et al., 2013; Prabu and Jayanti, 2011). Apart from its high energetic and economic potential (Budzianowski, 2012; Eftekhari et al., 2012; Nakaten et al., 2014a, 2014b, 2014c), UCG may cause environmental impacts such as ground subsidence and groundwater pollution (Burton et al., 2006; Couch, 2009; Durucan et al., 2014; Hewing et al., 1978; Sury et al., 2004). In order to completely avoid or significantly mitigate these potential environmental concerns, the UCG reactor is generally operated below hydrostatic pressure to hinder the outflow of UCG process fluids into adjacent aquifers (Burton et al., 2006; Seifi et al., 2011, 2014). Changes in permeability and generation of fractures in the overburden as a result of the *in situ* combustion process may introduce potential migration pathways for UCG contaminants like organic (phenols, benzene, PAHs and heterocyclics) and inorganic pollutants (ammonia, sulphates, cyanides, and heavy metals) (Humenick, 1978; Kapusta and Stańczyk, 2011; Liu et al., 2007; Walters and Niemczyk, 1984). As groundwater pollution is recognized to be the most relevant environmental risk related to UCG (Klimenko, 2009), extensive investigations on the formation, release, and migration of contaminants have to be conducted at the laboratory and field scale (Kapusta et al., 2013).

Major contributions to the environmental impact mitigation can be achieved by improving the understanding of coupled thermo-mechanical processes in the rocks surrounding the UCG reactor. However, these are difficult to investigate for deep UCG operations in the field, so that the current knowledge on these processes is mainly based on laboratory experiments (Stańczyk et al., 2010, 2011) and UCG field trials at shallow depths, e.g., Angren (110 m) in Uzbekistan, Chinchilla (140 m) in Australia, Hanna (80 m) and Hoe Creek (30–40 m) in the USA (Burton et al., 2006; Couch, 2009). During UCG, temperatures of more than 1500 °C can be reached in the UCG reactor and its close vicinity, and thus the temperature-dependent coal and rock behavior in the reactor vicinity is expected to be of the uttermost importance for assessment of UCG- related permeability changes in the rocks surrounding the UCG reactor. Next to mechanical stress changes due to excavation effects resulting from the reactor growth, thermal stresses also induce permeability changes. Permeability in consideration of the difference between hydrostatic and UCG reactor pressure, controls fluid in- and outflow into and out of the reactor, respectively (Blinderman and Anderson, 2004). This affects the drying of coal, pyrolysis gas flow from the coal into the reactor, oxidant and synthesis gas flow from the reactor, gasification efficiency as well as convective heat transfer into surrounding rocks (Buscheck et al., 2009; Su et al., 2013; Wolf and Bruining, 2007).

Coupled numerical models can be applied to assess the mechanical integrity of the UCG reactor and its surrounding rocks. Wolf and Bruining (2007) found in their study on the interaction between underground coal fires and the respective roof rocks that the combustion process and

permeability behavior, influenced by the thermo-mechanical behavior of the overburden rock, are the essential processes to be considered. Although, the study focused on shallow coal fires, similar behavior is expected in underground coal gasification of deeper seated coal seams. A 3D model for combined reactive heat and mass transport comprising thermo-mechanical failure behavior has been developed by Biezen (1996). With his approach, an understanding of the development of an underground coal gasification reactor is obtained taking into account thermo-mechanical failure properties of coal and rocks, as well as thermo-mechanically induced spalling of both, roof rock and coal. Simulation results show that a high permeability zone between the injector and producer develops, which leads to the formation of a single channel at the bottom of the coal seam. However, permeability changes in the overburden are not considered by this model. Hettema et al. (1998) studied the effect and influence of thermal spalling on differently heated Felser sandstones under the presence of water in thermal shock experiments. The pore pressure increases in the reactor vicinity, whereby the opening of the pores and micro-cracks can lead to a significant increase in permeability (Bernabe, 1987). However, Hettema et al. (1998) concluded that even for sedimentary rocks, which have the potential to spall by steam pressure alone, spalling probably occurs by a combination of steam pressure and a fracturing mechanism associated with high compressive thermal stress.

Several early studies on UCG demonstrated that roof rock behavior has an important effect on reactor stability and ground subsidence (Mortazavi, 1989; Thompson et al., 1977; Tian, 2013). Thermo-mechanical coupled models implemented by Tian (2013) and Najafi et al. (2014) aimed at the investigation of UCG induced ground subsidence based on the Controlled Retracting and Injection Point (CRIP) UCG configuration. Numerical studies performed by Tian (2013) therefore focused on the temperature impact and implementation of thermo-mechanical Hoek-Brown (TMHB) and Mohr-Coulomb models, whereas Najafi et al. (2014) analyzed the stress distribution in the vicinity of UCG panels to estimate the required protection pillar width for commercial scale UCG operation. Their simulation results show increasing ground subsidence with the increase of the reactor size as well as the stress increased at the front of the face and pillar edge due the induced thermal stresses. Thermo-mechanical simulation results of rocks surrounding an UCG reactor elaborated by Yang et al. (2014) show the temperature distribution and stress increase (around 10%) as well as vertical displacements (0.073 m) above the coal seam after three days of gasification. Sarraf et al. (2011) present a 2D model for the growth of a UCG reactor based on the CRIP technology, which incorporates the combined effects of fluid flow through porous media, mass transfer of species, heat transfer and reaction kinetics. The resulting cavity shape and growth rate are in good agreement with experimental data from post-burn experiments, but thermo-mechanical rock behavior and permeability changes in surrounding rocks have not been taken into account in that study. The implementation of a comprehensive UCG simulation tool, which is able to numerically couple underground gasification thermodynamics with hydro-mechanical and reactive transport processes to predict reactor growth, synthesis gas composition and rate, and UCG process interaction with the host environment, accounting for site characteristics, oxidant composition and injection rate is computationally extremely challenging and was recently reported to be in development (Nitao et al., 2011).

Furthermore, most existing mechanical modeling studies focused on ground subsidence or stress changes by applying only coarsely refined structured numerical grids, resulting in a limited validity considering thermo-mechanical processes in the close reactor vicinity (Najafi et al., 2014; Tan et

al., 2008; Yang et al., 2014). Most of the present experimental studies on thermo-mechanical properties of rocks at high temperatures mainly considered crystalline rocks such as granites and marbles. Due to limited data availability on thermo-mechanical properties of sedimentary rocks, previous thermo-mechanical modeling studies generally did not incorporate the influence of thermo-mechanical parameters (Najafi et al., 2014; Wolf and Bruining, 2007) or used those of igneous rocks instead, e.g., Min (1983) and Sarhosis et al. (2013).

In the present study, a coupled thermo-mechanical model has been developed to assess permeability changes in the UCG reactor overburden based on a volumetric strain to permeability relationship after Chin et al. (2000). Simulations carried out for this study are not focusing on the investigation of rock spalling at the reactor boundary, reactor roof collapse and ground surface subsidence. The finite-difference thermo-hydro-mechanical simulator FLAC^{3D} (Itasca, 2014) was employed to analyze thermo-mechanical stress changes, displacements and volumetric strain increments around a UCG reactor using a specifically refined unstructured grid.

2.2 METHODOLOGY

2.2.1 MODEL GRID GEOMETRY, BOUNDARY CONDITIONS AND APPLIED SIMULATOR

The chosen model size and grid discretization of the implemented numerical model were adapted to calculation time, whilst model boundary conditions were placed at a distance far enough away to minimize their impact on the computational results. The implementation of the 2D UCG reactor model presented here is derived from Hanna trial data, numerical simulation results of UCG thermodynamics carried out by Luo et al. (2009) and literature data after Tian et al. (2011, 2012, 2013, 2014, 2015). The implemented numerical model uses the UCG reactor symmetry present along its vertical axis assuming that a half-radial symmetric reactor develops along the UCG panel. Hence, the present approach neglects the 3D tear-drop shape of the UCG reactor as reported by, e.g., Burton et al. (2006), but maintains its major geometric features (Figure 4). The two-dimensional geometry of the Hanna coal seam of 4 m thickness is uniformly expanded towards the model boundaries with the reactor bottom located at a depth of 250 m below ground surface. Model size was set to 40 m × 110 m and discretized by about 3000 elements with sizes of 0.16 m to 5 m in horizontal and vertical directions. Application of an unstructured mesh allowed us for a sufficient grid refinement to maintain numerical accuracy in the UCG reactor vicinity for the four considered geometrical reactor growth steps. Therefore, the implemented model grid enables a specific stepwise UCG reactor excavation based on a pre-defined low coal consumption rate (0.654 t per day and meter reactor length), and thereby prevents overestimations of mechanical excavation effects, which would introduce unrealistic grid point velocities into the numerical model, and consequently overestimate strains and mechanical failure. In numerical modeling of mechanical processes, specific mechanical excavation methods may lead to different stress paths, which have an important impact on failure modes around excavation boundaries. However, the behavior of rock mass can be only reasonably revealed, if the stress path is captured in a realistic manner (Zhao et al., 2010). Based on sensitivity studies using time-dependent forces derived from elements at the outer reactor boundaries, the four step excavation showed comparable grid point velocities during excavation as in a finer step excavation.

A stress boundary condition with a vertical stress of 4.1 MPa has been assigned at the top model boundary, representing the weight of overburden. Fixed boundary conditions were applied normal to the lateral boundaries and model bottom. Hence, displacements perpendicular to the model bottom and lateral boundaries were not allowed at the respective model boundaries, while the model top was allowed to freely displace in any direction. Based on grid size sensitivity analyses, the final unstructured grid was generated using the open source GMSH software package (Geuzaine and Remacle, 2009) and own grid conversion tools to transfer the resulting grid into the finite-difference software package FLAC^{3D}.

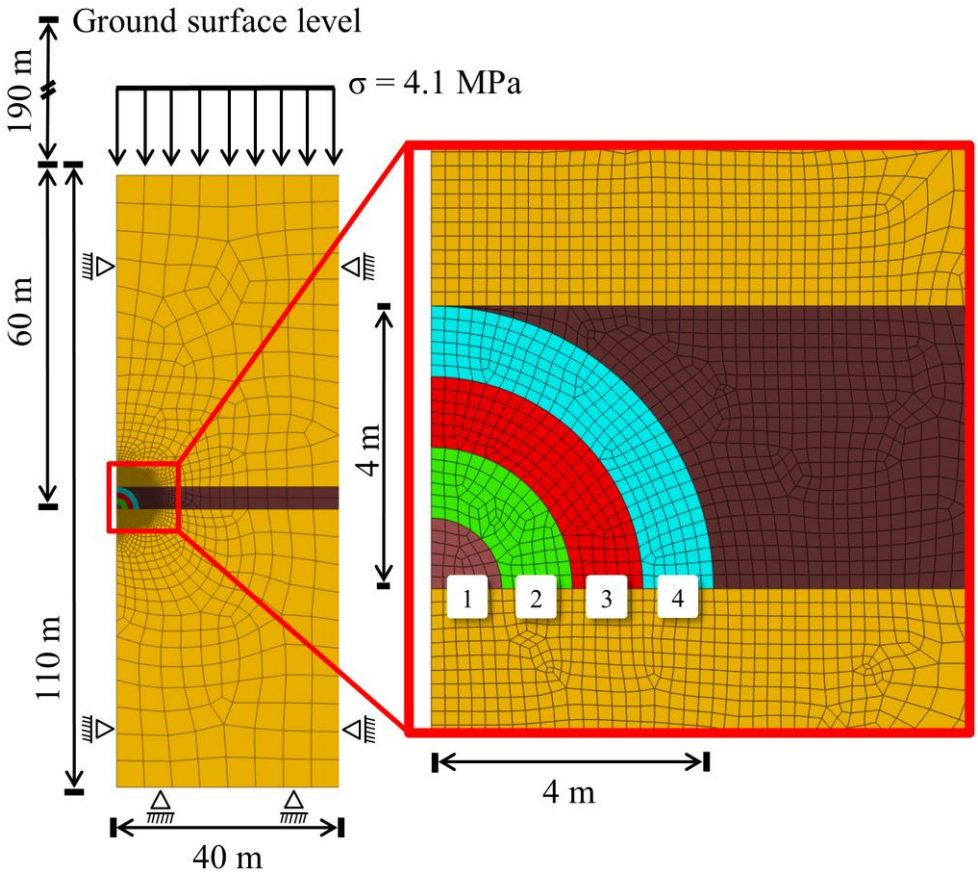

Figure 4: Geometry of the thermo-mechanical coupled 2D UCG model based on simplified geological data of the Hanna UCG trial. The model comprises two sandstone layers (colored in light brown) and one coal seam (colored in dark brown) with four geometric reactor growth steps considered in the simulations (light brown, green, red and turquois).

2.2.2 NUMERICAL MODEL PARAMETERIZATION AS WELL AS ROCK AND COAL PROPERTIES

Literature reviews and experimental studies carried out by Tian et al. (2011, 2012, 2013, 2014, 2015) summarize the extensive laboratory research on rock specimens exposed to high temperatures undertaken in the last decades to investigate the temperature influence on thermo-mechanical on physical, thermal and mechanical rock properties. These research efforts indicate that mechanical rock properties are generally highly dependent on temperature, and that the characteristics of temperature dependency vary with rock types, rock initial features such as micro-cracks and structure as well as with the experienced temperature gradient (heating rate)

(Tian et al., 2011, 2012, 2013, 2014, 2015). In addition to the previously mentioned review on international literature, Tian et al. (2011, 2012, 2013, 2014, 2015) provide new experimental study results on temperature-dependent thermo-mechanical rock properties, especially addressing the thermo-mechanical parameters of sedimentary rocks at temperatures of up to 1000 °C. Temperature-dependent thermal properties (linear thermal expansion coefficient, specific heat capacity, thermal conductivity) are not yet published for claystones (Tian et al., 2014). Since this modeling study focused on the temperature-dependent permeability development in the UCG reactor vicinity, all simulations have been implemented with thermal parameters derived for sandstone from published laboratory testing studies (see Figure 5 and Figure 6) (Badzioch et al., 1964; Clauser and Huenges, 1995; Hajpál and Török, 1998; Min, 1983; Shoemaker et al., 1977; Singer and Tye, 1979; Somerton, 1992; Tian, 2013; Yin et al., 2011). The normalized trends of thermo-mechanical coal properties after high temperature treatment are based on derived from a review carried out by Min (1983). All data applied in the thermo-mechanical model are compiled in Table 1, whereby typical initial values of density (ρ) and Poisson's ratio (ν) were assumed based on literature data (Gercek, 2007; Somerton, 1973) and maintained constant for all lithological units. As a generally accepted law on temperature influence on the Poisson's ratio (e.g., Gercek, 2007) has not been published so far, the Poisson's ratio is assumed to be independent of temperature in our simulations.

Density of sedimentary rocks decreases with increasing temperature due to volumetric expansion and/or the release of volatile matter, but the magnitude in decrease is relatively small compared to that of virgin rocks (Tian et al., 2011, 2012, 2013, 2014, 2015). The density is maintained constant for all geological units, whereas the linear thermal expansion coefficient (α) was chosen to be temperature-dependent as discussed below in more detail.

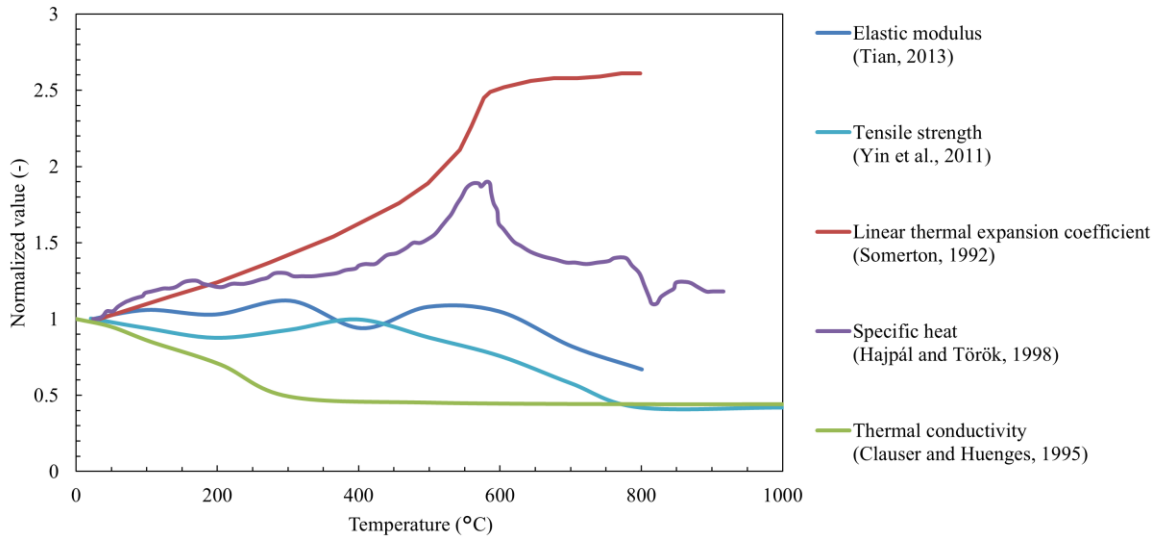

Figure 5: Trend of normalized thermo-mechanical properties of sandstones as a function of temperature.

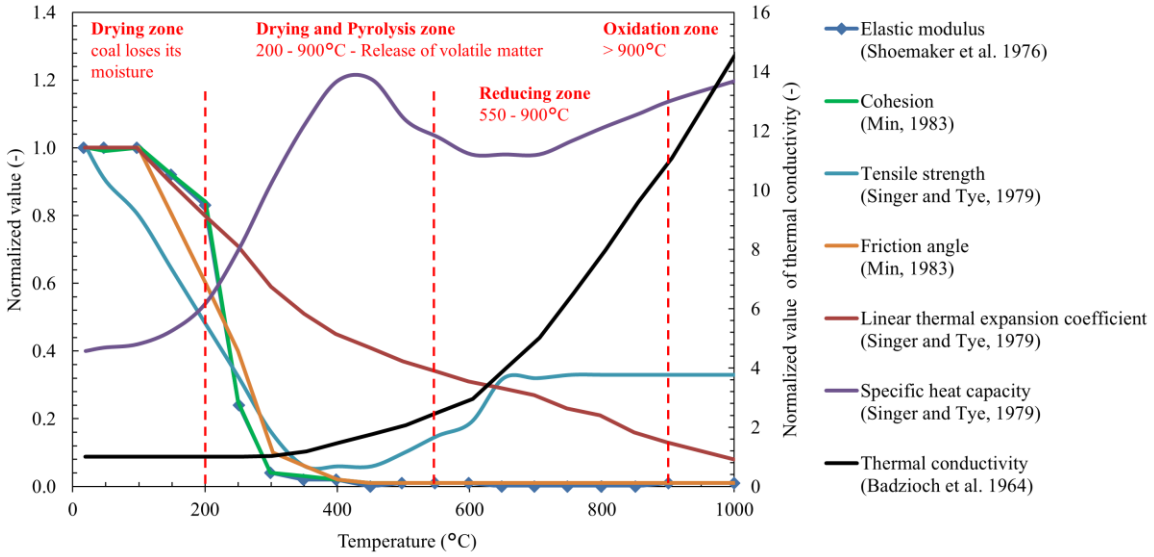

Figure 6: Trend of thermo-mechanical coal properties as a function of temperature. Red dashed lines delimit temperature regions representing the temperature zones exhibiting specific thermo-mechanical coal behavior.

Table 1: Initial thermo-mechanical rock properties applied for numerical model parameterization.

Input Parameter	Unit	Sandstone	Coal
Mechanical parameters			
Elastic modulus (E) $f(T)$	GPa	4	2
Tensile strength (σ_t) $f(T)$	MPa	5	0.27
Friction angle (φ) (constant for rock)	°	32	20
Cohesion (c) (constant for rock)	MPa	5	0.1
Poisson ratio (ν) (constant)	-	0.35	0.44
Density (ρ) (constant)	kg/m^3	2200	1300
Thermal parameters			
Linear thermal expansion coefficient (α) $f(T)$	K^{-1}	1.6×10^{-5}	5.0×10^{-6}
Specific heat capacity (C_P) $f(T)$	J/kg K	1363	2000
Thermal conductivity (λ) $f(T)$	W/m/K	2.30	0.23

2.2.3.1 SANDSTONE PROPERTIES AS FUNCTION OF TEMPERATURE

As summarized by Tian et al. (2011, 2012, 2013, 2014, 2015), significant experimental research on mechanical and thermal rock properties during and after high temperature treatment has been carried out in the scope of underground coal gasification research, whereby the results indicate that temperature-dependent parameters have to be considered in numerical simulations on high temperature rock mechanical processes (e.g., Bauer and Johnson, 1979; Clauser and Huenges, 1995; Hajpál and Török, 1998; Hettema et al., 1992; Somerton, 1992; Yin et al., 2011). Thus, temperature dependent thermo-mechanical properties of sandstone assigned to the models considered here include the elastic modulus (E), tensile strength (σ_t), linear thermal expansion coefficient (α), specific heat capacity (C_P) and thermal conductivity (λ, Figure 5). The normalized

values shown in Figure 5 are the respective ratios of these values at the tested temperature to those determined at initial conditions (Table 1) as a function of temperature. Experimental results have indicated that the nature of changes of rock strength properties with increasing temperature is not consistent for sedimentary rocks, but it is generally accepted that elastic modulus and strength of rocks decrease with increasing temperature (Tian et al., 2011, 2012, 2013, 2014, 2015). It is obvious that thermal property behavior of sedimentary rocks is related to its mineral composition. Somerton (1992) reported that less dense feldspars and clays are known to have lower thermal conductivities compared to quartz. Although, differences in mineral compositions have some effect on the magnitude of thermal effects, experimental results of linear thermal expansion coefficient tests on sandstone samples show that the quartz content has a dominant effect on its expansion (Somerton, 1992). The linear thermal expansion coefficient of sandstone increases in a continuous linearly manner with temperature and notably above 500 °C until the α–β quartz phase inversion at approximately 575 °C is reached, and then remains constant. Hajpál and Török (1998) observed that the specific heat capacity of sandstones increases with increasing temperature and reaches its maximum in the range of 550 °C to 700 °C, and decreases thereafter. In accordance with other studies on sedimentary rocks, Clauser and Huenges (1995) reported a generally decreasing trend in thermal conductivity with increasing temperature for sandstone. For sedimentary rocks in general, they showed that further factors influencing thermal conductivity are porosity and the origin of the particular sediment.

2.2.3.2 COAL PROPERTIES AS FUNCTION OF TEMPERATURE

Initial parameterization of coal (Table 1) considered data from the review of experimental testing data on temperature-dependent thermo-mechanical properties for bituminous coals carried out by Min (1983). From the thermal trends of the coal's elastic modulus (E) and tensile strength (σ_t), its cohesion (c) and friction angle (φ) were assumed and applied for model parameterization (Min, 1983). The implemented temperature-dependent thermal coal properties comprise the linear thermal expansion coefficient (α), specific heat capacity (C_P) and thermal conductivity (λ) (Figure 6, Badzioch et al., 1964; Min, 1983; Shoemaker et al., 1977; Singer and Tye, 1979). Coal undergoes a number of pyrolysis reactions during heating (Min, 1983). A significant decrease of the elastic modulus, tensile strength, cohesion and friction angle occurs at temperatures above 200 °C due to the release of volatile matter. Further notable property changes occur in the drying and pyrolysis temperature regions close to the coal liquefaction temperature at 300 to 350 °C, where softening and highly viscoelastic behavior occur (Barr-Howell et al., 1985; Shoemaker et al., 1977). In the present study, it is assumed that coal exposed to temperatures above 400 °C is either gasified or collapsed into a reactor forming a rubble pile. These transitions are not explicitly implemented, however, the loss in strength is considered through the implemented temperature-dependent mechanical properties. Thereto, all three mechanical properties (elastic modulus, cohesion and friction angle) are assumed to significantly decrease tending towards zero. Model elements experiencing temperatures above 400 °C do not have any strength assigned.

2.2.3 COUPLING OF VOLUMETRIC STRAIN INCREMENTS TO POROSITY AND PERMEABILITY CHANGES

Conditions in the UCG reactor and its combustion zone are strongly influenced by the influx of water, which is controlled by the host rock permeability and the gradient between hydrostatic and UCG reactor pressure (Buscheck et al., 2009). Hence, UCG operation, i.e., especially UCG reactor temperature, is determined by a complex interaction between hydro-mechanical effects and related permeability changes as well as coal properties and oxidant composition. In order to determine permeability changes, various approaches to this problem have been developed, but the impracticability of describing discrete fracture systems in detail has limited the specificity of analyses (Neuzil, 2012). Studies on the relation between principal stresses and discrete fracture permeability have been mainly motivated by interest in effects of tectonics and engineered excavations (e.g., Brown and Bruhn, 1998; Zhang et al., 2007). Thermally-induced mechanical and permeability changes around excavations are often addressed in the context of nuclear waste disposal (Min et al., 2005). In addition to the excavation damage zone, that is created in the excavation near-field exposing a high potential for changing rock permeability, also thermal stress effects generated in the near-field have been an issue of great concern (e.g., Hudson et al., 2008; Min et al., 2005; Min, 1983; Rutqvist et al., 2009; Tsang et al., 2005). Changes in permeability of simulated fractured rock masses were calculated with a set of stress-dependent empirical equations that account for both, normal and shear dilation (Min et al., 2004). The results show that permeability changes are small, i.e., a factor of two and generally decreasing around a nuclear waste repository, and thermally induced dilation was not observed (Min et al., 2005). However, the evolution of stresses and permeability changes around excavation zones is analyzed for different rock types (crystalline rock, rock salt, and indurated and plastic clays), at different times scale and much lower temperatures (Min et al., 2004, 2005).

Wolf and Bruining (2007) expected that the combustion process, the heat transfer and permeability behavior influenced by the thermo-mechanical behavior of the overburden rock are essential elements to be considered. For an initial uniform permeability field in the study presented by Wolf and Bruining (2007), the reactive free convection model was used to obtain a temperature distribution, which was then used in a compaction model to derive an updated permeability distribution. In the present study, deformation is associated with volume changes affecting rock and coal permeability, so that the rock compaction behavior in the UCG reactor vicinity was simulated by using an isotropic elastoplastic constitutive model using applying the material properties shown in Table 1. For modeling thermal and mechanical stress-induced permeability changes, the permeability is related to volumetric strain using the stress-induced relationship developed by Chin et al. (2000):

$$\phi = 1 - (1 - \phi_0)e^{-\Delta\varepsilon_v} \tag{1}$$

$$K = K_0 \left(\frac{\phi}{\phi_0}\right)^n \tag{2}$$

where ϕ is the porosity at a given volumetric strain ε_v; ϕ_0 the initial porosity; K the permeability at a given ε_v; K_0 the initial permeability; and n a power-law exponent (porosity sensitivity exponent) with a value range of 2 to 25 depending on stress and lithology (David et al., 1994; Yale, 1984). David et al. (1994) found a linear correlation of the logarithmic permeability and bulk

porosity for all tested sandstones. Therefore, permeability scales in form of a power-law with porosity (Equation 2). Experimental results from David et al. (1994) show that a rather large permeability loss corresponds to a moderate porosity reduction, which results in high values for the porosity sensitivity exponent (n). The effect of this exponent will be further discussed in the Results and Discussion section. Relating permeability to porosity and volumetric strain enables straightforward permeability change calculations in our coupled thermo-mechanical model. Our assumptions comprise a homogeneous and isotropic rock considering thermo-mechanical properties independent of pore pressure. Consequently, the applied model allows us to assess the damage zone in the reactor vicinity, which is associated with a strong permeability increase. In the developed model, calculated permeability changes are not reversible, what can be explained by the permanent increase in fracture aperture due to shear and tensile dilation in the rock. Furthermore, the thermo-mechanical simulations carried out for this study focus on an extreme case of spatial temperature distribution by neglecting fluid flow into and out of the reactor as well as the steam jacket present in the hanging wall.

2.2.4 SCENARIO ANALYSIS

Two different simulation scenarios were applied to carry out a sensitivity analysis for a coupled thermo-mechanical simulation of one day and 50 days length, respectively. Simulations were essentially carried out in two steps: the first step represents the initial setup of the numerical grid, material properties, boundary conditions, and initialization of the *in situ* stress as previously discussed. This initial model was then run to achieve a mechanical equilibrium (defined by the maximum unbalanced force present in the model), and used from there as initial state model for all simulations discussed in the following. Secondly, the UCG reactor was excavated in one step for the sensitivity analysis, whereas for the 50 day simulation, the reactor sizes were generated in a stepwise manner depending on the given coal consumption rate (0.654 t per day and meter reactor length). A constant temperature of 1000 °C was applied at the reactor boundary for each excavation step and the model was calculated to mechanical equilibrium for each thermal time step. The temperature-dependent rock and coal properties have been implemented in a tabular format in the numerical model for each element and time step. Thereto, FISH (Itasca macro programming language) functions were implemented and called for these properties at each iterative step in the coupled numerical analysis. In all cases, the coupled simulations were run separately for each excavation step until the achievement of a mechanical equilibrium before proceeding with the next excavation step.

2.3 RESULTS AND DISCUSSION

2.3.1 TEMPERATURE DEPENDENCY OF THERMO-MECHANICAL ROCK PROPERTIES

Mechanical processes in the UCG reactor vicinity are strongly influenced by mechanical and thermal properties, which are in turn controlled by the temperature distribution in the surrounding coal and its adjoining rock, provided that properties are considered to be temperature-dependent. Changes in the reactor temperature result in different mechanical behavior, whereby each parameter has a different development and a varying influence on total displacements in time (Figure 5 and Figure 6). For the sensitivity analysis, all four radial reactor zones were excavated at once and a temperature of 1000 °C was applied for one day at the reactor

walls. Except for the parameter to be investigated within the sensitivity analysis, all other model input parameters were maintained constant at initial conditions in time. The results of total displacements are plotted along three profiles (Figure 7) for comparison of the simulations using temperature-independent and temperature-dependent properties (Figure 8).

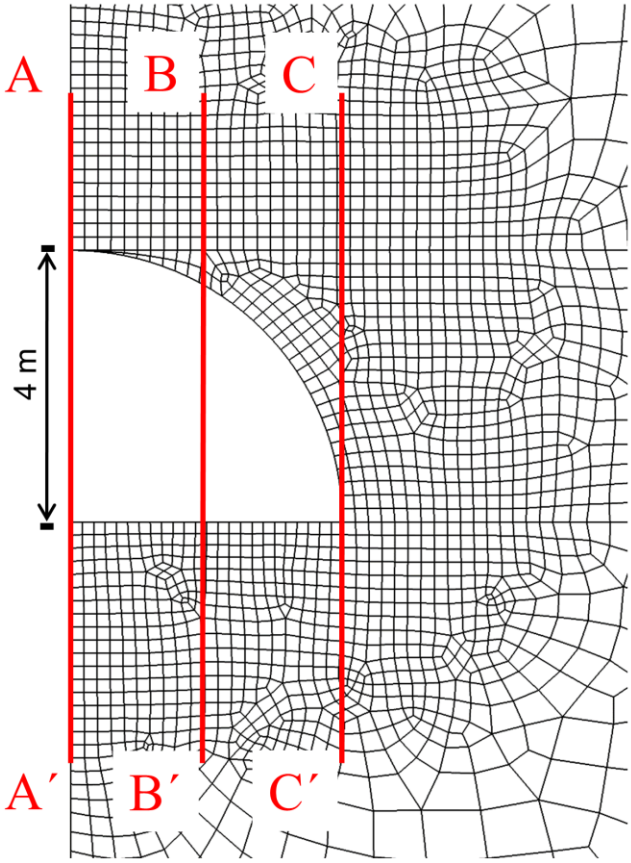

Figure 7: Position of the total displacement profiles in the 2D model.

The proposed methodology enabled us to identify the most relevant thermo-mechanical parameters in the simulation and to highlight, which of those have to be taken into account in thermo-mechanical environmental impact assessments of UCG operations. Parameters inducing the highest displacement variations were identified and quantified. Displacement profiles plotted in Figure 7 exhibit significant differences between simulations considering temperature-independent and dependent rock parameters. In general, the displacement magnitudes of temperature-dependent simulations are higher in regions of notable temperature changes.

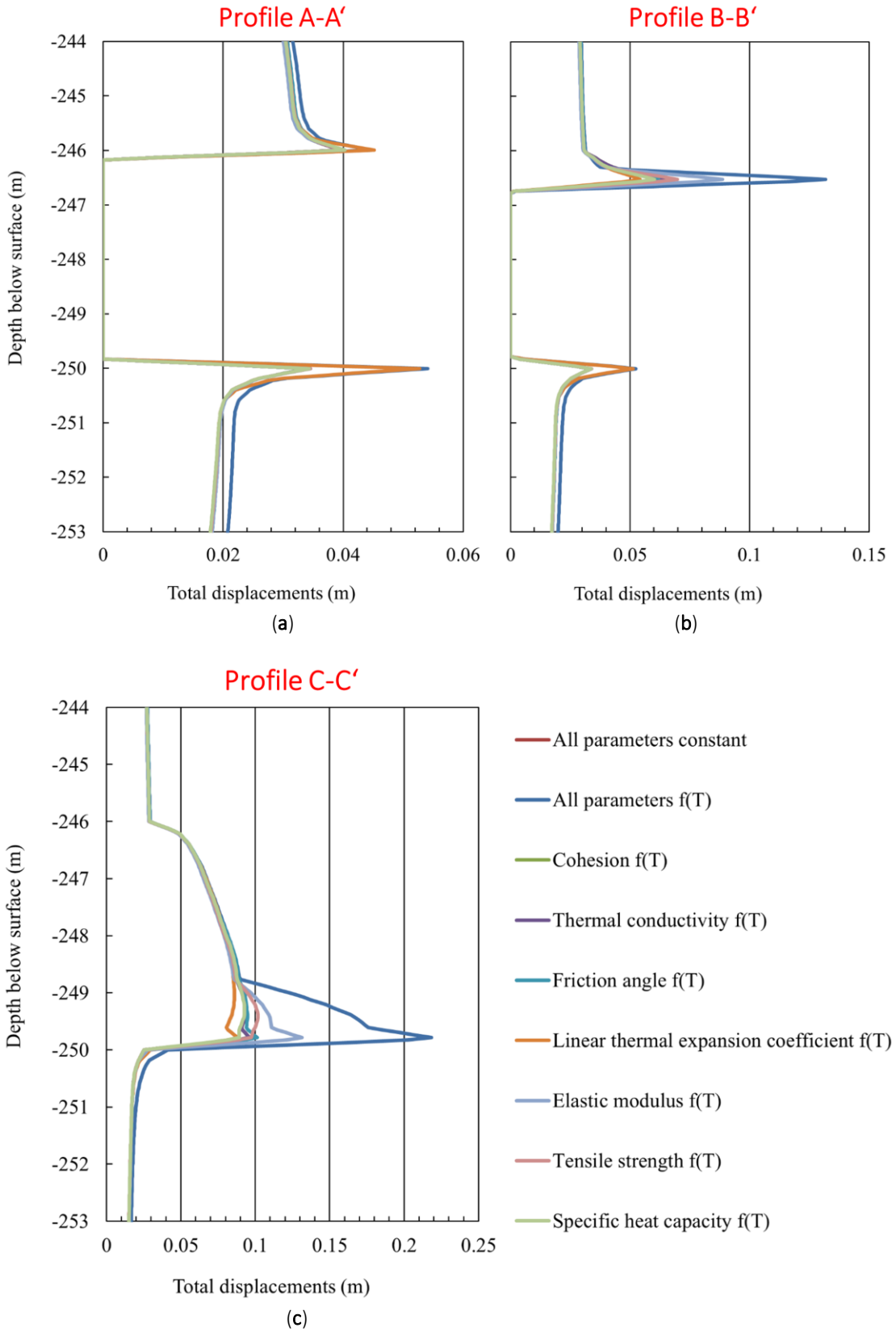

Figure 8: Profiles of total displacements (a–c) after one day of simulation show that the thermo-mechanical rock behavior is mainly influenced by the linear thermal expansion coefficient (α), tensile strength (σ_T) and elastic modulus ($\boldsymbol{E}$).

At the upper and lower reactor to sandstone boundary, the experienced high temperatures have the highest impacts on total displacements, especially due to the influence of the sandstone's linear thermal expansion coefficient. Maximum total displacements at the reactor bottom of about 6 cm are achieved, which is about 2 cm higher compared to the temperature-independent parameter based simulation (Profiles A-A´ and B-B´ in Figure 8). Due to only minor temperature-dependent variations in elastic modulus and tensile strength, the stability of the sandstone layer is not affected even at high temperature conditions. Hence, none of the other investigated parameters is found to be sensitive to displacements in the sandstone layer. The simulated total displacements in the coal seam at 246 m to 250 m depth (Figure 8, Profiles B-B´ and C-C´) illustrate that tensile strength and elastic modulus are the parameters most sensitive to consideration of their temperature-dependency. Significant changes in total displacements at the reactor hanging wall can be observed (about 22 cm in total), where the relative difference compared to the simulations with temperature-independent properties is up to 10 cm. Considering the development of the nominal values in Figure 6, it becomes obvious that the simulated displacements are related to a significant decrease in strength at temperatures above 200 °C.

The sensitivity analysis shows that maximum total displacements resulting from the consideration of temperature-dependent parameters are generally higher compared to those without temperature-dependent parameters. This is further influenced by the dynamic development of the spatial temperature distribution in the reactor vicinity, and thus the related changes in thermo-mechanical material properties affecting rock strength as well as the *in situ* stress regime. Furthermore, the sensitivity analysis shows that thermo-mechanical behavior of the given rocks is mainly influenced by the linear thermal expansion coefficient, tensile strength and elastic modulus. Nevertheless, for the 50 day simulation, specific heat capacity and thermal conductivity were maintained as temperature-dependent to account for a maximum realistic spatial temperature distribution in the reactor vicinity.

2.3.2 DISTRIBUTION OF TEMPERATURE WITH TEMPERATURE-DEPENDENT AND -INDEPENDENT MATERIAL PROPERTIES

Heat transport in the present simulations is driven by heat conduction only. Since heat conductivity and heat capacity are determined by low values in both lithological layers (Table 1), their change with increasing temperature is in the range of one order of magnitude, and thus induces a significant temperature increase (≥ 200 °C) in the close reactor vicinity only. Figure 9 shows the distribution of the temperature in the reactor vicinity after 50 days simulation with temperature-dependent and temperature-independent properties. For both simulations, the maximum of the high temperature (≥ 200 °C) distance to the reactor boundary is in the range of the coal seam thickness and even larger (0.85 m), if temperature-dependent parameters are not considered.

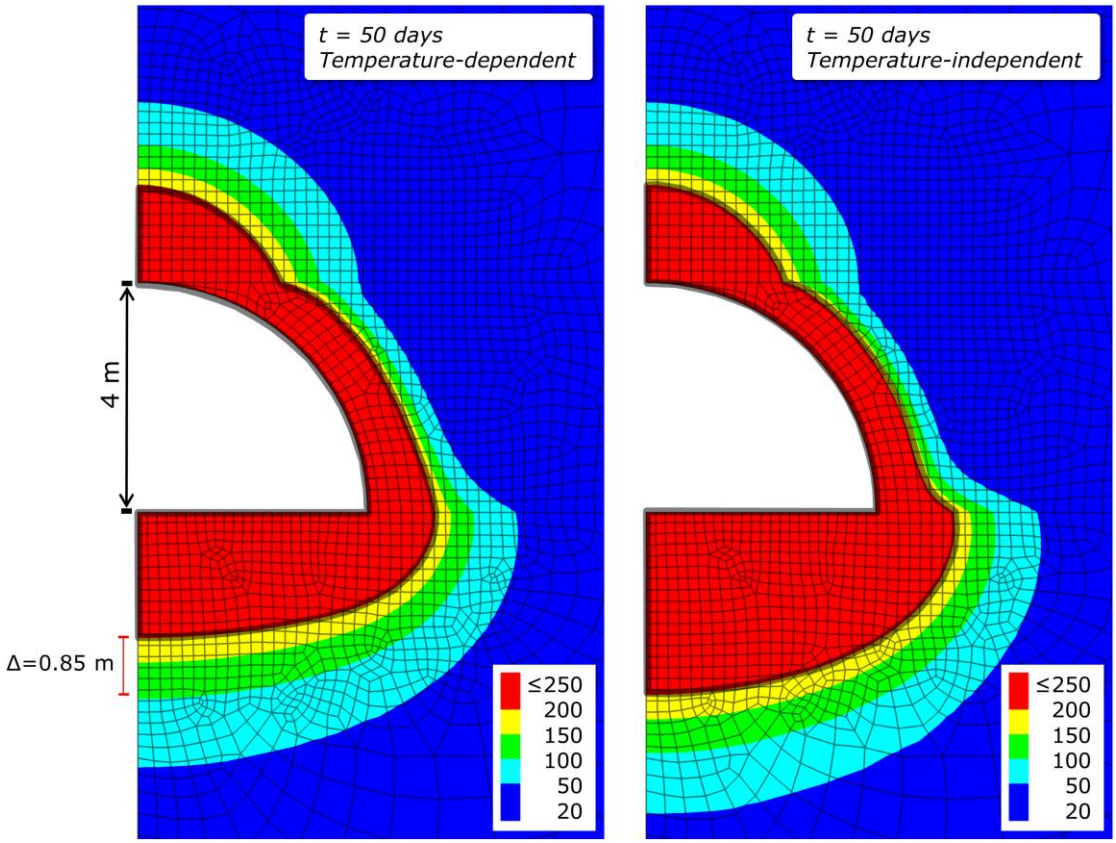

Figure 9: Temperature distribution in the reactor vicinity after 50 days of simulation with (a) temperature dependent and (b) temperature-independent material properties.

A comparison of the distribution of the thermal conductivity for temperature-dependent and temperature-independent parameters is shown in Figure 10. Due to the decrease in thermal conductivity with increasing temperature for sandstone, the magnitudes are reduced to about the half (1.2 W/m/K) of the initial value in reactor vicinity due to high temperature impact. The temperature of 1000 °C at the reactor boundary is applied at each reactor growth step, at especially results in the formation of a broader temperature field at the reactor bottom in the temperature-independent simulation (increase by 0.85 m at temperatures ≥ 200 °C). The influence of the exposure of the reactor underburden to high temperatures is significantly longer compared with that experienced by the reactor overburden in that case.

The increase in thermal conductivity of coal by about one order of magnitude in regions with temperatures above 900 °C is observed close to the reactor boundary only. Hence, the effect of considering temperature-dependent parameters is very limited for the resulting temperature distribution.

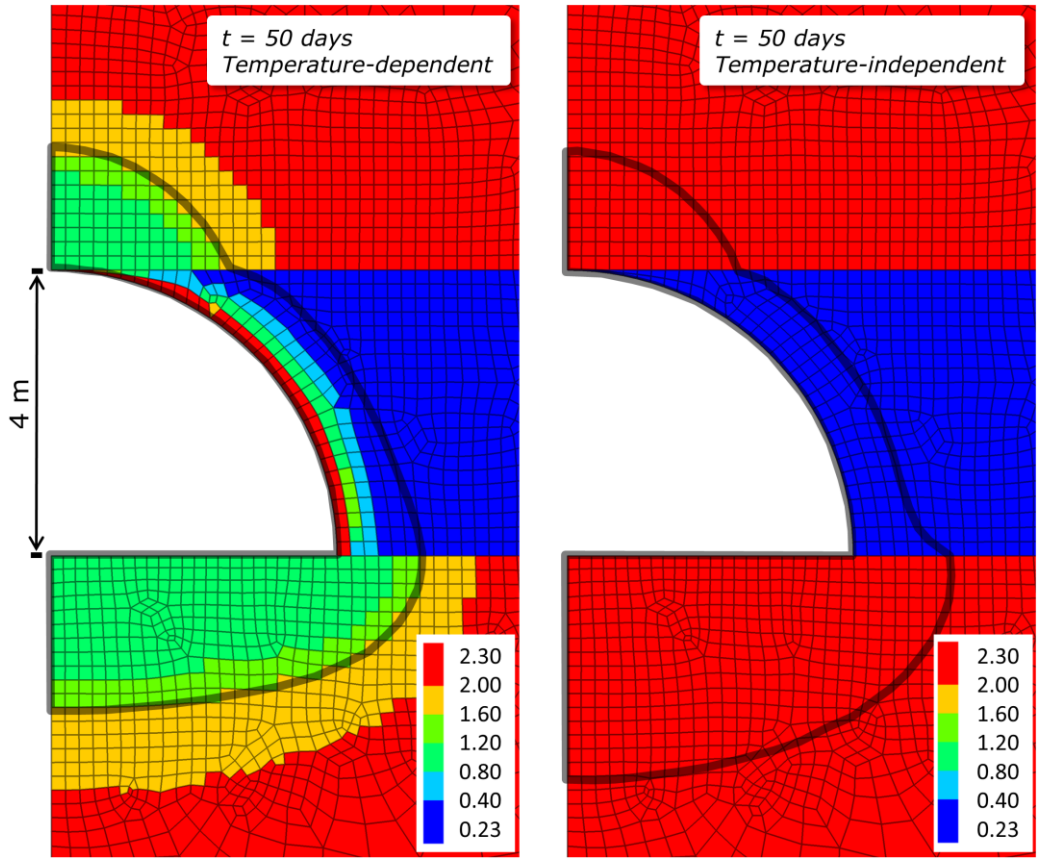

Figure 10: Distribution of the thermal property thermal conductivity (W/m/K) after 50 days of simulation with (a) temperature-dependent and (b) temperature-independent properties (initial values). The grey solid line represents the 200 °C isotherm.

2.3.3 DISTRIBUTION OF TOTAL DISPLACEMENTS IN THE UCG REACTOR VICINITY

A stepwise reactor zone excavation can minimize the overestimation of mechanical excavation effects (high grid point velocities at the simulation start), and was therefore applied in the displacement analysis considering temperature-dependent and -independent rock and coal parameters. Total displacements after 50 days of simulations show notably higher displacement magnitudes for the stepwise reactor excavation with temperature-dependent compared with temperature-independent material properties. Due to the high temperature present at the reactor boundary, temperature-dependent tensile strength and elastic modulus of coal drop significantly. The coal strength tends towards zero inducing high displacement magnitudes above 0.25 m (Figure 11). The observed vertical distribution of total displacements using temperature-dependent properties is twice as high with more than 0.05 m in the hanging wall. Here, the spatial distributions of the total displacements mainly differ for the coal seam in the lateral extent. Major property changes of coal due to increasing temperature result in a loss of strength, and thus a different displacement pattern. Simulations using temperature-independent parameters show a larger zone of total displacements in the foot wall compared to the temperature-dependent ones. The mechanical properties of sandstone exhibit significantly lower changes with temperature compared to coal and are mainly influenced by the thermal expansion coefficient. Although the

trend of this property is increasing with temperature, our sensitivity analysis reveals rather minor changes (2–4 mm) in total displacements.

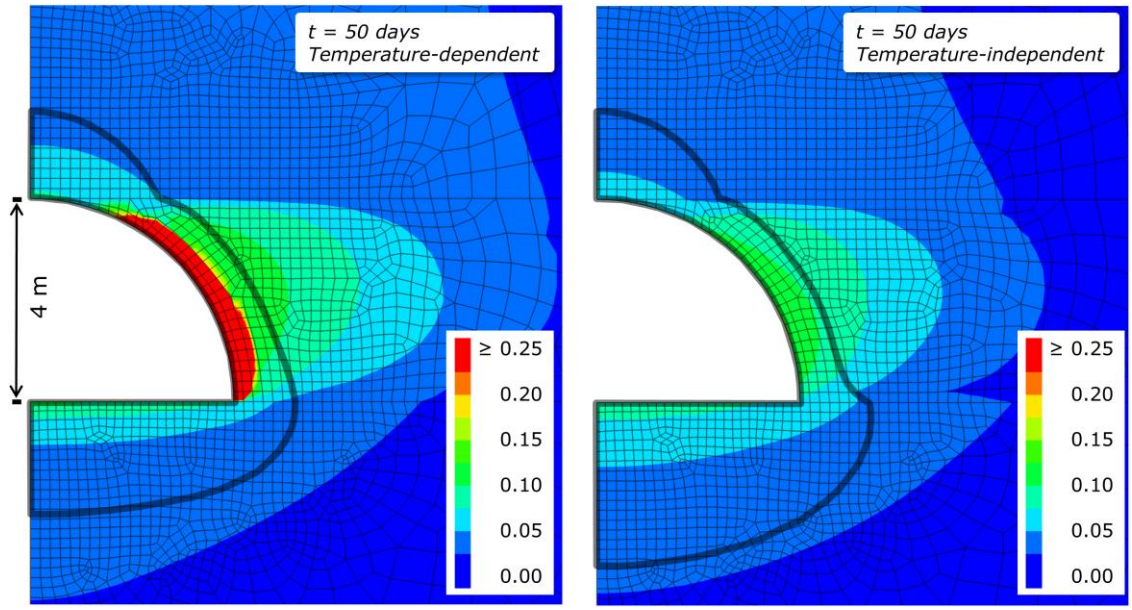

(a) (b)

Figure 11: Distribution of total displacements of surrounding rocks in the UCG reactor vicinity after stepwise reactor zone excavation with (a) temperature-dependent properties and (b) temperature-independent material properties after 50 days of simulation.

2.3.4 PRINCIPAL STRESS DISTRIBUTION IN THE UCG REACTOR VICINITY

During the UCG process, the experienced high temperatures generate a high thermal gradient of limited spatial extent for temperature-dependent as well as -independent properties, and thus induce thermal stresses in the surrounding rock masses. Rock strength and behavior under high temperatures differ notably from those at initial conditions. Therefore, the assigned thermo-mechanical parameters in the model are essential to analyses of stress distribution in the reactor vicinity. The present simulations were carried out neglecting pore pressure, and thus pore fluid heat capacity and thermal conductivity were not taken into account. Figure 12 shows the vertical profiles of the minimum (σ_3) and maximum (σ_1) principal stresses along the horizontal reactor center from the model top to its bottom (190–300 m below ground level), after reaching the state of equilibrium (before excavation) and after 50 days of simulation (following the excavation). The initial principal stresses increase linearly with depth and show a significant peak in the coal seam region due to the coal's higher Poisson's ratio. The maximum principal stress after the excavation is in the order of 20 to 22 MPa for temperature-dependent and independent parameters. A significant stress increase in the sandstone surrounding the reactor develops due to the excavation process and temperature effects.

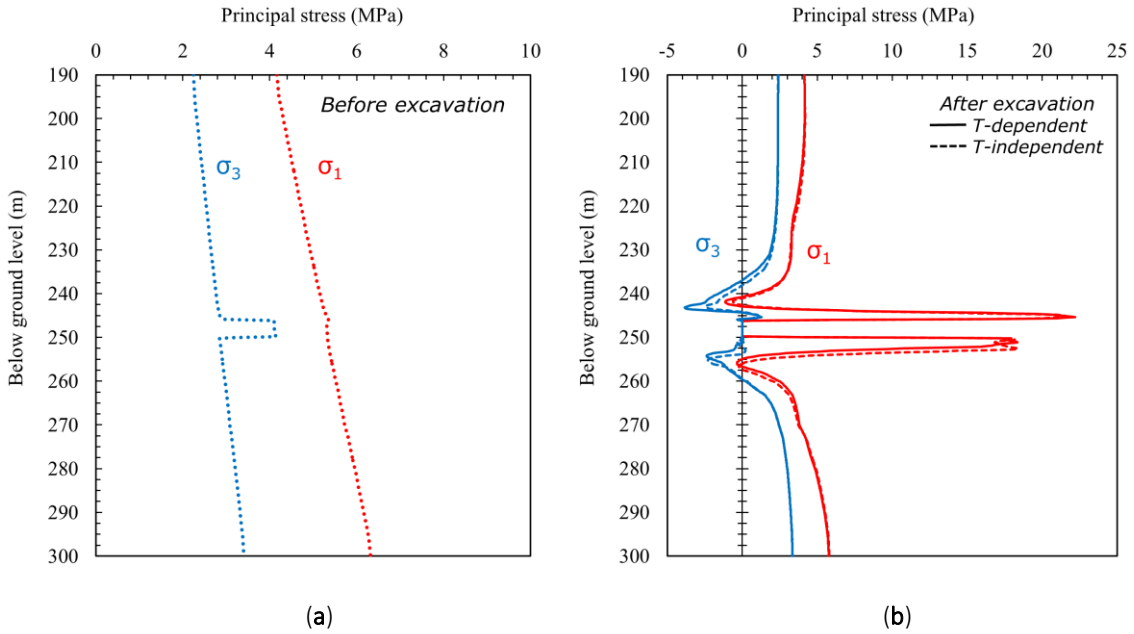

Figure 12: Profile of maximum ($\sigma_1 = \sigma_v$) and minimum ($\sigma_3 = \sigma_H$) principal stresses at the left model boundary plotted against depth (a) before excavation (initial stress state) and (b) after 50 days of simulation with temperature-dependent and -independent parameters.

The rock plasticity behavior is shown and discussed in detail below; however, local stress field changes occur, if rock strength (Table 1) is exceeded. Figure 13 shows the distribution of the minimum and maximum principal stresses in the reactor vicinity. An arching effect evolving due to a temperature-induced reduction in coal strength in the close reactor vicinity shifts the main load-bearing section of the coal seam to about 10 m lateral distance from the reactor boundary, where a minimum principal stress of 8 MPa (compressive regime) is observed (Figure 13). The same lateral stress-pattern is found for temperature-dependent and -independent properties. For the temperature-dependent simulation, in response to changes in the stress field of the growing reactor zone and increase in spatial temperature distribution, minimum principal stresses are in the order of −4 MPa (tensile regime) above the cavity. Although stress differences are in the order of maximum 2 MPa in the affected region above the reactor, pure tensile failure is observed in the simulations for temperature-dependent simulations only (Figure 14a). Due to the lower temperature distribution below the reactor, the temperature-induced stress increase is overestimated for the simulation using temperature-independent parameters.

Apart from the differences in principal stresses above and below of the reactor vicinity, stress changes are negligible in simulations using temperature-dependent and -independent parameters. However, stress distribution is strongly dependent on the reactor growth and design, and therefore may induce higher impacts with temperature-dependent parameters for UCG channel or even parallel multi-channel design.

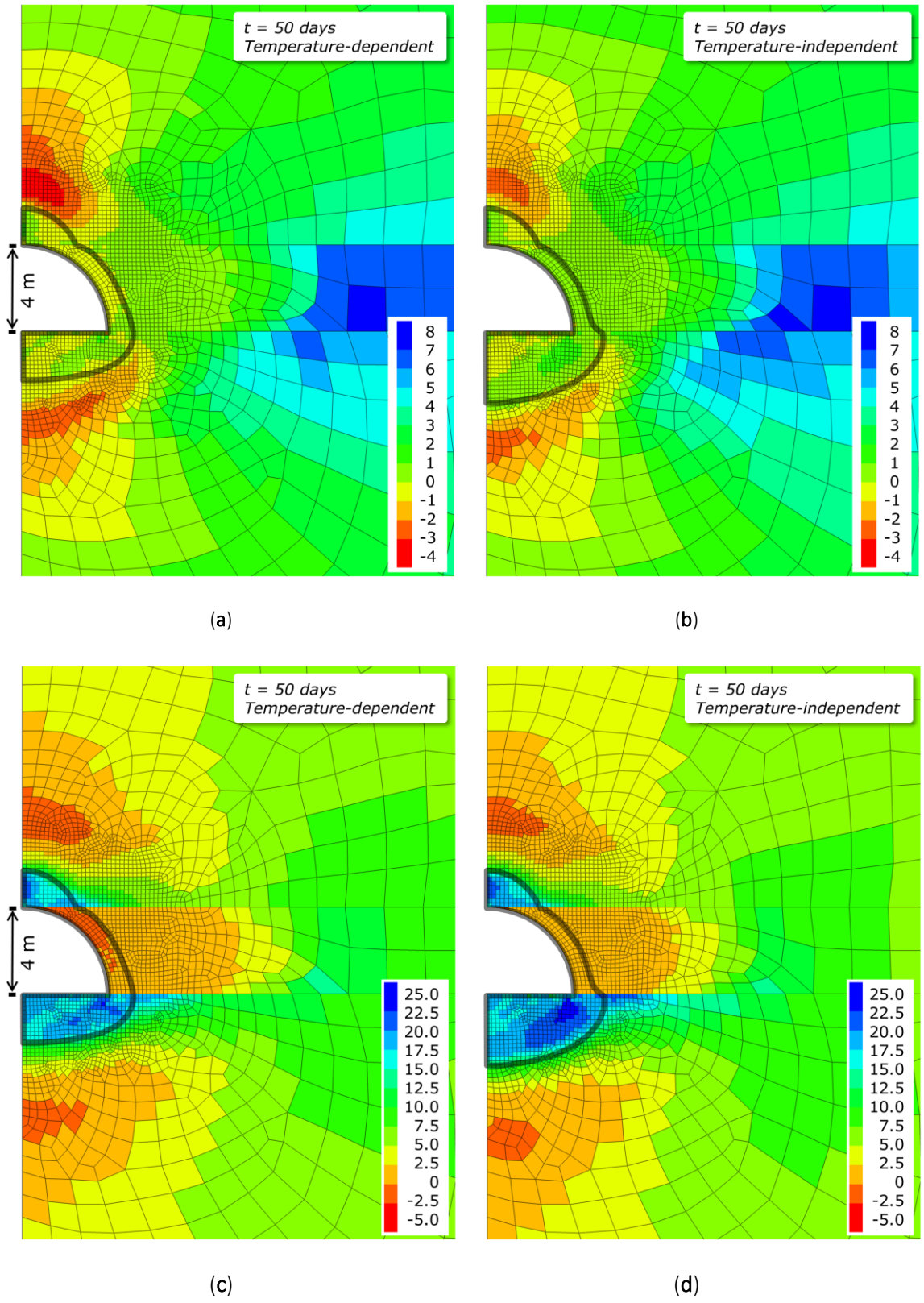

Figure 13: Minimum ($\sigma_3 = \sigma_H$) principal stress (in MPa) with (a) temperature-dependent and (b) -independent properties and maximum ($\sigma_1 = \sigma_v$) principal stress (in MPa) with (c) temperature-dependent and (d) -independent properties after 50 days of simulation. The grey solid line represents the 200 °C isotherm.

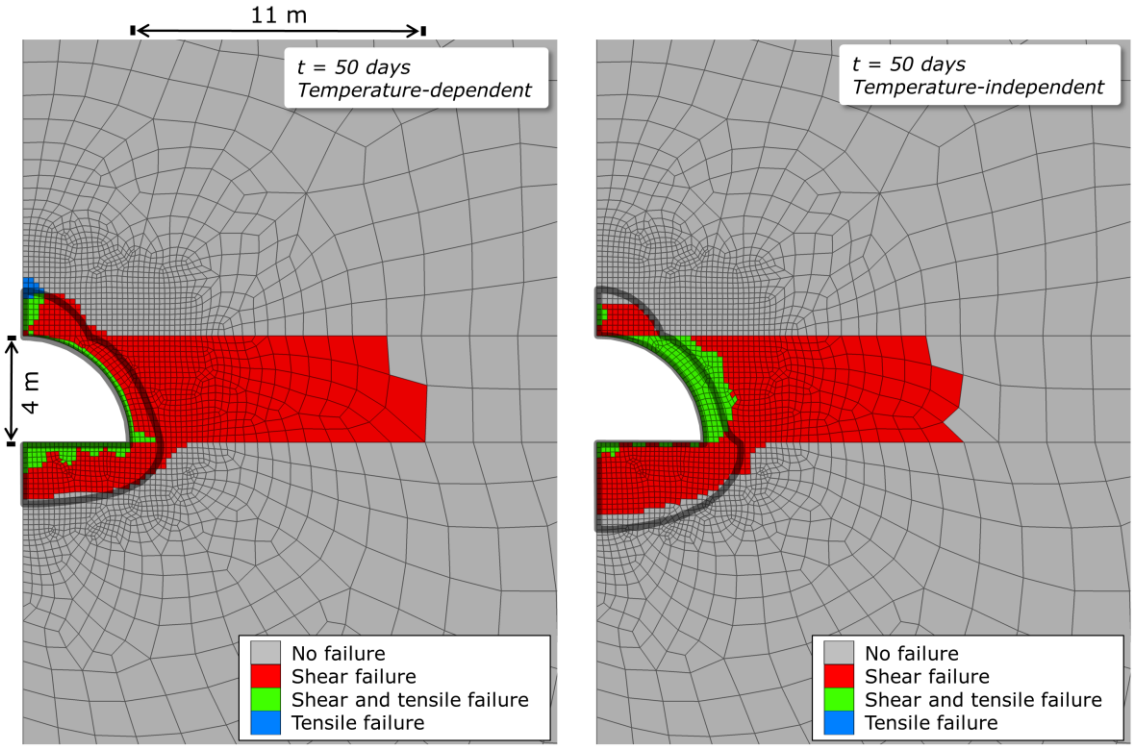

Figure 14: Distribution of shear and tensile rock failure experienced by rocks surrounding the UCG reactor after stepwise reactor zone excavation with (a) temperature-dependent and (b) -independent properties after 50 days of simulation. The grey solid line represents the 200 °C isotherm.

2.3.5 PLASTICITY BEHAVIOR OF ROCKS SURROUNDING THE UCG REACTOR

In the numerical computation, the Mohr-Coulomb failure criterion is applied, which can be expressed as:

$$\tau = \sigma_n \cdot tan(\varphi) + c \tag{3}$$

where τ is the rock shear strength; σ_n the effective normal stress; and c and φ the cohesion and internal friction angle, respectively. If failure in the rock matrix occurs, the stress state for that element is recalculated and the updated stress state then applied for further failure assessment. Shear and tensile failure (green) dominate at the reactor boundary after 50 days of simulation, followed by a region of pure tensile failure (blue) (Figure 14a). Tensile failure mainly occurs in the hanging wall above the reactor, and is dominant in the simulation using temperature-dependent parameters. This region is strongly influenced by the increase in temperature, and thus reduced rock strength and associated changes in stresses as plotted in Figure 12 and Figure 13. Coal mainly experiences shear failure (red) exhibiting about three times the length of the coal seam thickness in the simulations with and without temperature-dependent parameters (Figure 14). The region of shear failure is determined by stress changes induced by excavation effects. If coal is heated, it becomes softer and plasticity increases allowing for higher displacements and volumetric strain increments. However, the temperature distribution increase is limited to the close reactor vicinity (about 2 m in maximum for simulations using temperature-dependent parameters) due to the lower thermal conductivity of coal compared with sandstone at temperatures below 600 °C.

2.3.6 PERMEABILITY DISTRIBUTION IN ROCKS SURROUNDING THE UCG REACTOR VICINITY

The distribution of temperature and stresses in the UCG reactor vicinity is of utmost interest for the mechanical rock behavior and stability as well as the development of spatial permeability distribution in time. The latter may affect the potential flow of gasification educts and products as well as of fluids present in the reactor vicinity potentially determining the gasification process efficiency. Figure 15 shows the resulting volumetric strain increment distribution around the reactor after 50 days of simulation and the corresponding high temperature field (≥ 200 °C) distribution for simulations using temperature-dependent and temperature-independent material parameters.

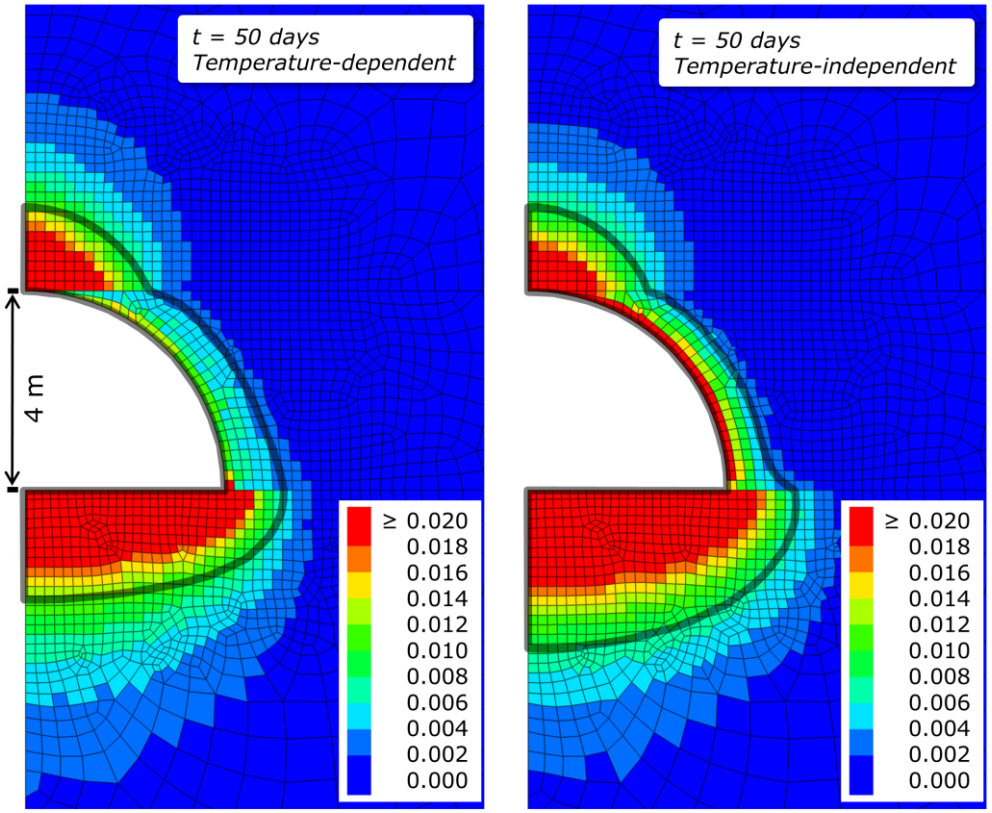

(a) (b)

Figure 15: Distribution of positive volumetric strain increments with (a) temperature-dependent and (b) -independent properties in UCG reactor vicinity. The grey solid line represents the 200 °C isotherm.

The magnitude of spatial changes in volumetric strain increments correlate with those of temperature increase (≥ 200 °C) for both simulation runs. However, this is discussed later in this manuscript. Elements exhibiting more than 2% volumetric strain increment are highlighted in red in Figure 15. The magnitude and distribution of volumetric strain increments cannot be directly compared to the total displacements presented in Figure 11, which are accumulated displacements at each gridpoint of the model; volumetric strain increments are the sum of the elastic and plastic components of strain of each element. Furthermore, the implemented model considers the different porosity data assigned to the coal and sandstone units, used in the calculation of permeability changes.

For the assessment of permeability changes, normalized permeabilities with an initially uniform distribution in the model were applied, while average rock-specific porosity values were derived from literature and assigned to the respective units (Table 2) (Somerton, 1992). Based on the calculated volumetric strain increments, the new permeability distribution is derived using Equation 2. Depending on the porosity and grain size of sandstones tested by David et al. (1994) and Yale (Yale, 1984), these exponents are ranging from 2 to 25 for sandstones. In the present model, data were assigned to represent sandstones with porosities below 10%. To understand and investigate the effect of the porosity sensitivity of permeability, we compare the results for three different permeability sensitivity exponents (namely n = 2, 13 and 25) within the given range (Figure 16).

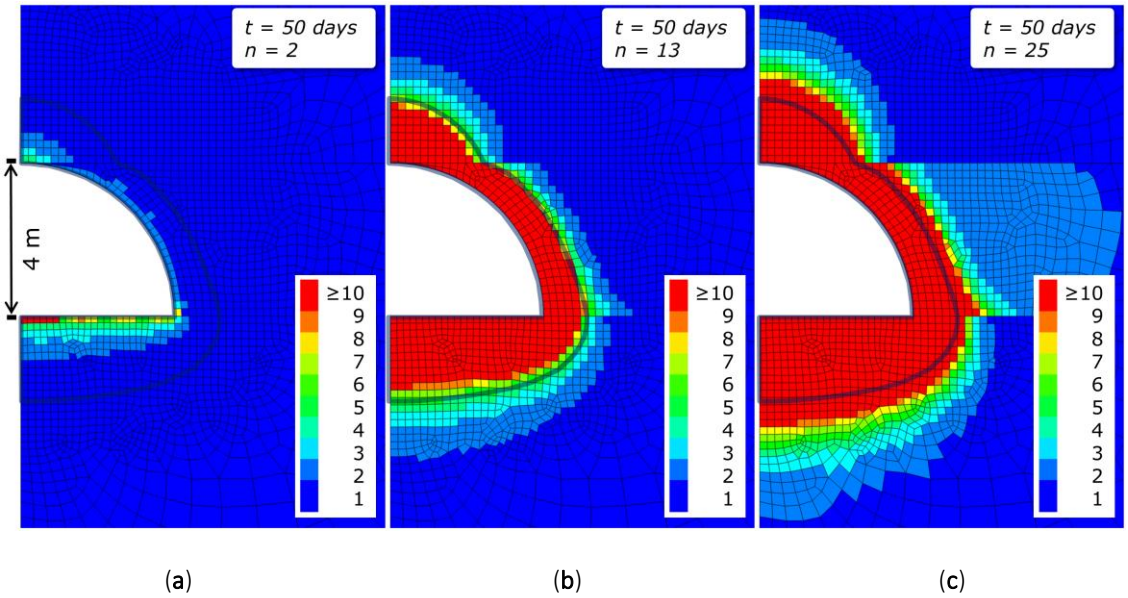

Figure 16: Porosity and permeability is expressed as function of volumetric strain increment following Chin et al. (2000) with porosity sensitivity exponents of (a) n = 2; (b) n = 13; and (c) n = 25. The grey solid line represents the 200 °C isotherm.

For an improved illustration of permeability changes, the values are limited to one order of magnitude permeability increase (red elements). For the smallest exponent value, a limited radius around the reactor is affected (< 0.5 m) only, concentrated at the reactor top and bottom. In contrast, the effect of the exponent is notably higher for the exponents n = 13 and 25. The permeability increase of more than one order of magnitude is evenly distributed around the reactor and up to about 1.5 m in the sandstone lithology. In that radius, fluid flow may be significantly affected by the local permeability increase, while relevant permeability changes in the coal seam exhibit only 50% of that radius.

Table 2: Initial averaged data applied for permeability change analysis (from Somerton, 1992 and Min, 1983).

Initial Values	Coal	Sandstone
ϕ_0	0.02	0.06
Normalized K_0	1	1
n	13	

The positive volumetric strain increment is strongly temperature-induced in the surrounding sandstones as shown in Figure 15, what is confirmed by the calculated permeability changes in the simulations using temperature-dependent and -independent parameters. Figure 17 illustrates that the comparison of permeability changes resulting from simulations using temperature-dependent and temperature-independent parameters exhibit only minor lateral differences (0.65 m) of about one order of magnitude in the reactor near-field. Particularly at the top of the reactor, these differences are negligibly small (0.17 m). Therefore, using temperature-dependent parameters affects the magnitude of the local total displacements and volumetric strain increments in the reactor near-field, but almost not their spatial distribution; hence, also not the resulting permeability distribution. Nevertheless, neglecting the temperature-dependent development of parameters may result in an overestimation of permeability changes in the close reactor vicinity.

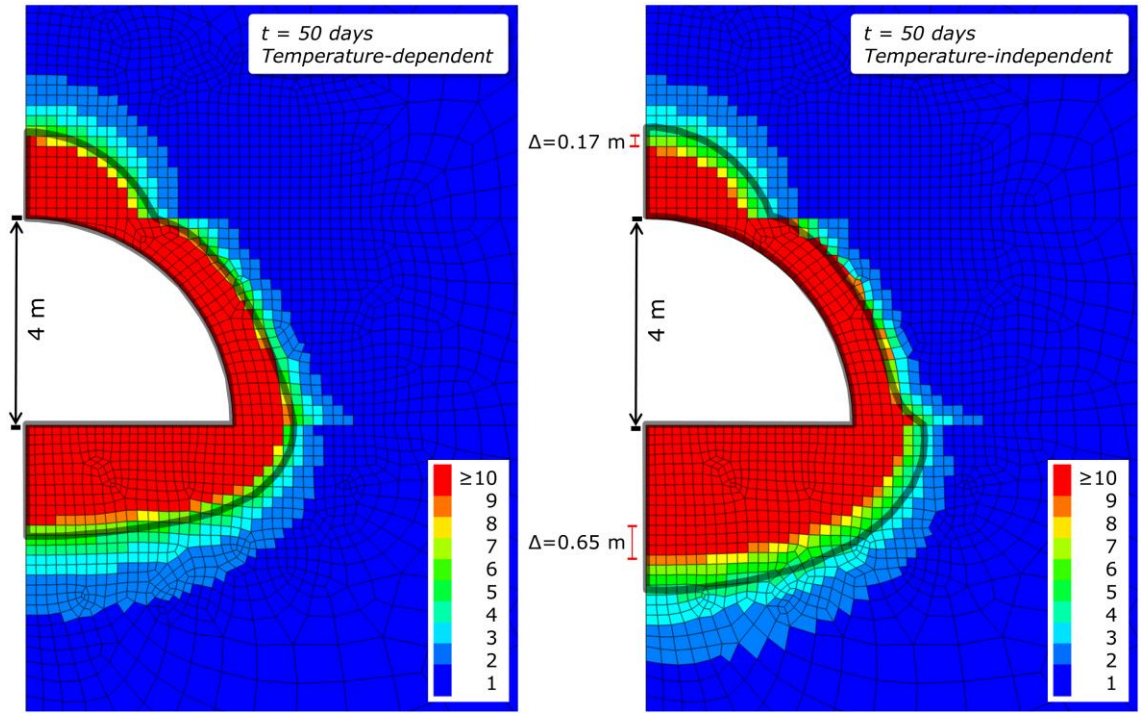

(a) (b)

Figure 17: Permeability changes (–) show negligible differences for (a) temperature-dependent and (b) temperature-independent parameters. The difference in regions of high permeability increase is only marginal, extending to 0.17 m above and 0.65 m below the reactor.

While various mechanisms have been investigated to explain the processes causing permeability changes in rocks experiencing variations in normal and shear stresses, the effect of mechanical stress on permeability in the context of a geotechnical excavation has been found to be confined mainly to the near-field of deposition holes, tunnels or boreholes (Min et al., 2013; Zoback, 2007). Permeability changes calculated under consideration of the given thermo-mechanical material properties are mainly mechanically-induced in the simulations carried out in the present study.

2.4 SUMMARY AND CONCLUSIONS

In the present study, we investigated the coupled thermo-mechanical impact of temperature-dependent parameters on permeability changes in the vicinity of a hypothetical underground coal gasification reactor by comparing simulation results based on thermo-mechanical parameters determined in recently published data from high-temperature experimental results. For that purpose, a 2D thermo-mechanical numerical model was implemented comprising three geological units as, e.g., given in the former Hanna UCG field trial in the USA. An elastoplastic constitutive law was assigned to the coal and sandstone units in the model. The spatial development of the UCG reactor with time was realized by a stepwise excavation in order not to overestimate the mechanical excavation effects, which would result in unreasonably high grid point velocities. At each excavation step, a constant temperature of 1000 °C was applied at the reactor boundaries to represent the heat generated by the gasification process in the coupled thermo-mechanical simulations. A parameter sensitivity analysis identified the parameters most sensitive to temperature. Then, a simulation time of 50 days was applied to compute the average time-dependent heat impact experienced by a 1 m long section of a typical CRIP-based UCG reactor.

Our simulation results demonstrate that the temperature-dependent thermo-mechanical properties elastic modulus, tensile strength and linear thermal expansion coefficient have a notable direct influence on stress changes and deformation, while thermal conductivity mainly influences the spatial temperature distribution around the UCG reactor, and thus only indirectly affects stress changes and deformation. Especially the temperature distribution in cavity vicinity is determined by the thermal conductivity and may result in overestimating the size of areas with high permeability changes unless temperature-dependent properties are considered. Therefore, it is obvious that the thermo-mechanical rock behavior is mainly influenced by the parameters thermal expansion coefficient, tensile strength and elastic modulus.

In the close reactor vicinity, the high temperatures induce positive volumetric strains. However, permeability changes calculated based on volumetric strain show only negligible differences between simulations using temperature-dependent and temperature-independent parameters. Hence, near-field models employed for the assessment of reactor growth induced by the thermodynamic gasification processes require temperature-dependent parameters for simulations, while far-field models can benefit from neglecting temperature dependence, which in turn increases the computational efficiency significantly by not adapting the thermo-mechanical parameters of each model element after each calculation step.

Shear and tensile failure occur at multiple locations in the reactor near-field in the thermo-mechanical model due to stepwise excavation effects applied to simulate the reactor growth and thermally induced stresses. The region of shear failure in lateral direction is about three times the

length of the coal seam thickness in the present case and mainly stress-induced and independent of temperature, since an arching effect develops with time. At the reactor top, a field of pure tensile failure is observed in the sandstone for the temperature-dependent simulation results. High temperatures at the reactor boundary induce a decrease in rock strength and determine stress changes; thus, generate tensile failure mainly in the temperature-dependent simulations.

The present study considers sandstones as over- and underburden of the target coal seam. Other rock types usually present in geological coal deposits, such as claystones, siltstones and shales, were not specifically addressed due to the limited availability of experimental data on temperature-dependent thermal properties (linear thermal expansion, specific heat capacity and thermal conductivity).

3D modeling will be applied in the next step to enable the assessment of complex site-scale geological models with regard to environmental UCG impacts. The model presented here will be thereto extended by a thermo-hydro-mechanical coupling to include fluid flow out of and into the UCG reactor. Detailed knowledge on site geology as well as permeability of potentially existing discontinuities is generally not available. Therefore, coupled numerical models allow for the assessment of potential permeability changes and mechanical integrity of UCG reactors, what is of uttermost importance for a safe and environmental-friendly UCG operation.

3 Fault Reactivation Can Generate Hydraulic Short Circuits in Underground Coal Gasification — New Insights from Regional-Scale Thermo-Mechanical 3D Modeling

Abstract

Underground coal gasification (UCG) has the potential to increase worldwide coal reserves by utilization of coal deposits not mineable by conventional methods. This involves combusting coal *in situ* to produce a synthesis gas, applicable for electricity generation and chemical feedstock production. Three-dimensional (3D) thermo-mechanical models already significantly contribute to UCG design by process optimization and mitigation of the environmental footprint. We developed the first 3D UCG model based on real structural geological data to investigate the impacts of using isothermal and non-isothermal simulations, two different pillar widths and four varying regional stress regimes on the spatial changes in temperature and permeability, ground surface subsidence and fault reactivation. Our simulation results demonstrate that non-isothermal processes have to be considered in these assessments due to thermally-induced stresses. Furthermore, we demonstrate that permeability increase is limited to the close reactor vicinity, although the presence of previously undetected faults can introduce formation of hydraulic short circuits between single UCG channels over large distances. This requires particular consideration of potentially present sub-seismic faults in the exploration and site selection stages, since the required pillar widths may be easily underestimated in presence of faults with different orientations with respect to the regional stress regime.

3.1 INTRODUCTION

Underground coal gasification aims at *in situ* conversion of coal deposits, currently not mineable by conventional methods and production of a high-calorific synthesis gas, applicable for power generation, natural gas substitution and chemical feedstock production. In UCG, target coal deposits are developed by directional drilling and then converted into a synthesis gas by sub-stoichiometric combustion, using gasification agents based on oxygen-enriched air and steam. Synthesis gas constituents are mainly hydrogen, carbon monoxide, carbon dioxide and methane in addition to nitrogen and minor components such as sulfuric acid (Bhutto et al., 2013; Blinderman et al., 2008; Burton et al., 2006; Friedmann et al., 2009; Kempka et al., 2011b; Klebingat et al., 2016; Nakaten et al., 2013; Yang et al., 2016).

Apart from the high economic potentials, UCG may effect site-specific environmental impacts, including fault reactivation, induced seismicity and ground surface subsidence. Furthermore, potentially induced changes in overburden hydraulic conductivity may result in pollution of shallow aquifers (Sirdesai et al., 2015; Sury et al., 2004). Especially thermo-mechanical effects and/or fault reactivation may introduce potential migration pathways for hazardous environmental contaminants, mainly composed of organic and inorganic pollutants (Couch, 2009; Friedmann et al., 2009; Sury et al., 2004). Site-specific coupled thermo-mechanical processes occurring in rocks adjacent to a deep UCG reactor are generally not well known in the field, because of the difficulty to quantify all occurring chemical reactions during the UCG process and their effects on UCG reactor size and shape (Najafi et al., 2015). Current knowledge on these processes is mainly based on laboratory experiments (Hettema et al., 1998; Kapusta and Stańczyk, 2011; Stańczyk et al., 2011; Tian, 2013; Tian et al., 2011, 2012, 2013, 2014, 2015; Wolf and Bruining, 2007) and a few successful UCG field trials. Since the 1930s, more than 50 pilot-scale UCG operations have been carried out worldwide. These developments have been concentrated in the former Union of Soviet Socialist Republics (USSR), Europe, U.S., South Africa, Australia and China and were predominantly undertaken at shallow depths, e.g., at Angren (110 m) in Uzbekistan, Chinchilla (140 m) in Australia, and Hanna (80 m) and Hoe Creek (30–40 m) in the U.S. (Burton et al., 2006; Durucan et al., 2014; Najafi et al., 2015; Sajjad and Rasul, 2014; Yang et al., 2016).

Developing an UCG model to quantify the process performance and to obtain reliable predictions for a new UCG development before proceeding to the gasification stage requires a sound understanding of its physical theory as well as knowledge on how to integrate field test and laboratory data in the analysis (Khan et al., 2015). Khan et al. (2015) concluded that each potential UCG site will be unique, so that design parameters (i.e., coal seam depth, thickness, inclination, coal properties, moisture content, water influx, etc.) have to be addressed before initiating the site operation and performance parameters are taken into account. Due to the high financial effort associated with UCG field trials, mathematical and numerical modeling has become an important methodology to study the coupled processes influencing UCG performance. However, the complexity of simultaneously occurring physical and chemical processes, such as chemical reactions and their kinetics, transport phenomena (i.e., heat and mass), turbulent flow patterns in the reactor, water influx from the surrounding rock mass and thermo-mechanical processes related to geological boundary conditions and stress regimes is remarkably high (Khan et al., 2015;

Nitao et al., 2011; Nourozieh et al., 2010). Almost all previous UCG studies applied one-dimensional (1D) or two-dimensional (2D) models to account for selected coupled processes (Sirdesai et al., 2015), which only have a limited validity in predicting the performance of UCG field trial operation, especially when considering the generally high heterogeneity and complexity of geological systems. For instance, it is known that 2D models may overestimate the magnitude of ground surface subsidence and stresses in pillars (Adhikary et al., 2016). Consequently, three-dimensional (3D) numerical 3D models, representing known geological features in high details are required for reliable predictions of site-specific UCG performance.

Nowadays, it is possible to develop and apply 3D models of varying complexity due to the significantly lower demand in computational time with the availability and advancement of innovative modeling and coupling techniques as well as parallel computations. In order to enhance the features of a 3D model and to apply the model for the assessment and prediction of UCG performance considering thermo-mechanical impacts, it is imperative to incorporate coal seam properties and geology of the target site into the model. Hereby, our previous findings (Otto and Kempka, 2015a, 2015b) emphasize that model simplifications with regard to the consideration of thermo-mechanical parameters in far-field numerical models can significantly reduce the computational time, while preserving the validity of the numerical results.

Taking into account these findings, coupled simulations based on complex 3D regional-scale models were employed in the present study to assess the potential formation of hydraulic short circuits between single UCG channels. For that purpose, a coupled thermo-mechanical 3D model has been developed to allow investigating the regional-scale geomechanical impacts of a hypothetical UCG operation at the Polish Wieczorek mine located in the Upper Silesian Coal Basin.

3.2 MATERIALS AND METHODS

3.2.1 NUMERICAL MODEL GEOMETRY, PARAMETRIZATION AND BOUNDARY CONDITIONS

Based on well log data and geological cross-sections of the Polish Wieczorek mine in the Upper Silesian Coal Basin, a 3D structural geological model was implemented and integrated into a numerical thermo-mechanical model. The finite-difference thermo-hydro-mechanical simulator FLAC^{3D} (Itasca, 2014) was employed to analyze thermo-mechanical stress changes, displacements and volumetric strain increments around the UCG reactors, using a specifically refined unstructured grid.

Table 3 shows the mechanical parameterization of the subdivided lithological units of the model, carried out using averaged data from Chećko (2013), whereby thermal properties for Layers 5-10 were derived from published data (Table 4). Fault properties were assumed with zero cohesion, a friction angle of 20° and dilation angle of 10°. We assigned the FLAC^{3D} Mohr–Coulomb model (elastoplastic constitutive law) to all lithological layers in the numerical model. The spatial model size is 10 km × 10 km × 5 km, comprising ten lithological units (dipping 8° S), a double fault (dipping 82° NW) penetrating the target coal seam and 13 UCG channels of 2000 m length. Each UCG channel consists of 40 single reactors of 11 m in height, 20 m in width and about 50 m in length. The model is discretized by about 1.5 million elements of 3.66 (close UCG reactor vicinity) to 800 m

(model boundaries) extent in horizontal and vertical directions (Figure 18), whereby grid element sizes increase towards the lateral and bottom model boundaries. Further, 28,928 elements were implemented as ubiquitous joint elements, introducing a plane of weakness respecting the fault dip direction and angle. We meshed the model using hexahedral grid elements and maintained a rectangular UCG reactor shape to limit the total amount of elements. Local grid refinements were applied in the near-reactor and near-fault areas to properly account for local thermo-mechanical effects. Hereby, the chosen model size and grid discretization were optimized by grid sensitivity analyses, while the model boundary conditions were maintained at a pre-defined distance to avoid any impact on the simulation results in the area of interest. Velocities perpendicular to the model bottom and to the lateral boundaries were set to zero at the respective model boundaries, while the model top was defined as free surface. Exact fault geometries were considered by the implementation of the previously addressed ubiquitous joint elements to integrate the spatially varying fault dip direction and angle.

Most of hydraulic fracturing test and focal mechanism data indicate the predominance of a strike-slip stress regime with a maximum horizontal stress orientation (S_{Hmax}) in northwest to southeast direction (S_{Hmax} azimuth of 167°) in the Upper Silesian Coal Basin in Poland (Jarosinski, 2005a). We incorporated this stress regime into the 3D model, whereby the vertical stress gradient results from the gravitational load of the overburden.

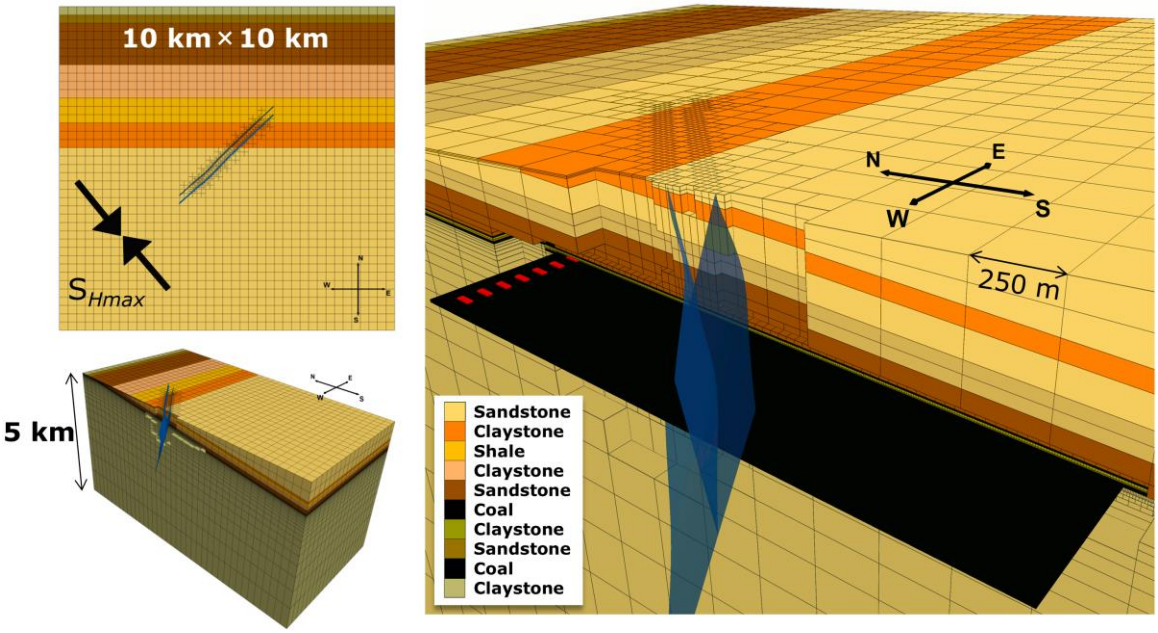

Figure 18: Geometry of the coupled thermo-mechanical 3D UCG model with the implemented double fault (blue) from three different perspectives: orientation of the maximum horizontal stress (S_{Hmax}) and lateral model dimensions in: plane-view (top left); 3D cross-section view (bottom left); and close-up 3D cross-section view (right) with the target coal seam and UCG channels considering a coal pillar width of 60 m. The model comprises ten lithological units with a target coal seam thickness of 11 m at depths from 370 to 580 m.

After calibrating the numerical model with regard to the present stress regime, an equilibrated mechanical state was achieved. This state served as starting data set for all simulations carried out in the scope of the present study. In order not to overestimate ground surface subsidence and stresses in 3D models as discussed by Adhikary et al. (2016), UCG reactor growth is considered to occur simultaneously in 50-m steps along the pre-defined UCG channels, determined by an

average gasification front progress of 1 m/day. The selected reactor growth rate is in good agreement with the empirical model presented by Najafi et al. (2015), allowing for predication of UCG reactor growth rates under various operational and geological boundary conditions. Data published on previous field-scale UCG activities exhibit reactor growth rates varying from 0.35 to 1.2 m/day. A constant temperature of 1000 °C was applied at the boundary of each active reactor after its excavation, whereby the *in situ* temperature was set to 30 °C following the local geothermal gradient. The numerical model was calculated until a mechanical equilibrium was achieved following each thermal time step of 50 days duration. The temporal temperature development in the rocks adjacent to the UCG channel was taken into account according to the cool-down process documented by Sarhosis et al. (2013). After the mechanical equilibrium state is achieved, the next reactor growth step is undertaken. Our present simulations neglect pore pressure, and thus pore fluid heat capacity and thermal conductivity are not taken into account, while the driving force for heat transport is conduction. Furthermore, the thermo-mechanical simulations carried out in this study focus on an extreme case of spatial temperature distribution, neglecting fluid flow into and out of the reactor as well as the steam jacket developing in the hanging wall.

Table 3: Mechanical parameters used for all undertaken simulation runs (from Chećko, 2013).

Lithological Units	Young's Modulus (GPa)	Tensile Strength (MPa)	Friction Angle [1] (°)	Cohesion [2] (MPa)	Poisson's Ratio (-)	Density (kg·m^{-3})	Dilation Angle (°)
Sandstone (Layer 1)	7.5	2.0	31	14.9	0.21	2115	-
Claystone (Layer 2)	8.2	2.7	31	19.0	0.27	2458	-
Shale (Layer 3)	8.2	2.3	31	17.2	0.25	2399	-
Claystone (Layer 4)	7.8	2.6	31	18.2	0.27	2397	-
Sandstone (Layer 5)	8.8	2.0	31	15.9	0.21	2407	-
Coal (Layer 6)	0.7	0.6	31	3.8	0.35	1281	-
Claystone (Layer 7)	8.0	3.8	31	10.9	0.27	2465	-
Sandstone (Layer 8)	8.5	1.9	31	15.3	0.21	2262	-
Target coal seam (Layer 9)	0.7	0.6	31	3.8	0.35	1281	-
Claystone (Layer 10)	80	3.8	31	10.9	0.27	2465	-
Fault	-	-	20	0	-	-	10

[1] Friction angle derived from Byerlee (1978); [2] cohesion determined by means of compressive strength and friction angle.

Table 4: Thermal parameters applied for Layers 5–10 in all simulation runs (from Cała et al., 2014; Małkowski et al., 2013; Somerton, 1992; Speight, 2005; Tan et al., 2008).

Lithological Units	Linear thermal Expansion Coefficient (K^{-1})	Specific Heat Capacity (J·kg^{-1}·K^{-1})	Thermal Conductivity (W·m^{-1}·K^{-1})
Sandstone (Layer 5)	1.6×10^{-5}	1210	4.67
Coal (Layer 6)	3.3×10^{-5}	1130	0.5
Claystone (Layer 7)	7.9×10^{-5}	970	2.57
Sandstone (Layer 8)	1.6×10^{-5}	1210	4.67
Target coal seam (Layer 9)	3.3×10^{-5}	1130	0.5
Claystone (Layer 10)	7.9×10^{-5}	970	2.57

3.2.2 SCENARIO ANALYSIS AND UCG PANEL DESIGN

In order to analyze the impact of temperature and pillar width on the spatial stress distribution and potential changes in rock permeability in the UCG channel vicinity, two UCG designs with pillar widths of 60 and 140 m (schematically shown in Figure 19) were taken into account. Each reactor has a theoretical capacity of 2.97 PJ/a over a lifetime of 5.5 years (2000 days), considering a coal calorific value of 29 MJ/kg.

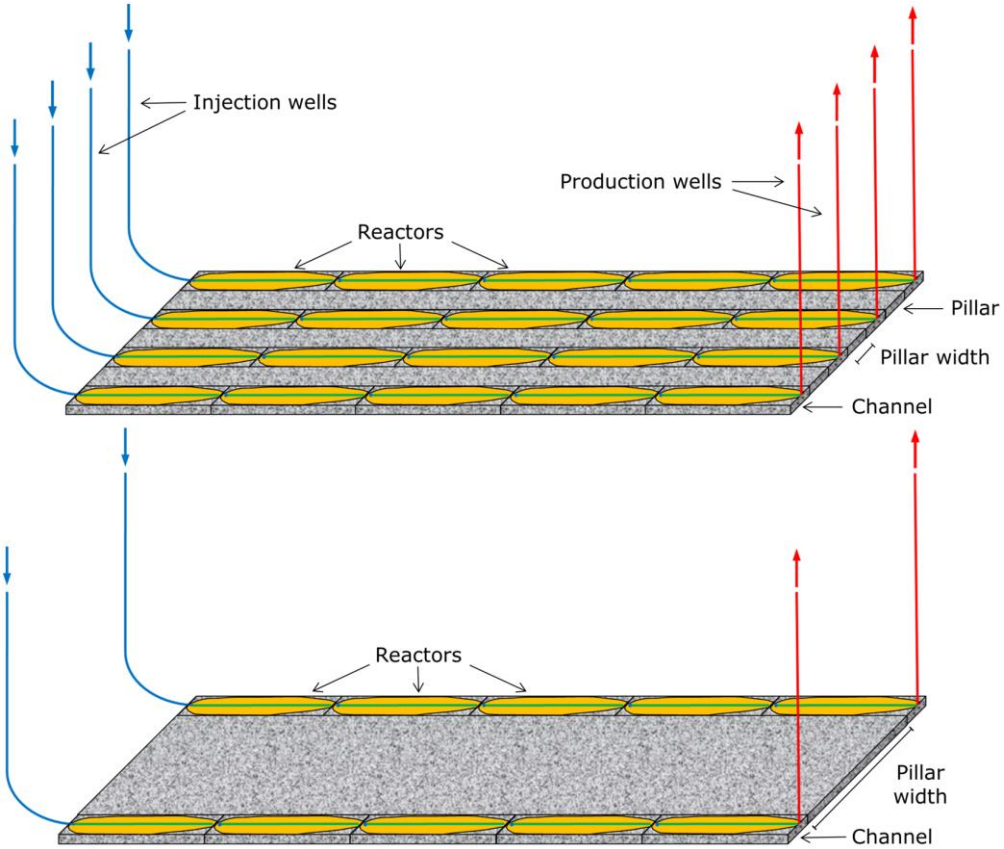

Figure 19: Conceptual design of the UCG CRIP (Controlled Retracting Ignition Point) methodology for different reactor-to-pillar-width ratios applied in our assessment: ratio of 1:3 (60 m pillar width) (top); and ratio of 1:7 (140 m pillar width) (bottom), modified after Blinderman (2016).

Identification of potential fluid migration pathways is of utmost interest in UCG operations to avoid hydraulic short circuits between two or more UCG channels as well as between UCG channels and potentially present shallow groundwater aquifers. Hydraulic short circuits between UCG channels render the gasification process uncontrollable in view of pressure and fluid mass balance monitoring and maintenance.

Fluid flow along geological faults is determined by zones of hydraulic weaknesses, generally represented by the fault damage zone, and thus fault integrity assessments has to focus on the identification of such weak fault segments. Using 3D seismic data as a basis for these assessments is state-of-the-art (Ligtenberg, 2005). In tectonic field-work studies (e.g., Koledoye et al., 2003; Price and Cosgrove, 1990; van der Zee, 2002), it has been shown that large-scale faults generally represent highly complex zones composed of different fault segments, multiple fault strands, Riedel shears, splay faults, dilatational jogs and relay ramps (Ligtenberg, 2005). These individual

fault elements can be sub-seismic, and therefore not apparent in 3D seismic data. However, these faults can become extremely relevant at the intermediate scale in UCG operations, since potential fluid migration pathways in between single UCG channels may be established in case of their reactivation.

3.3 SIMULATION RESULTS

In this paragraph, simulation results, such as permeability changes, vertical displacements, stress state at specific fault elements and fault integrity are presented for the six different simulation scenarios considered. First, different horizontal distances between the single UCG channels (60 and 140 m pillar widths) are presented for isothermal (pure mechanical simulation with constant temperature of 30 °C) and non-isothermal settings. In particular, we compare isothermal with non-isothermal simulation results for the scenarios with a 60 m pillar width to assess the thermal impact on induced stresses, resulting in rock expansion occurring in the surrounding lithological layers. Then, varying stress regimes (strike-slip, normal faulting and reverse faulting) and maximum principal stress (S_{Hmax}) orientations (normal and parallel to the fault) are investigated in view of fault integrity. For the model set-up with a pillar width of 140 m, the focus was on assessing the impacts of different regional stress regimes, including normal, reverse and strike-slip on fault integrity. Furthermore, we oriented the maximum horizontal stress parallel to the fault to generate maximum shear and reduce normal stresses at the fault plane, and hence trigger fault reactivation, resulting in potential hydraulic short circuits between single UCG channels.

3.3.1 VERTICAL TEMPERATURE DISTRIBUTION IN THE UCG CHANNEL VICINITY

High temperatures during the UCG process generate a high thermal gradient of limited spatial extent, and hence induce thermal stresses in the surrounding rocks. Experimental studies by different authors (Hettema et al., 1993; Liu et al., 2016b; Tian et al., 2014, 2015) show that rock strength and behavior at enhanced temperatures differ notably from those at normal temperatures, considering purely mechanical conditions. Figure 20 exemplarily shows the temperature variation along a vertical profile in the UCG channel vicinity (depth of coal seam 367-378 m below ground level) at different times (50, 100, 200, 300, 500 and 1000 days). Since heat conductivity and heat capacity are determined by generally low values in the surrounding lithological layers of the target coal seam, a significant temperature increase (≥ 200 °C) is induced in the close reactor vicinity (distance up to 7.5 m) only. The varying temperature gradients above and below the target coal seam result from different thermal conductivities depending on the lithology (Table 4).

A comparison of the assessed isothermal and non-isothermal scenarios by means of spatial distribution of permeability, vertical displacements, state of stress at specific fault elements and fault integrity is provided in the following.

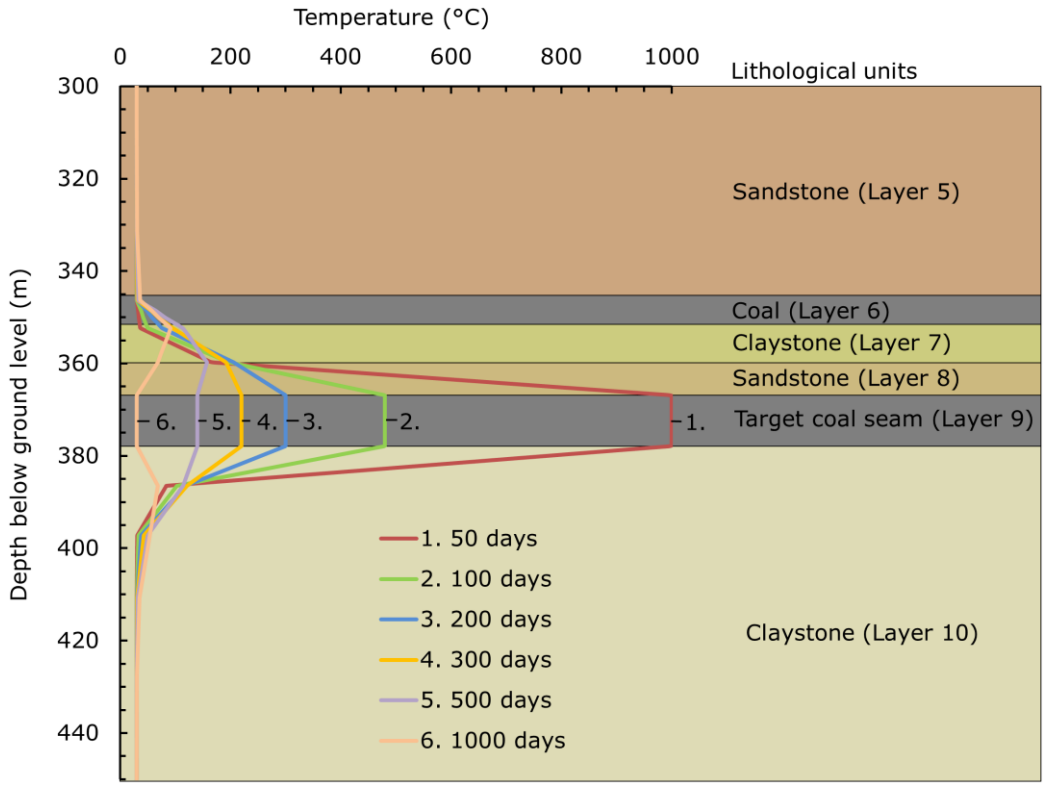

Figure 20: Temperature variation along a vertical profile through the coal seam (Layer 9) at different simulation times. The high temperature (≥ 200 °C) region is limited to the close channel vicinity and reaches a maximum extent of 7.5 m after 200 days of simulation above and 50 days below the target coal seam (Layer 9).

3.3.2 PERMEABILITY DISTRIBUTION IN THE ROCKS SURROUNDING THE UCG CHANNELS

The distribution of stresses in the UCG channel surroundings is required for the quantification of mechanical rock behavior and fault integrity as well as the spatial variation in the permeability distribution with time. The latter may affect the potential flow of gasification oxidants and products as well as of groundwater present in the reactor vicinity, potentially determining the gasification process efficiency and environmental impacts. Porosity and permeability changes in the vicinity of UCG reactors can be expressed as function of volumetric strain increment as shown in our previous studies (Otto and Kempka, 2015a, 2015b). For the assessment of permeability changes, normalized permeabilities with an initially uniform distribution in the model were applied, while average rock-specific porosities, depending on the present lithology were derived from literature and assigned to the respective model layers (Table 5). Based on the calculated volumetric strain increments, a new permeability distribution was derived following Chin et al. (2000), using dedicated porosity sensitivity exponents for each geological unit (Table 5).

Table 5: Initial averaged data applied for permeability variation analysis (from Min, 1983; Somerton, 1992; and Tian et al., 2014).

Lithological Units	Initial Values [1]		
	ϕ_0	*Normalized* K_0	n
Claystone (Layer 7)	0.0875	1	13
Sandstone (Layer 8)	0.06	1	13
Target coal seam (Layer 9)	0.02	1	13
Claystone (Layer 10)	0.0875	1	13

[1] The initial values are ϕ_0 = porosity, K_0 = permeability and n is a power-law exponent (porosity sensitivity exponent) as described in Chin et al. (2000) and Otto and Kempka (2015a, 2015b).

Figure 21 shows the resulting changes in permeability in the UCG channel vicinity at the end of the operational time for the isothermal and non-isothermal scenarios with a 60 m pillar width. For a proper illustration of these changes, the values are limited to one order of magnitude increase (red elements). For the isothermal scenario, only a limited region at the reactor walls of up to 4 m is affected. In contrast, the changes in positive volumetric strain increment, and hence permeability in the surrounding rocks are mainly temperature-induced as shown in Figure 21 (bottom) for the non-isothermal scenario. A permeability increase by more than one order in magnitude is distributed around the UCG channel and laterally extends up to about 4 m into the coal seam from the channel walls and up to 7 m in vertical direction.

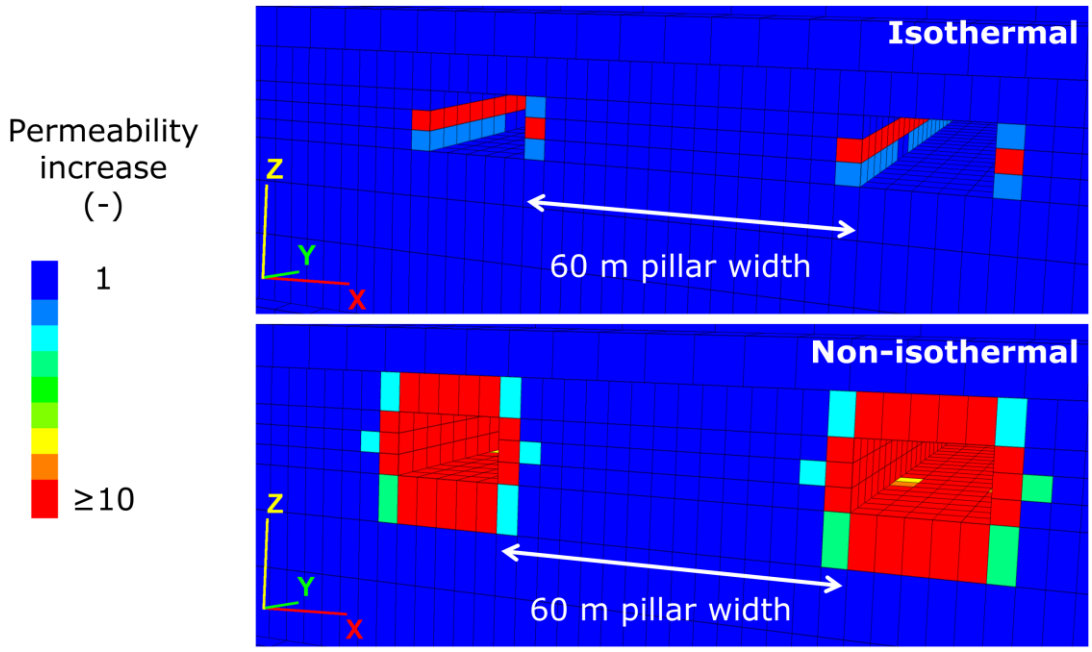

Figure 21: Normalized permeability changes (–) for the: isothermal (top); and non-isothermal (bottom) scenarios with a pillar width of 60 m show significant differences in their spatial distribution due to the lack of temperature-induced stress effects in the non-isothermal scenario.

3.3.3 VERTICAL DISPLACEMENTS AT 2000 DAYS (END OF OPERATION)

Figure 22 shows the vertical displacements induced by mechanical effects related to the excavation of the UCG channels for the isothermal and non-isothermal scenarios with 60 m pillar

width at the ground surface (top) and in cross-section views (profiles A–B in Figure 22, bottom). The temperature-induced stresses result in different spatial distributions of vertical displacements. An oval-shaped subsidence pattern above the excavated area is observed in both simulation scenarios, although exhibiting different magnitudes at the surface. The highest vertical ground surface displacement in the isothermal scenario is about −0.055 m, while that in the non-isothermal scenario amount to ca. −0.03 m. The profile views (Figure 22, bottom) show the development of vertical displacements below the ground surface, exposing the highest subsidence with depth increasing from the ground surface down to the excavated channels (−520 m). For the isothermal scenario, the pattern of displacements is less homogeneous compared to that in the non-isothermal scenario.

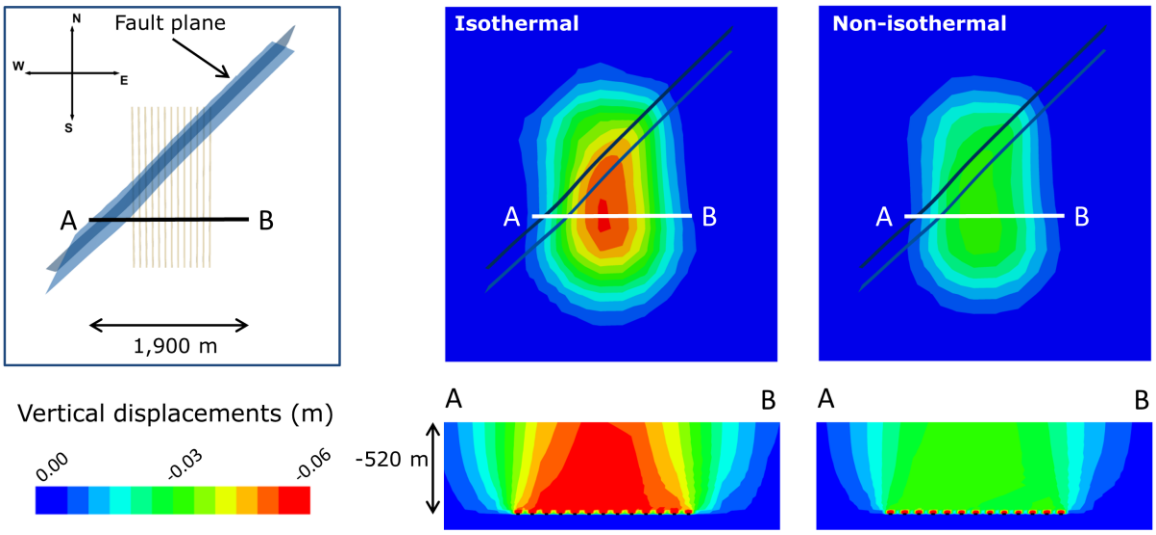

Figure 22: Plane views of the vertical displacement distribution at the ground surface (top) and cross-sections (bottom) for the isothermal (middle) and non-isothermal (right) scenarios after 2000 days of simulation (end of operation). The location of the UCG channels and the fault plane with regard to the plotted cross-section is illustrated in the upper left sub-figure.

The different pattern of vertical displacements has its origin in local temperature effects, resulting in high vertical displacements (up to −0.27 m) in the hanging wall as well as positive vertical displacements at the foot wall (thermal expansion of up to 0.24 m), induced by thermal expansion effects (Figure 23, right). For the isothermal simulation scenario, only vertical displacements directly above the reactor of up to −0.10 m (pure mechanical excavation effects) occur in the absence of thermal expansion effects, e.g. at the reactor bottom (Figure 23, left).

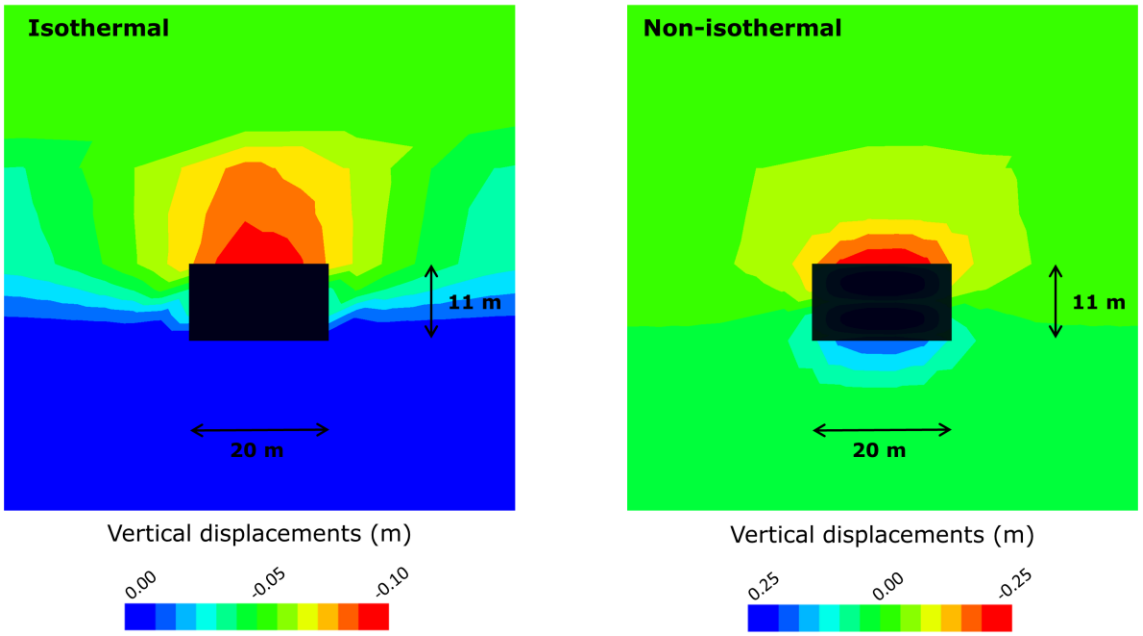

Figure 23: Vertical displacements in close vicinity of one UCG channel located at the A–B profile shown in Figure 22 for the: isothermal (left) and non-isothermal (right) scenarios.

3.3.4 STRESS STATES AT FAULT ELEMENTS

Figure 24 illustrates the stress states at the elements intersected by the fault plane in Layers 6 to 10 for the strike-slip stress regime, assessed at end of the operational time in the isothermal (Figure 24, left) and non-isothermal (Figure 24, right) simulations with 60 m pillar widths. Here, fault failure is observed in both simulations, though exhibiting varying characteristics due to the induced thermal stresses in the non-isothermal scenario. Thereby, the maximum normal stress is increasing from 23 to 52 MPa, while the maximum shear stress increases from 7 to approximately 14 MPa, when comparing the isothermal with the non-isothermal simulation, respectively.

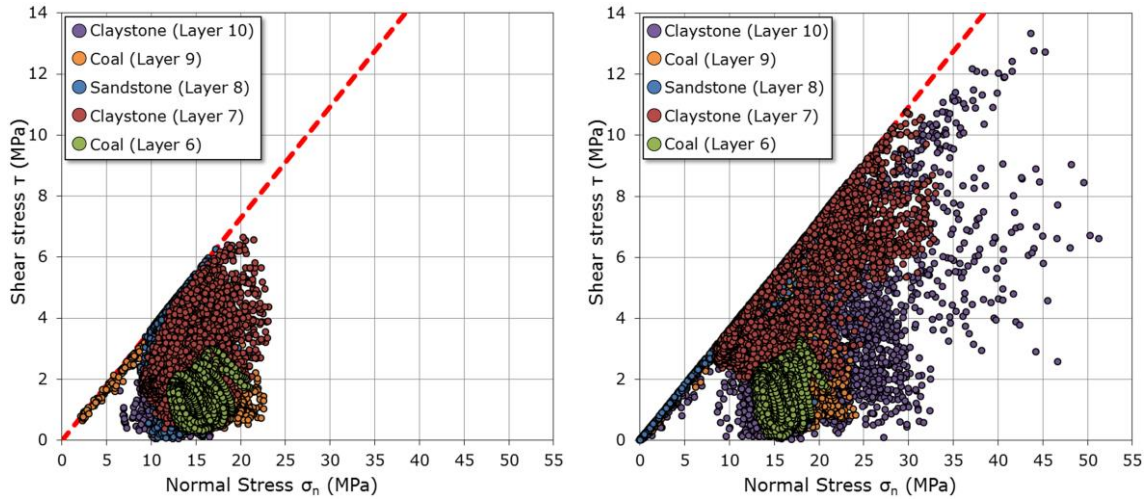

Figure 24: Normal versus shear stress plots for the fault elements in: isothermal simulation (left) and non-isothermal simulation (right) at end of the operational time. Coulomb failure line plotted as dashed red line.

3.3.5 FAULT INTEGRITY

The fault acts as discontinuity in terms of its mechanical properties, with the lowest values of friction angle and zero cohesion (Table 3). This implies that fault elements represent the region of highest probability for the occurrence of shear and tensile failure. Results of fault integrity assessments for the isothermal (Figure 25, top) and non-isothermal (Figure 25, bottom) scenarios are illustrated in Figure 25. The stepwise channel excavation induces mechanical stresses in the coal pillars and their surrounding rocks. Therefore, shear failure is mostly localized in the close channel vicinity. Tensile failure is not observed at the fault plane in the isothermal scenario. The results do not show any coalescence of reactivated fault regions by means of shear failure in the scenario with 60 m pillar width. Figure 25 (top) shows the results obtained after 2000 days of UCG operation for the non-isothermal scenario. The temperature leads to an increase in shear failure, and further produces tensile failure in the close reactor vicinity as a result of the additionally induced thermal stresses. In this scenario, coalescence of reactivated fault areas by shear failure at the fault plane in adjacent lithological layers above and below the coal seam is observed (Figure 25, bottom). Formation of hydraulic short circuits, and hence the development of potential fluid migration pathways between the respective UCG channels is very likely. Consequently, the decrease in fault integrity is significantly underestimated, if the thermal stresses acting on the coal pillars are neglected, as given in the isothermal simulations.

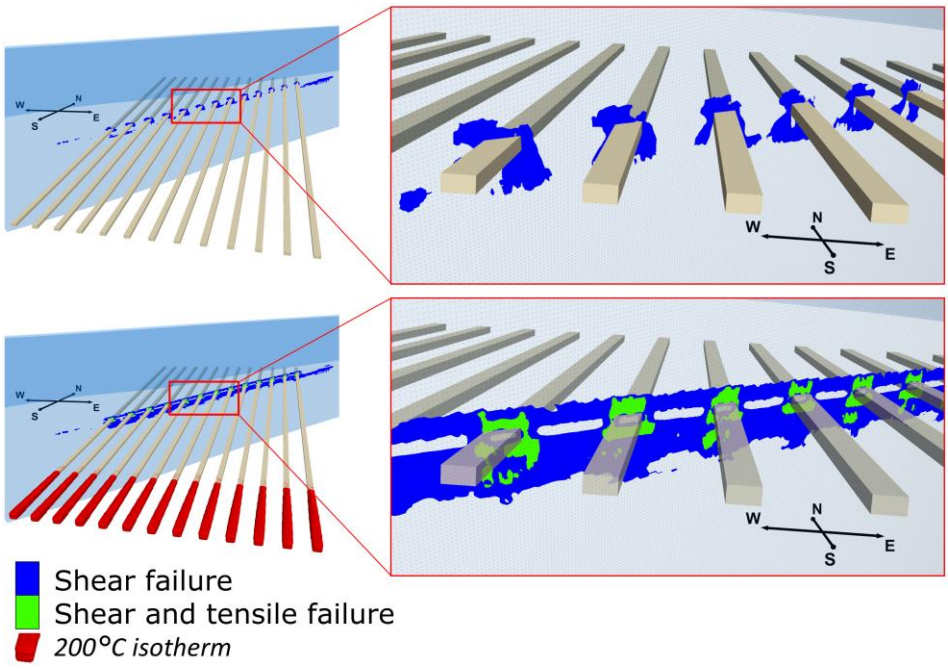

Figure 25: 3D view (left) and close view (right) of shear and tensile failure occurring at the fault plane in the isothermal (top) and non-isothermal (bottom) scenarios with 60 m pillar widths at a simulation time of 2000 days (end of UCG operation). UCG channels are represented by transparent grey shapes.

3.3.6 INFLUENCE OF PILLAR WIDTH ON FAULT STABILITY

Figure 26 (top) shows the coalescence of fault reactivation regions by means of shear and tensile failure, observed at the fault plane for the non-isothermal scenario with 60 m pillar width and that with 140 m pillar width. The patterns of shear and tensile failure are concentrated around the channels, whereby tensile failure induced by thermal stresses is located in close channel vicinity.

Areas of failure between the channels do not exhibit any general pattern and create no potential hydraulic short circuits between any channels. In contrast to the 60 m pillar width scenario, a defined coalescence of reactivated fault areas is not observed.

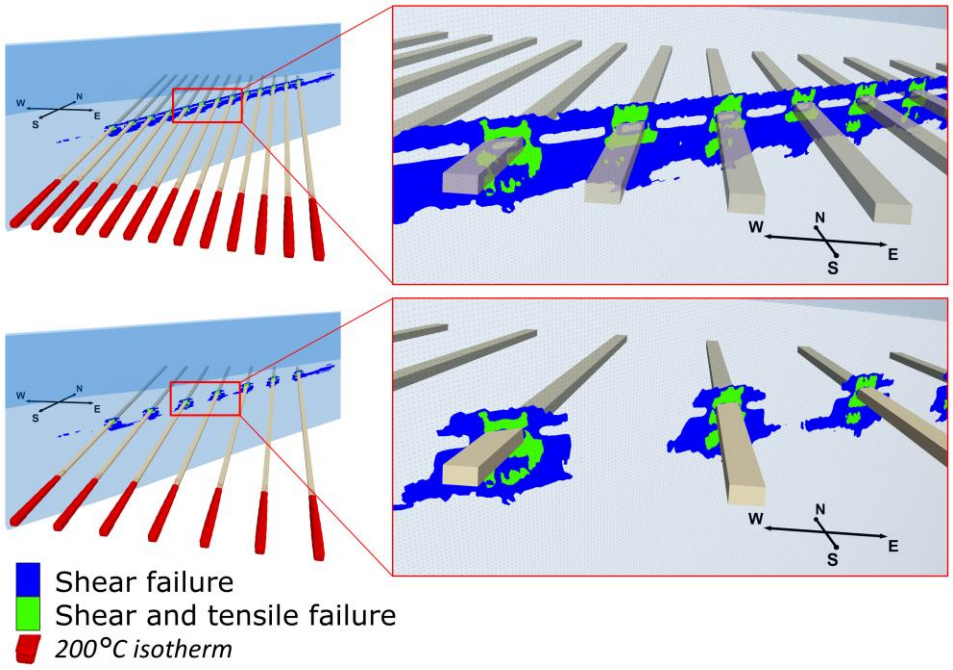

Figure 26: 3D distant (left) and close (right) views of shear and tensile failure at the fault plane for the non-isothermal scenarios with 60 m (top) and 140 m (bottom) pillar widths at a simulation time of 2000 days (end of UCG operation).

3.3.7 INFLUENCE OF STRESS REGIME ON FAULT STABILITY

According investigations on recent stress regimes in Poland, the heterogeneity in the present stress field is very high. Jarosinski (2005a, 2005b, 2006) summarized an extensive set of stress-related data for Poland, taking into account borehole breakout analyses, hydraulic leak-off tests, earthquake focal mechanism solutions and regional intraplate motions derived from GPS measurements. These data allow for assumptions regarding geodynamics in specific Polish geological basins, with the presence of frequent breakouts showing that tectonically driven anisotropy of horizontal stresses is a common feature. The S_{Hmax} direction in Eastern Poland is roughly N–S oriented and differs significantly from the stress regime in Western Europe. Jarosinski (2006) reported that this deviation is produced by the tectonic push from the south, which is successively compensated in the Upper Silesian Basin segment. Furthermore, stress directions are also ambiguous due to the interplay of several additional tectonic factors in the western part of Poland. Although most of hydraulic fracturing data and earthquake focal mechanism solutions indicate the presence of a strike-slip stress regime in Eastern Poland, the limited data available from Western Poland suggest the presence of a normal faulting stress regime (Jarosinski, 2005a, 2005b).

In order to assess the impact of different stress regimes and S_{Hmax} orientations on fault integrity, we conducted a sensitivity analysis, considering two strike-slip stress regimes (S_{Hmax} perpendicular and parallel to the fault plane), one normal and one reverse faulting stress regime scenario. In all cases, coupled simulations were run with the parameterization of the non-isothermal 140 m pillar

width scenario. Figure 27 shows the fault integrity at 2000 days (end of operation), where the largest reactivated fault area by shear and tensile failure develops for the strike-slip faulting regime, in which the S_{Hmax} orientation is parallel to the fault plane. Here, areas of shear and tensile failure expose a clear coalescence below the coal seam in the western part of the fault (Figure 27, distant view). For the normal faulting stress regime, a similar characteristic of the fault areas, reactivated by tensile failure compared to the previously described scenario can be noticed. However, a coalescence of reactivated fault areas by shear failure is not observed, since areas of shear failure are much less pronounced. The smallest reactivated fault area in this comparison is observed for the reverse faulting stress regime (Figure 27, bottom). In that scenario, only close reactor vicinities are affected by a lower occurrence of shear and tensile failure, compared to the strike-slip stress regime with the S_{Hmax} orientation parallel to the fault plane. For the reverse faulting stress regime scenario, coalescence of reactivated fault areas is not observed in the simulations. The impact of S_{Hmax} orientations on fault reactivation becomes obvious by comparing the two strike-slip regime scenario simulation results. Larger areas of shear and tensile failure mainly occur in layers above and below the target coal seam.

The perpendicular S_{Hmax} orientation towards the fault plane leads to a notable reduction in fault reactivation. Compared to the strike-slip stress regime, the normal and the reverse faulting stress regimes indicate the same characteristics of rock failure in the coal seam. For the layers above and below, this also applies for the reverse faulting stress regime. Here, a slightly smaller area of shear and an even smaller area of tensile failure with similar characteristics are observed. Nevertheless, in the normal faulting stress regime a larger fault reactivation area forms in the adjacent rock layers, compared to the strike slip regime, especially for the areas of tensile failure. Significant differences become apparent in the comparison of the reverse and normal faulting stress regimes as well. Here, especially the tensile failure characteristics of the reverse faulting regime differ from the normal faulting one, since their lowest extent is observed here. For the undertaken simulations and model set-up, the strike-slip faulting regime with S_{Hmax} parallel to the fault plane and the reverse faulting regime encompass the worst- and best-case scenarios, respectively.

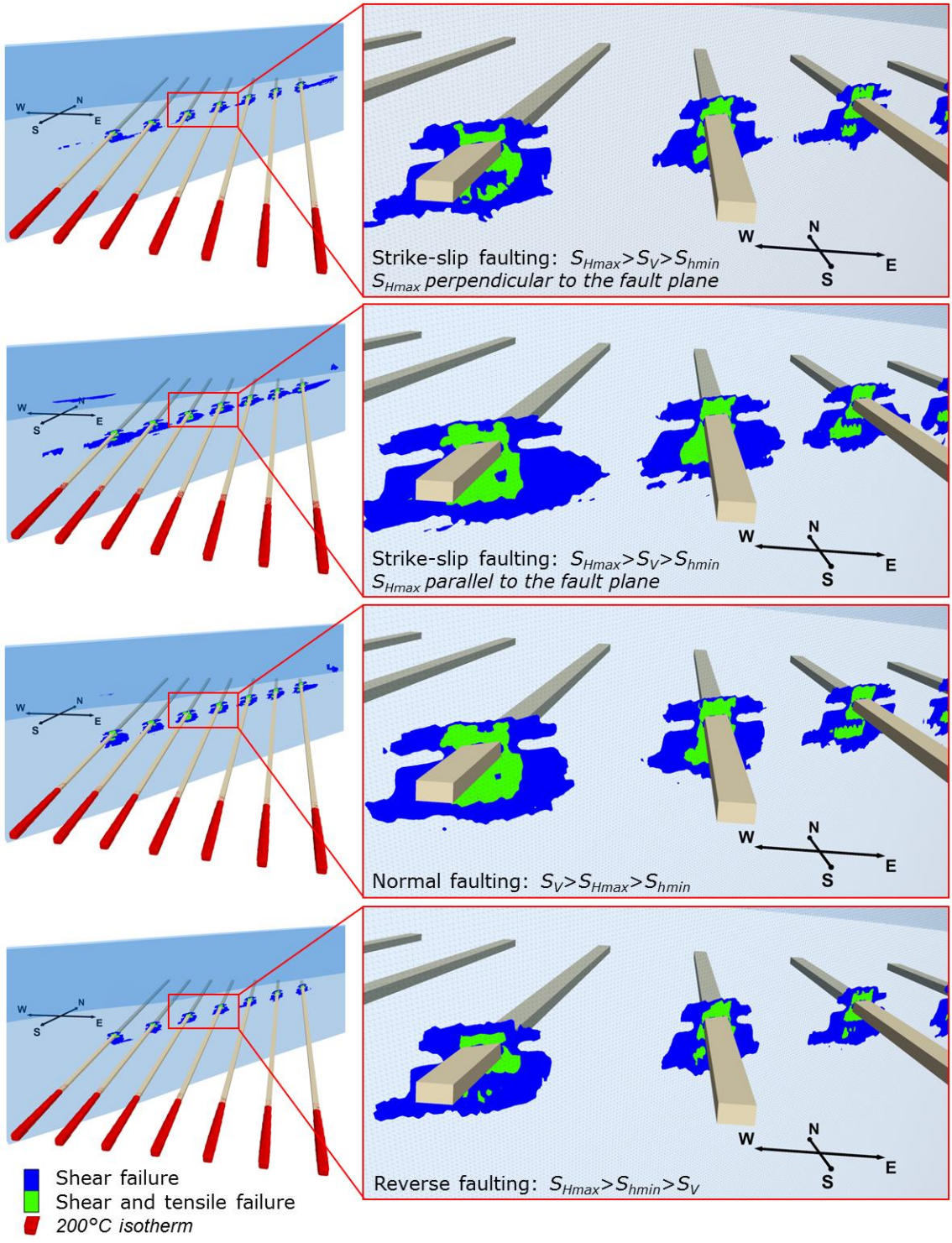

Figure 27: 3D distant (left) and close (right) views of shear and tensile failure at the fault plane in (from top to bottom) the two strike-slip (S_{Hmax} perpendicular to the fault plane and S_{Hmax} parallel to the fault plane) as well as the normal and reverse faulting stress regimes for the non-isothermal scenario with 140 m pillar width at a simulation time of 2000 days (end of UCG operation).

3.4 DISCUSSION

The impacts of enhanced and high temperatures on thermo-mechanical rock properties have been investigated during the last decades to improve process quantification and prediction in

different engineering topics, including nuclear waste disposal, geothermal heat recovery and UCG (Liu et al., 2016a, 2016b; Min et al., 2005; Somerton, 1992; Tian et al., 2012, 2014). Hereby, the linear thermal expansion coefficient was identified as one of the key parameters, governing volumetric and stress changes in rocks exposed to high temperatures (≥ 200 °C). Enhanced temperatures can induce high internal thermal stresses as a consequence of the thermal-expansion characteristics of different minerals, likely to result in thermal cracking and a decrease in rock strength (David et al., 1999; Liu et al., 2016b; Somerton, 1992; Tian et al., 2012, 2014).

Our simulation results show the impact of high temperatures, comparing isothermal and non-isothermal scenarios in a complex 3D model setting in the context of UCG operation, considering stress states at fault elements, permeability changes in UCG channel vicinity, vertical displacements and fault integrity in terms of hydraulic short circuit formation. Since heat conductivity and heat capacity are determined by generally low values for sedimentary rocks (Table 4), a significant temperature increase (≥ 200 °C) is only induced in the close UCG reactor vicinity. Figure 20 shows that the maximum extent of high temperature (≥ 200 °C) from the reactor boundary is about 7.5 m (reached after 200 days).

Further, the reliable prediction and management of mining-induced surface subsidence is one of the environmentally challenging issues in the context of coal mining (e.g., Adhikary et al., 2016; Sury et al., 2004). Luo et al. (2009) developed a UCG subsidence prediction methodology and showed that overlying strata and ground surface subsidence behavior in UCG operation is relatively similar to that in conventional longwall coal mining. Depending on UCG panel design, channel dimensions and coal seam depth, the maximum surface subsidence calculated by Li et al. (2015) (0.039 m) and Sirdesai et al. (2015) (0.038 m) is in the range of our simulation results (0.055 m). Even if the strength of overlying strata above the gasified coal seams can increase under the influence of temperature as suggested by Li et al. (2015) and observed in experiments by Liu et al. (2016b) at temperatures between 100 and 450 °C due to cementation reactions effecting weakening, increasing temperature tends to a general decrease in rock strength (Evans and Kohlstedt, 1995; Liu et al., 2016a; Tian et al., 2015). However, microstructural changes in mineralogy and the associated variation in strength are not considered in our simulations. In fact, vertical displacements at the ground surface calculated in our simulations are about 50% higher in the isothermal scenario and notably less homogeneous compared to those in the non-isothermal one at the end of the operational time. At that moment, the non-isothermal simulation has not achieved a thermo-mechanical equilibrium state due to sustained thermally-induced stresses, whereby the high temperatures effect a thermal expansion of the heated surrounding rocks in the affected strata. Considering the development of high vertical displacements in the UCG channel vicinity (Figure 23), it becomes obvious that the simulated displacements are related to thermally-induced stresses.

Thermo-mechanical stresses due to coal extraction and thermal loading, resulting from the UCG process also induce permeability changes. Permeability, in consideration of the difference between hydrostatic and UCG reactor pressure, controls fluid in- and outflow into and out of the reactor, respectively (Blinderman and Anderson, 2004; Otto and Kempka, 2015a). Figure 21 illustrates that permeability changes resulting from isothermal and non-isothermal simulations exhibit significant deviations in the close UCG channel vicinity. Here, fluid flow is likely to be affected by the local permeability increase, which is of relevance in the determination of the

temporal and spatial steam jacket extent, surrounding a UCG reactor (Blinderman and Anderson, 2004; Blinderman and Jones, 2002). Nevertheless, isothermal and non-isothermal simulations of both 60 m pillar width scenarios show that permeability changes only occur in close UCG channel vicinity, whereby hydraulic short circuit formation between single channels is not observed in the absence of geologic faults. Therefore, the increase in local permeability due to mechanical and thermal stresses does not compromise UCG operation for a pillar width of 60 m. Simulation results rather suggest that pillar widths of 30 m (equals a coal-seam-thickness-to-pillar-width-ratio of about 1:3) would suffice to avoid hydraulic short circuit formation between single UCG channels in our study area.

However, similar to conventional longwall mining, where roof support by coal pillars is required, dimensions of pillars are relevant in UCG operations when using the CRIP technology. In this case, a protection pillar is left in the coal seam to mitigate the formation of stress peaks in the hanging wall during the gasification of each channel. This avoids uncontrolled fluid cross-flow and isolates single channels during their operation, minimizing ground surface subsidence and allowing the channels to be flushed and/or cooled at the end of UCG operation (Najafi et al., 2014). However, a wider protection pillar results in a lower coal yield, and thus counteracts economic aspects of UCG operation. Najafi et al. (2014) presented an approach to estimate the required protection pillar width in CRIP-based UCG operation and compared purely mechanical with thermo-mechanical simulations. They showed that temperature induces thermal stresses and reduces the pillar strength, what is also demonstrated in the present study. However, Najafi et al. (2014) focused on side abutment stresses occurring around the pillars, whereby a maximum lateral failure zone of about 3.25 m in a 3.5 m thick coal seam was observed. They did not consider fault planes as regions of mechanical weakness and potential fluid migration pathways in their model. Our fault integrity analyses show that shear and tensile failure significantly increase due to thermal stress propagation, what may result in a coalescence of shear failure. If distances between UCG channels are not sufficiently high, this behavior can trigger fault reactivation, and therefore form potential hydraulic short circuits between single UCG channels, but also generate mining-induced seismicity (Hasegawa et al., 1989; Sen et al., 2013).

In addition to variable pillar width, different stress regimes were considered in the coupled thermo-mechanical simulations to assess their impact on fault integrity in terms of hydraulic short circuit formation. The results show a significant influence of the stress field and S_{Hmax} orientation on fault integrity. Even for a pillar width of 140 m, a coalesce of reactivated fault areas is feasible as shown for the scenario based on a strike-slip stress regime with the S_{Hmax} orientation parallel to the fault plane (Figure 27, second sub-figure). Simulations assessing fault integrity exhibit a high uncertainty if only limited data on the local stress regime is available. Additionally, non-detectable sub-seismic faults of various orientations can create hydraulic conduits between UCG reactors and shallower strata, and thus generate environmental hazards related to UCG operation, such as migration of UCG pollutants into shallow freshwater aquifers. In this context, thermo-mechanical processes are the key for quantification of potential leakage pathway formation and the potential for groundwater contamination (Vorobiev et al., 2008). A large fault, as implemented in the present model, would be highly undesirable and can impede UCG in practice. The risks include gas losses, contaminant migration and uncontrolled water influx (Burton et al., 2006). However, recent numerical simulations on fault reactivation are mainly associated to hydraulic fracturing (Rutqvist et al., 2013), CO_2 storage (Cappa and Rutqvist, 2011; Tillner et al., 2016) and geothermal

heat recovery (Jacquey et al., 2015), whereas the process of fault reactivation was not yet adequately represented in the field of underground coal gasification (Khan et al., 2015).

3.5 SUMMARY AND CONCLUSIONS

In the present study, we investigated the impact of the temperature distribution in the vicinity of an UCG reactor on hydraulic conductivity changes, ground surface subsidence, and especially on the fault integrity at a hypothetical commercial-scale underground coal gasification site by coupled thermo-mechanical simulations. For that purpose, we carried out six simulation scenarios, considering two different pillar widths and four different stress regimes, using a 3D thermo-mechanical model with a double fault. Model parameterization was undertaken using comprehensive well log data and geological cross-sections from the Polish Wieczorek coal mine in the Upper Silesian Basin. A simulation time of 2000 days was investigated, considering the time-dependent heat conduction experienced during UCG reactor growth and progress of UCG channels, realized by a simultaneous stepwise excavation of the single UCG reactors of 50 m length.

High temperatures applied at the reactor boundary determine stress changes by thermally-induced strains as presented in the comparison of stress states at the fault elements (Figure 24). Neglecting temperature effects in complex regional-scale UCG simulations by running purely mechanical simulations, which in turn would significantly increase the computational efficiency of the simulations, is not feasible, since shear and tensile failure would be notably underestimated. A significant temperature increase (≥ 200 °C) is only induced in the close reactor vicinity (7.5 m).

Although the difference in surface subsidence is negligibly small (−0.03 to −0.055 m) between the isothermal and non-isothermal simulations, and possibly even underestimated at specific time steps, high differences are apparent above and below the UCG channels. High vertical displacements (up to −0.27 m) in the hanging wall as well as positive vertical displacements at the foot wall (up to 0.24 m) are observed in the non-isothermal scenario. The absence of thermal effects (no thermal expansion) leads to significantly lower vertical displacements of −0.10 m in the isothermal simulation scenario. The permeability change derived from the calculated volumetric strain increment is limited to the close UCG reactor vicinity. The range with the highest spatial permeability increase, exceeding a factor of more than ten is less than the coal seam thickness and almost identical to the high-temperature region (≥ 200 °C). Consequently, one may assume that the increase in permeability in the close UCG channel vicinity does not form hydraulic short circuits, and thus not compromise a commercial-scale UCG operation with low pillar widths in the absence of geologic faults.

However, our simulation results also show that fault reactivation can significantly contribute to formation of hydraulic short circuits between single UCG channels by means of fault shear and tensile failure. In general, isothermal simulations underestimate the development of potential hydraulic short circuits. Further, formation of hydraulic short circuits can induce fractures, linking UCG channels to previously isolated shallow freshwater aquifers. Hence, a significantly larger pillar width between single UCG channels may be required to avoid running an uncontrolled UCG operation in our study area, whereby a coal-seam-thickness-to-pillar-width-ratio of about 1:14 ensures a safe operation. However, selected pillar widths determine the coal yield, and thus UCG

economics, even though ground surface subsidence is reduced by increased pillar widths. Consequently, sub-seismic faults, not detected by seismic and drill-core interpretations, can form potential fluid migration pathways. The extent of fault reactivation strongly depends on the local stress regime and orientation of the maximum horizontal stress towards the fault plane (Figure 27). Our undertaken scenario-based sensitivity analysis on fault integrity, considering four different stress regimes reveals their high impact on the fault reactivation characteristics. The strike-slip stress regime with the S_{Hmax} orientation parallel to the fault plane represents the worst-case scenario of possible shear and tensile failure in the present study.

One limitation of the presented study is the fact that fluid flow is not considered in the model, so that the effect of the steam jacket is not taken into account, resulting in a probable overestimation of the spatial temperature increase in the vicinity of the UCG channels. Another limitation is determined by the chosen reactor shape (quadrilateral instead of radial), reducing the UCG reactor stability due to a limitation of the arching effect. These assumptions were made to maintain a good balance between the required computational time and model accuracy.

In conclusion, sub-seismic faults of unknown orientations can exhibit a major threat for a safe, environmental-friendly and economical UCG operation and require careful consideration by 3D coupled numerical modeling, involving the assessment of uncertainties regarding the fault parameters and regional stress regime. Considering these insights, 3D models become increasingly important to obtain reliable assessments of UCG impacts, despite the still high computational effort. Site-specific UCG assessments should therefore comprise sufficient geological data to constrain the pattern of structural overprints that may influence the integrity of present and undetected fault systems, local coal seams and their overlaying strata. Considering these data, coupled 3D thermo-mechanical UCG modeling provides a solid foundation for optimal UCG channel design and assessment of its operational and environmental impacts, supporting to overcome the enormous challenges in UCG commercialization.

4 Prediction of Steam Jacket Dynamics and Water Balances in Underground Coal Gasification

Abstract

Underground coal gasification (UCG) converts coal to a high-calorific synthesis gas for the production of fuels or chemical feedstock. UCG reactors are generally operated below hydrostatic pressure to avoid leakage of UCG fluids into overburden aquifers. Additionally, fluid flow out of and into the reactor is also determined by the presence of the steam jacket, emerging in close reactor vicinity due to the high temperatures generated in UCG operation. Aiming at improving the understanding of the substantial role of the steam jacket in UCG operations, we employ numerical non-isothermal multiphase flow simulations to assess the occurring multiphase fluid flow processes. For that purpose, we first validate our modeling approach against published data on the U.S. UCG field trials at Hanna and Hoe Creek, achieving a very good agreement between our simulation and the observed water balances. Then, we discuss the effect of coal seam permeability and UCG reactor pressure on the dynamic multiphase flow processes in the reactor's vicinity. The presented modeling approach allows for the quantification and prediction of time-dependent temperature and pressure distributions in the reactor vicinity, and thus steam jacket dynamics as well as reactor water in- and outflows.

4.1 INTRODUCTION

Underground coal gasifying (UCG) has the potential to increase worldwide coal reserves by the utilization of coal deposits not mineable by conventional methods (Blinderman et al., 2008; Burton et al., 2006; Couch, 2009). It is based on combusting coal in situ to produce a high-calorific synthesis gas, which can be applied for electricity generation as well as fuel or chemical feedstock production at the surface. This re-emerging technology could provide a relevant contribution to the development of Clean Coal Technologies, if accompanied by carbon capture and storage, e.g., in the reactor cavities generated in the coal following the cease of operation (Durucan et al., 2014; Kempka et al., 2011a; Nakaten et al., 2014a). Apart from its high economic potentials (Nakaten et al., 2013, 2014b, 2014c), UCG may induce environmental impacts such as freshwater aquifer pollution by synthesis gas and/or by-product leakage (Camp and White, 2015; Campbell et al., 1979; Humenick, 1978; Kapusta et al., 2013; Klebingat et al., 2016; Liu et al., 2007).

The gasifying zone propagates between injection and production wells in the UCG reactor, which is partially filled with caved coal rubble from the overburden. The rate of reactor growth depends on a number of factors, some of which can be controlled, such as the rate of air or steam injection, as well as the geological boundary conditions affected by the chemo-thermo-hydro-mechanical properties of the coal and its overburden (Akbarzadeh Kasani and Chalaturnyk, 2017; Buscheck et al., 2009; Najafi et al., 2015; Otto and Kempka, 2015a; Shirazi et al., 2013; Sury et al., 2004).

Coal permeability and hydraulic pressure, determine the pressure gradient between the reactor and overlying aquifers and control the water inflow into the reactor and the flow of UCG products out of the reactor into the surrounding rock as well as the convective heat transfer between the reactor, the coal, and its overburden (Buscheck et al., 2009; Morris et al., 2009). Next to mechanical stress changes triggered by coal excavation, thermal stresses also induce permeability changes in the reactor's close vicinity (Otto et al., 2016; Otto and Kempka, 2015a, 2015b). Furthermore, permeability affects natural convection that transports fluids along with heat and potential UCG by-products into the overburden. Close to the reactor, fluid flow is also determined by the high reactor temperatures. In this context, the presence of water plays an especially vital role in the UCG process, providing a source of hydrogen for the steam-char and methanation reactions, which contribute significantly to the calorific value of the synthesis gas (Krantz et al., 1980). Water also favors the water-gas-shift reaction, which trades carbon monoxide for hydrogen (Krantz et al., 1980). In addition, phase transitions between liquid and gaseous water in the close reactor vicinity consume heat, which is required by the endothermic steam-char reaction. As a result, a layer of steam surrounds the UCG reactor, termed the steam jacket. In order to prevent or significantly mitigate potential environmental impacts, UCG reactors are generally operated below hydrostatic pressure, hindering the outflow of UCG process fluids into adjacent aquifers (Saulov et al., 2010; Shafirovich and Varma, 2009). Although, the difference between reactor and hydrostatic pressure produces an inflow of groundwater into the reactor, preventing UCG by-product leakage, on the other hand, the emerging steam jacket reduces the heat consumption by water evaporation and controls the spatial water inflow into the reactor, allowing operators to maintain an efficient and sustainable operation (Blinderman and Jones, 2002; Burton et al., 2006; Perkins and Love, 2010).

Many efforts have been undertaken towards understanding the complex and strongly coupled thermo-hydro-mechanical processes in UCG (Akbarzadeh and Chalaturnyk, 2013, 2014b; Akbarzadeh Kasani and Chalaturnyk, 2017; McKee and Santoro, 1980; Nitao et al., 2011; Sarhosis et al., 2013; Yang et al., 2016). Numerical modeling has been an important methodology to study these processes in view of UCG performance and sustainability. However, most of the earlier UCG modeling efforts assumed reduced complexity to achieve reasonable computational runtimes. Further, the former model's applicability is limited to specific and isolated cases, resulting in models that can hardly predict the performance of previous and future UCG operations (Khan et al., 2015). With the current advancement in numerical modeling software tools and increasingly powerful computational hardware, 3D models with a reasonable complexity, e.g., supra-critical multi-phase fluid flow, can be efficiently employed (Khan et al., 2015).

The present study addresses thermo-hydraulic processes in UCG to improve the understanding of UCG steam jacket dynamics and multiphase fluid flow in the reactor's close vicinity. For that purpose, we apply a scientific numerical simulator to investigate the influence of reactor pressure and coal permeability on water flow into and out of a UCG reactor as well as the spatial and temporal variation of pressure and temperature in view of the steam jacket dynamics. We first employ the well-documented U.S. UCG field trials at Hanna and Hoe Creek for model validation, and then apply our validated modeling approach to demonstrate the effect of coal seam permeability and reactor pressure on the complex multiphase fluid flow processes in the reactor vicinity. Our objective is to improve the understanding of the sub- and supercritical multiphase flow processes in the UCG reactor vicinity and the associated steam jacket formation in space and time. In the present study, coupled mechanical and/or chemical modeling approach was consciously not taken into account in favor of model validation against published operational data, i.e., water balances. Further, the high complexity of the coupled processes in UCG is likely to produce superimposing effects in the simulation results, avoiding a proper understanding of the mechanisms responsible for vapor phase formation and multiphase flow. Therefore, we decided to focus on thermo-hydraulic processes in the present study only to account for steam jacket dynamics as a result of formation fluid vaporization in the high-temperature reactor near-field.

4.2 METHOD AND NUMERICAL MODEL DESCRIPTION

The simulation of hydraulic multiphase-flow processes in UCG is complex in view of reaching numerical convergence, since temperature and pressure are likely to cross the critical point of water. In this case, a transition from subcritical to supercritical mixture properties occurs, demanding non-isothermal compositional multiphase flow simulations to account for three-phase water flow, including the occurring phase transitions. In the present study, we applied the numerical simulator MUFITS (Multiphase Filtration Transport Simulator) (Afanasyev, 2013a) for modeling the thermodynamic processes in the UCG reactor vicinity. MUFITS is a scientific multiphase flow simulator and provides different modules for the analysis of non-isothermal multiphase flows in porous media (Afanasyev et al., 2016; Afanasyev, 2013a, 2015b). In contrast to the classic numerical approach, wherein pressure and temperature are used to determine the multiphase thermodynamic equilibrium, MUFITS uses pressure-enthalpy-mixture compositional variables (Afanasyev, 2012, 2013a). Fluid mixture properties are specified by the thermodynamic potential:

$$\Lambda(P, h, \boldsymbol{x}) \tag{4}$$

which is determined by pressure (P) and total enthalpy (h). Here, $\boldsymbol{x}$ is the mixture molar composition and Λ is the molar entropy. The potential (Equation (4)) is represented using a polynomial spline in the ($P, h, \boldsymbol{x}$) space, which coefficients are calculated before the hydrodynamic simulations (Afanasyev, 2013b).The thermodynamic potential is used in the conditional extremum problem (Equations (5)–(7)), which corresponds to the entropy maximum conditions in the thermodynamic equilibrium ($P, h_t, \boldsymbol{x}_t$ = constant, t denotes the total parameters of the mixture) (Afanasyev, 2013a, 2013b):

$$\sum_{i=1}^{3} \Lambda_i V_i = \Lambda_i \rightarrow max,\ \Lambda_i = \Lambda(P, h_i, \boldsymbol{x}_i) \tag{5}$$

$$\sum_{i=1}^{3} h_i V_i = h_t, \sum_{i=1}^{3} \boldsymbol{x}_i V_i = \boldsymbol{x}_t, \sum_{i=1}^{3} V_i = 1 \tag{6}$$

$$0 \leq h_i \leq 1 \tag{7}$$

where, V is the phase molar fraction and the subscript i =1, 2, 3 refers the i-th phase of the binary mixture. Therefore, MUFITS can be used to describe single-, two- and three-phase states of mixtures under a wide range of pressures and temperatures, minimizing numerical convergence issues (Afanasyev et al., 2015, 2016, Afanasyev, 2013a, 2015b). A detailed description and the corresponding problem solution method as formulated in Equations (5)–(7) is given by Afanasyev (Afanasyev, 2012). For modeling of water flow in porous media, mass (Equation (8)) and energy conservation equations (Equation (9)) are used to maintain mass balances, while Darcy's law (Equation (10)) is employed for fluid transport (Afanasyev, 2013a, 2013b):

$$\frac{\partial}{\partial t}\left(\phi \sum_{i=1}^{3} \rho_i m_{ij} s_i\right) + div\left(\sum_{i=1}^{3} \rho_i m_{ij} \boldsymbol{w}_i\right) = \mathrm{Q}_i, \qquad j = 1, 2 \tag{8}$$

$$\frac{\partial}{\partial t}\left(\phi \sum_{i=1}^{3} \rho_i e_i s_i + (1-\phi)\,\rho_s e_s\right) + div\left(\sum_{i=1}^{3} \rho_i \tilde{h}_i \boldsymbol{w}_i - \lambda grad T\right) = \mathrm{Q}_e \tag{9}$$

$$\boldsymbol{w}_i = -K \frac{k_{ri}}{\mu_i}(grad P - \rho_i \boldsymbol{g}), \qquad i = 1, 2, 3 \tag{10}$$

where, i and j represent the phases and components, respectively, ϕ is the porosity, ρ is the density, m_{ij} is the j-th component mass fraction in the i-th phase, s is the saturation, $\boldsymbol{w}_i$ is the Darcy velocity, $\mathrm{Q}_i(\mathrm{Q}_e)$ is the (energy) influx out of the point source, e is the internal energy, $\tilde{h}$ is the mass enthalpy, λ is the effective heat conduction coefficient, T is the temperature, K is the absolute permeability, k_r is the relative permeability, μ is the viscosity, $\boldsymbol{g}$ is the gravitational acceleration and the subscript s refers to the host rock parameters. For this study, heat conduction and convection were included by using the MUFITS 2016.C BINMIXT module (Afanasyev, 2013b).

4.3 MODELING APPROACH VALIDATION USING UCG TRIAL DATA

4.3.1 FIELD-TESTS HANNA II AND HOE CREEK II

During the mid to late 1970s, the U.S. Department of Energy financed eight field tests at shallow depths in Wyoming to determine the feasibility of UCG (Thorsness and Cena, 1985). The Laramie Energy Technology Center (LERC) conducted five pilot tests at the Hanna and the Lawrence Livermore National Laboratory (LLNL) three tests at the Hoe Creek site. The well-documented results of these field tests have been presented in numerous publications and reports (e.g., Aiman et al., 1979; Barbour and Covell, 1988; Bartke et al., 1985a, 1985b; Brandenburg et al., 1977; Camp and White, 2015; Campbell et al., 1975; Fischer et al., 1975; Gunn and Krantz, 1987; LaFleur et al., 1984; Nordin, 1992; Thorsness and Cena, 1985). Yang et al. (2016) reviewed the recent global developments, research progress and technical innovations as well as the economic feasibility of UCG over the past ten years. Since the present study focuses on literature data on water balance calculation models introduced by Camp (1980), Camp et al. (1980), Krantz et al. (1980) and Levie et al. (1980) for the Hanna II Phase 2 and Hoe Creek II tests, these field trials are briefly introduced here. The Hanna II test was conducted in a 9-m thick subbituminous coal seam with overlying sandstone strata at 83 m depth. A linked vertical wells (LVW) configuration with a distance of 18 m was used, whereby about 1800 tons of coal were gasified in 25 days (Bartke et al., 1985b; Fischer et al., 1975; Levie et al., 1980). At the Hoe Creek site, the stratigraphic sequence consists of sandstones, claystones, siltstones and two coal seams. The deeper coal seam with a thickness of 8 m at 38 m depth was the target seam here (Buscheck et al., 2009; Campbell et al., 1979). The Hoe Creek II test was conducted for 58 days and consumed a similar amount of coal as the Hanna II Phase 2 one, also using a LVW configuration with an identical well distance (Nordin, 1992). Cross-sections following the Hanna II and Hoe Creek II field tests, taking into account operational monitoring data and post-burn coring show reactor growths up into the coal seam roof (Akbarzadeh and Chalaturnyk, 2014a; Bartke et al., 1985b; Levie et al., 1980), whereby roof collapse particularly occurred at the Hoe Creek II site. As a consequence of the operational procedure and hydrogeological boundary conditions, product gases migrated from the Hoe Creek II reactor into adjacent aquifers, which became contaminated with UCG by-products such as tars and organic compounds (Nordin, 1992). Contamination of shallow freshwater aquifers following the Hoe Creek II tests became a main concern in UCG operation, but this is not in the direct focus of this study.

4.3.2 PREVIOUS EXISTING MODELS TO QUANTIFY WATER BALANCES

The semi-analytical model (Camp, 1980; Camp et al., 1980; Krantz et al., 1980), which has been developed in the 1970s to predict water flow into and out of the UCG reactor incorporates isothermal unsteady-state radial flow (permeation) as well as spalling-enhanced dehydration (drying) of coal and overburden rocks. These two mechanisms were mathematically integrated with a semi-analytical reactor growth model and applied to predict the water balances in the two field tests introduced before. The produced amount of water from the UCG reactors was observed at the production wells, and is therefore zero when water from adjacent rocks is not flowing into the UCG reactor or water flow from the reactor into the adjacent rocks does not occur. Water flow into and out of the UCG reactor is strongly determined by the direction of the pressure gradient

between the reactor and the adjacent aquifer. In the model developed by Camp (1980), outflow from the reactor is only considered if a water column of at least about 0.3 m (one foot) height is displaced out of the close reactor vicinity. It has to be noted that this assumption is only taken into account for the Hanna model, but neglected in the Hoe Creek one. Camp (1980) assumes the reactor to have a cylindrical shape, growing radially according to the daily coal consumption and due to the occurrence of the aforementioned spalling-enhanced drying mechanism. The integrated semi-analytical reactor-growth model provides the daily water flow from this mechanism and supplies the water balance model with the reactor dimensions, which are increasing with time. Coal composition and its time-dependent consumption are calculated using material and energy balances (Boysen, 1978), while the average daily reactor pressure is taken from Gunn (1979). The coal consumed in both field trials and used in the semi-analytical models amounts to about 1340 m³ for the Hanna II Phase 2 and about 1400 m³ for the Hoe Creek II test (Camp, 1980). The model predictions are in very good agreement with the observed daily and total water production at the wellheads for the Hanna II Phase 2 and Hoe Creek II field tests (Camp, 1980). Camp's modeling results on the water permeation for both field tests are used for the validation of our non-isothermal multiphase flow modeling approach, comparing simulated and observed water flow into and out of the respective UCG reactors.

4.3.3 NUMERICAL MODEL IMPLEMENTATION

For the validation of our modeling approach, we conduct two numerical simulations and compare our results against published data on the observed water balances (Camp et al., 1980; Krantz et al., 1980). Based on comprehensive well log data as well as geological cross-sections of both field tests, two 3D thermo-hydraulic models are implemented. Due to the almost similar amount of coal consumed during both tests, Figure 28 shows the reactor dimensions at the end of operation for both field tests. Two lithological units, coal seam and overburden, are integrated into the numerical model, while a spatial model size of 50 m × 20 m × 20 m discretized by 20,000 1-m hexahedral elements is used. The model dimensions are chosen to locate the model boundaries far enough from the reactor boundaries to avoid hydraulic boundary effects that would compromise the simulation results. Grid discretization is adapted to maintain an optimum balance between the required computational time and the accuracy of the modeling results. For that purpose, the implemented model size and grid dimensions were optimized by sensitivity analyses, which are not discussed here due to the limited scientific interest.

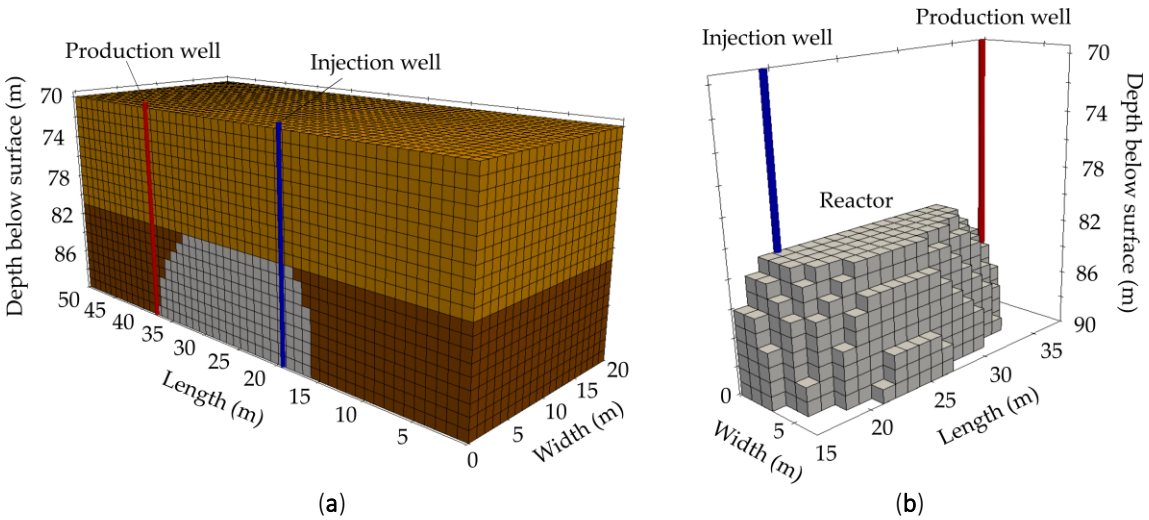

Figure 28: Cross-section of the employed numerical model grid with two lithological units (dark brown: coal seam; light brown: overburden) and the UCG reactor (grey) (a); Cross-section view of the spatial UCG reactor dimensions at the end of operation (b).

The implemented numerical model makes use of the UCG reactor symmetry along its vertical axis, assuming that a symmetric tear-drop shaped reactor growth along the link between the injection and production well develops with increasing operational time, whereby the areal sweep contours of the reactor are derived from Levie et al. (1980). Table 6 shows the model parameters used in the simulations of both field tests.

Table 6: Thermo-hydraulic rock properties applied for model parametrization (Bartke et al., 1985b; Buscheck et al., 2009; Camp, 1980; Min, 1983; Thorsness and Cena, 1985).

Parameter	Hanna II		Hoe Creek II	
	Coal Seam	Overburden	Coal Seam	Overburden
Density (kg/m³)	1350	2200	1350	2259
Specific heat capacity (J/kg K)	2000	1636	800	900
Thermal conductivity (W/m/K)	3.4	2.0	0.27	2.0
Porosity (-)	0.1	0.1	0.1	0.1
Horizontal permeability (mD)	5 [1]	5	100 [1]	120
Vertical-to-horizontal permeability ratio (-)	1/3	1/3	1/5	1/5

[1] Best-fit of permeability match against operational data of water flow into and out of the UCG reactor.

Hydraulic heads of 47 m (0.462 MPa) and 22 m (0.221 MPa) at the coal seam base are used in the Hanna and Hoe Creek simulations, indicating that both field tests were undertaken in the water-saturated zone (Camp, 1980). In both cases, relative permeability has to be considered in the prediction and evaluation of multiphase flow processes, since two-phase flow conditions develop due to the emerging water vapor phase at the calculated in situ pressures and temperatures. In different literature, heat transfer (Catton and Lee, 1987; Pakala, 2012), liquid phase (k_{rl}) and gas phase relative permeabilities (k_{rg}) are typically modeled as a function of liquid saturation (s_l):

$$k_{rl} = s_l^3 \tag{11}$$

$$k_{rg} = (1 - s_l)^2 \tag{12}$$

Relative permeability functions derived from Zhang et al. (2015) were tested in this context for the coal seam layer but show only a negligible effect on the water flow calculations in our models. Taking this finding into account and aiming at improving numerical convergence, we assume that the relative permeability functions given in Equations (11) and (12) are valid for both lithological layers, while capillary pressure effects can be neglected. For modeling purposes, Camp (1980) considered the coal seams and overburden layers at both sites to represent horizontal aquifers of infinite radial extent with isotropic permeabilities, vertically embedded in impermeable strata. Therefore, our lateral model boundaries are assumed to be open for fluid flow (Dirichlet boundary conditions with constant head), while the bottom boundary is closed for fluid flow (Neumann boundary condition), and the model top boundary uses Cauchy boundary conditions to represent a boundary closed for fluid flow, respecting the site-specific overburden aquifer thickness. After achieving hydraulic equilibrium, the simulations start with a time step size of 0.1 days in the Hanna (simulation time of 25 days in total) and Hoe Creek models (simulation time of 58 days in total), respectively. Considering the time-dependent coal consumption in each field test, we have integrated a reactor growth model with our simulation runs to account for the increasing interface between the reactor and its adjacent coal and rocks. In this context, constant linear pressure and temperature gradients (Dirichlet boundary conditions) derived from operational data (Bartke et al., 1985b) are assigned to grid elements representing the UCG reactor, spatially increasing with each time step (Figure 29). Due to the lack of temperature data for the Hoe Creek field test, a constant temperature of 600 °C (Lee, 1984) is applied here instead. Permeabilities were fitted for each layer for both field tests individually; the findings are discussed in the following section. The Camp (1980) model data have been time-corrected (time shift of about −3 days), using the operational pressure records (Bartke et al., 1985b).

4.3.4 MODEL VALIDATION RESULTS AND DISCUSSION

Our simulation results plotted in Figure 29 show the pressure dependency of the water in- and outflow (black) during the 25-day UCG operation at Hanna. Here, low horizontal and vertical coal seam permeabilities of 5 and 2 mD were implemented, respectively. The overburden, characterized by low-permeable sandstones is assigned with the same values. During the first ten days of the test, the reactor pressure is below the hydrostatic pressure, resulting in a flow of groundwater into the reactor at a rate of up to 3 m³/day. With the increase of reactor pressure above the aquifer pressure, the pressure gradient is reversed in the aquifer direction and water flow out of the reactor occurs. The maximum observed peak in reactor pressure of about 0.65 MPa after 15 days leads to the highest simulated outflow of up to 4 m³/day. Comparing our simulation results against literature data exhibits a very good agreement, whereby a qualitative correlation between reactor pressure and water flows becomes obvious (Figure 29). Figure 30 shows the pressure history and simulation results on water in- and outflow for the 58-day Hoe Creek field test in comparison with the data in the literature. A higher coal seam permeability of 100 mD in the horizontal and 20 mD in the vertical direction, derived from simulations undertaken for history-matching permeability, results in a very good agreement of our Hoe Creek simulation results with the published data (Camp, 1980).

According to Stone and Snoeberger (1976), most horizontal permeability measurements reported values between 225 and 408 mD. Therefore, an average value of 350 mD is used in Camp's (1980) model. However, this high permeability is not confirmed by our best-fit permeability derived from history-matching. An overburden permeability with 120 mD in the horizontal and 22 mD in the vertical direction is applied in our model following Buscheck et al. (2009). Potential explanations for the deviation in coal seam permeability between our best-fit model and the Camp (1980) data are discussed below.

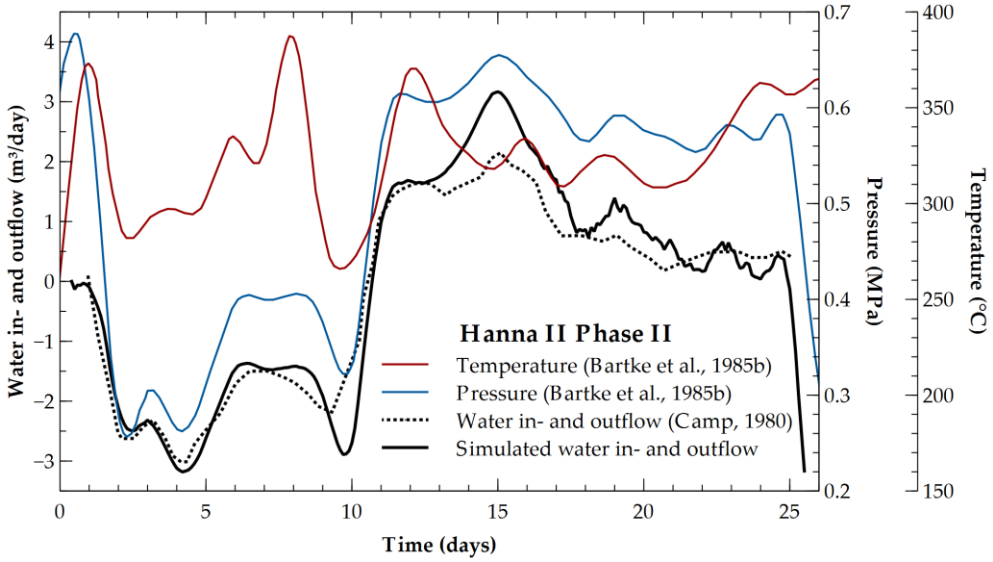

Figure 29: Simulation results of water in- and outflow at Hanna (solid black line) in comparison with the data in the literature (dashed black line) (Camp, 1980) show very good agreement and exhibit a strong pressure-dependency (blue line) (Bartke et al., 1985b) of the calculated water in- and outflows. Reactor pressure and temperature (red line) (Bartke et al., 1985b) are applied at all reactor elements as inner boundary conditions. Water outflow is positive here.

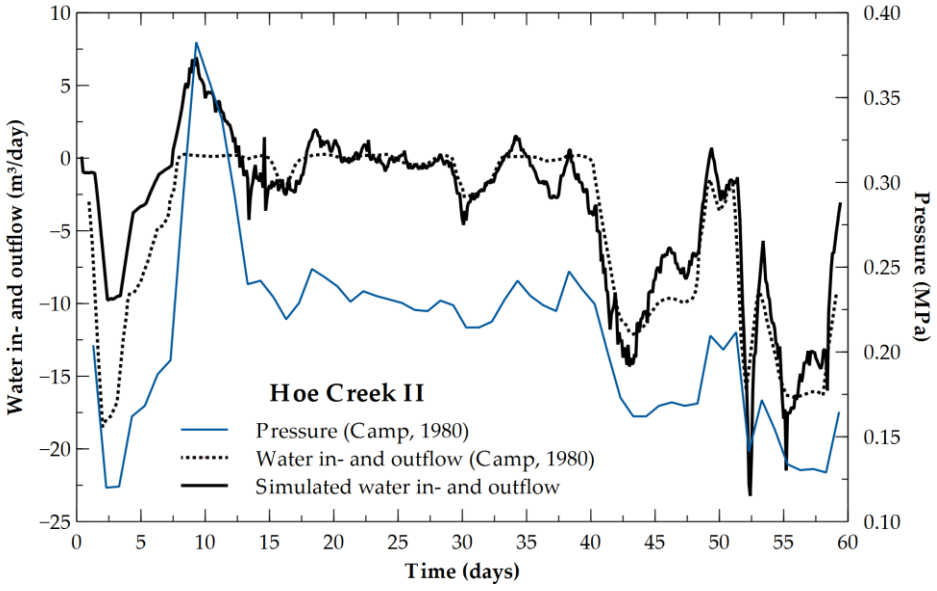

Figure 30: Simulation results on water in- and outflow for the Hoe Creek field test (solid black line) show a very good agreement with the data in the literature (dashed black line) (Camp, 1980), exhibiting a strong pressure-dependency (blue line) of water flow. Water outflow is positive here.

The reactor pressure during UCG operation was maintained below the hydraulic pressure, so that the Hoe Creek II field test is mainly characterized by water flow into the reactor. The water inflow rate is significantly higher than for the Hanna test, reaching up to 22.5 m^3/day. Only a short phase of water outflow of up to 8 m^3/day was determined at days eight to eleven, while water outflow for this field test does not occur in the literature data for the reasons discussed above.

The deviation of the calculated inflow values from the literature data mainly results from the following aspects. First, we allow hydraulic pressure to vary in the coal seam and the overburden aquifers during UCG operation. In contrast, Camp (1980) assumed a constant hydraulic coal seam aquifer pressure in his model. The simplified cylindrical geometry used by Camp (1980) exposes a smaller contact surface between the cylindrical reactor and its adjacent rocks, compared to the tear-drop reactor shape geometry used in our modeling approach. Also, we consider the observed reactor temperature as an inner boundary condition derived from the operational data, whereas the non-isothermal effects are neglected in the modeling done by Camp (1980). Furthermore, we implemented the observed pressure history in 0.1-day steps for both field tests instead of using daily-averaged data as Camp (1980) did. For instance, the pressure drop we determined in the Hanna simulation at day ten cannot be faithfully reproduced in his model. As a result, Camp's calculated inflow into the reactor is lower than in our simulation results. Due to the lack of published reactor pressure data for the Hoe Creek field test, we considered the pressure history provided with the Camp model documentation (Camp, 1980), which in turn may have reduced the quality of our match due to its one-day resolution in time**.** Finally, the best match of water inflow was achieved with 100 mD horizontal coal seam permeability for the Hoe Creek field test, whereas the literature data exhibits permeabilities between 225 and 408 mD at Hoe Creek site I (Stone and Snoeberger, 1976). The target coal seams (Felix No. 2) at Hoe Creek sites I and II are characterized by a highly anisotropic permeability tensor (Stone and Snoeberger, 1976), whereby most hydraulic tests were undertaken at the Hoe Creek I site. Here, the principal permeability tensor axes of the target coal seam correspond with the orientation of two sets of near-vertical fractures, which are likely to impose a high local permeability. Hence, hydraulic coal seam characteristics can be expected to vary substantially between the Hoe Creek sites I and II.

We conclude from this modeling exercise, using geological and operational data from two UCG field trials differing in terms of their duration and hydrogeological boundary conditions, that our modeling approach is capable of reflecting the most important non-isothermal multiphase flow processes required to calculate UCG reactor water balances. Thus, our modeling approach provides the required features to assess steam jacket dynamics in UCG.

4.4 EFFECT OF REACTOR PRESSURE AND COAL SEAM PERMEABILITY ON STEAM JACKET DYNAMICS

Usually, UCG operators aim at maintaining a small but nonetheless positive water inflow from the surrounding coal seam and overburden into the reactor to limit gas and heat losses and especially the leakage of UCG by-products, which may have potential environmental impacts such as groundwater contamination (Burton et al., 2006; Perkins and Love, 2010). The water inflow rate can be managed by adjusting the reactor operating pressure, determined by the injection and production wellhead pressures. Further, water flow behavior in the reactor vicinity is subject to multiphase flow processes, including steam jacket formation (regions with gas saturation > 0). Due

to relative permeability effects, the steam jacket can effectively retard fluid flow into the reactor and at the same time limit fluid leakage out of the reactor, and hence an understanding of steam jacket formation is substantial for efficient and sustainable UCG operation in terms of optimizing the synthesis gas quality and minimizing environmental impacts.

4.4.1 NUMERICAL MODEL GEOMETRY, INITIAL AND BOUNDARY CONDITIONS

A 2D numerical model is employed to analyze the thermo-hydraulic behavior, in particular the steam jacket dynamics in the UCG reactor vicinity. For that purpose, we carry out twelve different multiphase flow simulations with simulation times of 30 days each. Thereby, different reactor pressures (5% and 1% above as well as 1% and 5% below hydrostatic pressure, respectively) and coal seam permeabilities (1, 10, and 100 mD) are tested. The permeability of the implemented overburden sandstone (50 mD) is maintained constant in all simulations to focus on the effect of coal seam permeability only. The chosen model size and grid discretization are adapted according to the aforementioned grid and boundary condition criteria. Spatial model size is 40 m in width and 15 m in height, comprising two lithological units discretized by about 9600 hexahedron elements with edge sizes of 0.25 m (Figure 31). The model represents a 2D geological cross-section of a synthetic radial-symmetric UCG reactor with a coal seam thickness of 4 m, located at a depth of 250 m below the surface. In the present simulation runs, a static reactor shape with a radius of 4 m is used to represent the final reactor dimensions at the end of UCG operation (Figure 31). All data applied in the thermo-hydraulic model are compiled in Table 7, derived from literature data (Otto and Kempka, 2015a) and maintained constant for the lithological units during the entire simulation time. Hydrogeological sandstone properties are implemented for the overburden lithology (Otto and Kempka, 2015a).

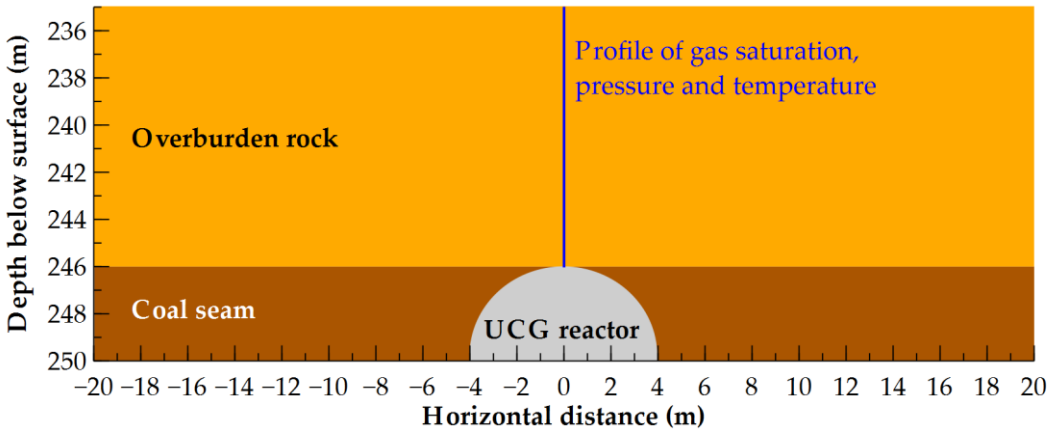

Figure 31: Cross-section of the 2D thermo-hydraulic model, comprising two lithological units with a radial UCG reactor shape at 246 to 250 m depth. The simulated gas saturation, pressure, and temperature profiles given in Figure 34 are plotted along the blue vertical profile given here.

Identical assumptions to those made for the previously introduced 3D models were considered with regard to relative permeabilities and capillary pressures. The lateral model boundaries were assumed to be open for fluid flow (Dirichlet boundary condition), whereas the top and bottom boundaries were closed for fluid flow (Neumann boundary condition). Following the Hoe Creek simulation implementation, a constant temperature of 600 °C was applied at the reactor elements, whereby the in situ temperature was set to 20 °C at all other elements.

Table 7: Thermo-hydraulic rock properties applied for 2D model parametrization (Otto and Kempka, 2015a).

Parameter	Coal Seam	Overburden
Density (kg/m³)	1300	2200
Specific heat capacity (J/kg K)	2000	1363
Thermal conductivity (W/m/K)	0.23	2.3
Porosity (-)	0.02	0.1
Permeability (mD)	1; 10; 100 [1]	50
Horizontal-to-vertical permeability ratio (-)	1/3	1/3

[1] The effect of coal seam permeability is analyzed in different simulation scenarios.

4.4.2 STEAM JACKET DYNAMICS IN THE UCG REACTOR VICINITY

Figure 32 shows the calculated maximum steam jacket extents at constant reactor pressure variations by +1% and +5% (top) as well as −1% and −5% (bottom) relative to the initial hydrostatic pressure at the coal seam top after 30 days of simulation. Hereafter, we only refer by +5% and +1% (for supra-hydrostatic pressures) as well as −1% and −5% (sub-hydrostatic pressures) to the hydraulic pressure regimes.

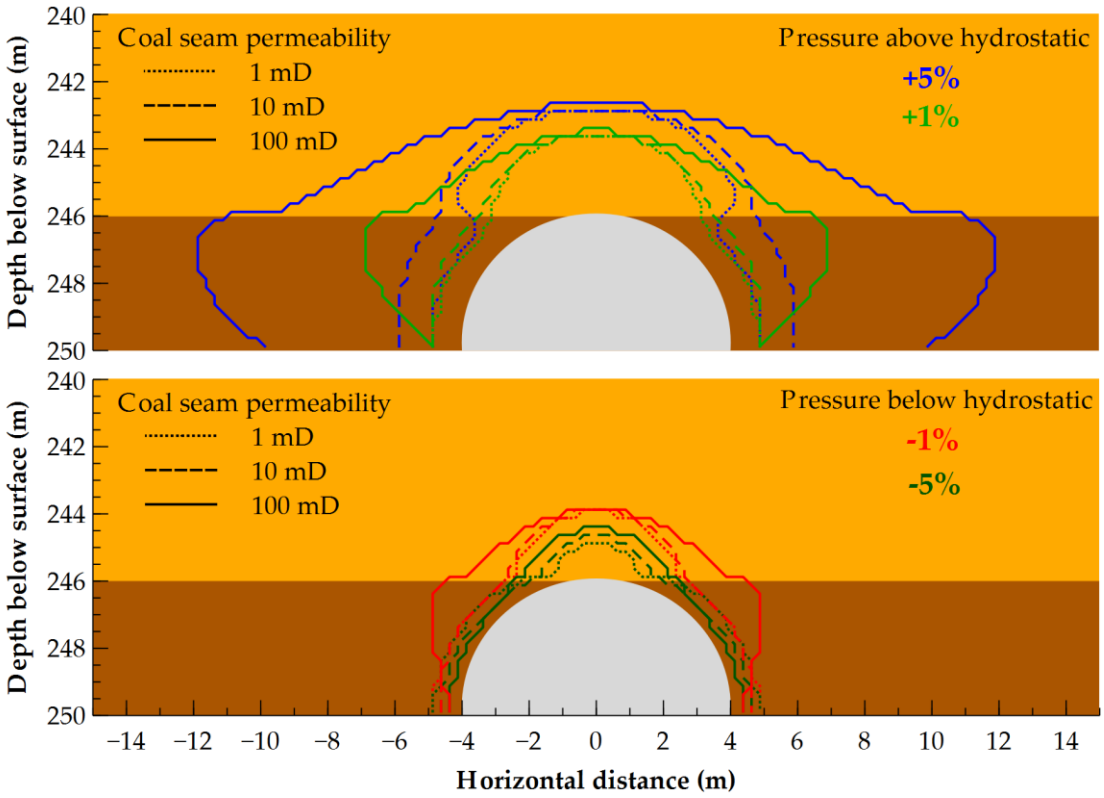

Figure 32: Simulated steam jacket extents after 30 days of UCG operation for different pressures above (top) and below (bottom) the initial hydrostatic pressure and for different assumed coal seam permeabilities (horizontal permeability of the overburden is maintained constant at 50 mD).

For each of these reactor pressure-driven scenarios, the effects of coal seam permeability on the spatial steam jacket extent are calculated for 1, 10, and 100 mD. The resulting water in- and outflows for each scenario, scaled to 1-m UCG reactor length are shown in Figure 33. The comparison of the steam jacket extents around the UCG reactor exhibits their strong dependency

on the reactor pressure. In vertical directions, these differ by about 1 m only due to the constant overburden permeability (50 mD in horizontal direction). For the +5% scenario, a maximum steam jacket extent of up to 3.5 m in the vertical and 8 m in the horizontal direction is observed for a coal seam permeability scenario of 100 mD. The lower the coal seam permeability the lower the horizontal steam jacket extent with 2 m for 10 mD and 1 m for 1 mD in the +5% scenario. The +1% scenario generates a maximum horizontal steam jacket extent of up to 3.5 m for a 100 mD permeability. Differences in the horizontal steam jacket extent for the +1% scenario are considerably lower (maximum of 0.25 m) for the coal seam permeabilities of 10 mD and 1 mD. In both scenarios, the maximum steam jacket extent is in the range of up to one meter. The slightly flattened shapes around the reactor result from the difference in permeabilities between the coal seam and the overburden as well as the horizontal-to-vertical permeability anisotropy. High temperatures at the reactor boundary induce steam jacket formation, even if the reactor pressure is operated below the hydrostatic one. Here, water inflow into the reactor (Figure 33) reduces the spatial steam jacket extent, whereby it is limited to a maximum of 1 m in the horizontal direction in all sub-hydrostatic reactor pressure-driven simulation scenarios. Varying coal seam permeabilities to 1, 10, and 100 mD shows that higher permeabilities result in higher water inflows (Figure 33), and thus a marginally lower spatial steam jacket extent at the coal seam base for the −1% and −5% scenarios (Figure 32).

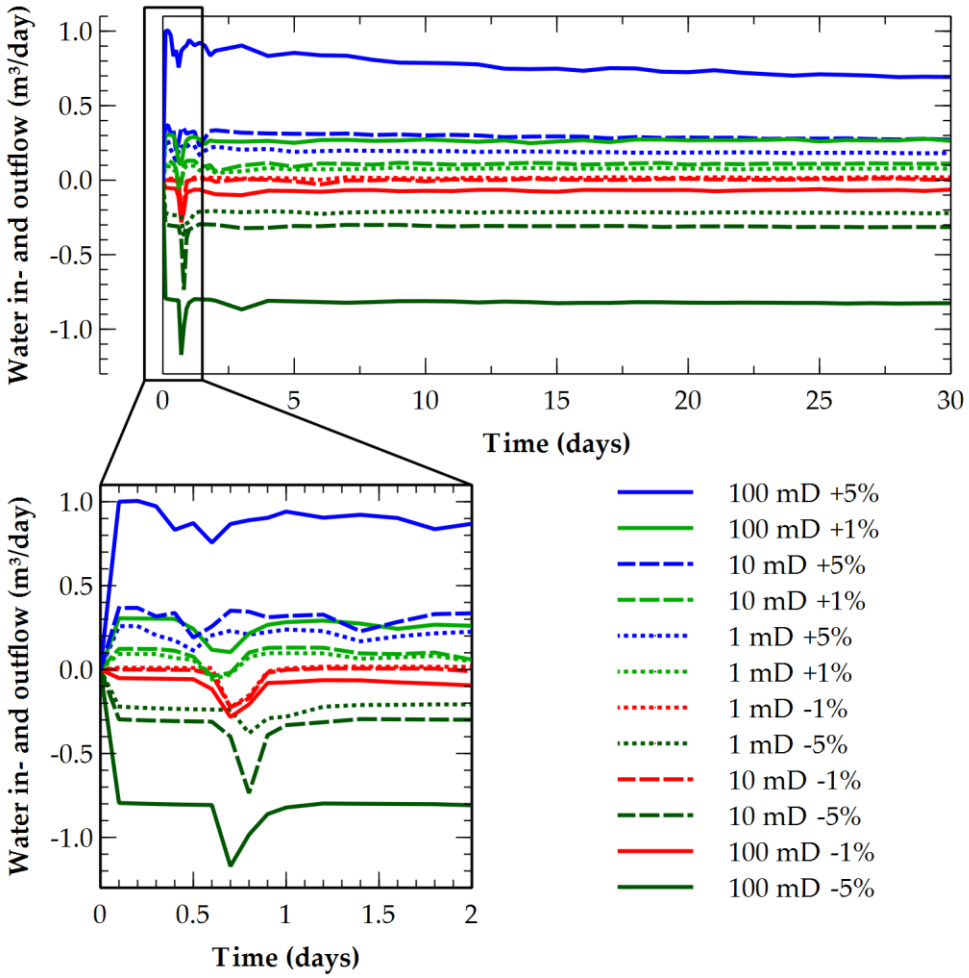

Figure 33: Simulation results of water in- and outflow scaled to 1-m reactor length in the twelve simulation scenarios for the entire simulation time (top) and for the first two days of simulation (bottom). Water outflow is positive here.

With decreasing depth, hydrostatic pressure decreases, while the reactor pressure is assumed to be constant during the entire simulation time. Therefore, the driving force for water inflow provided by the pressure gradient wanes towards the reactor top and results in local supra-hydrostatic pressure. This becomes apparent in the inverse trend of the steam jacket extent at the height of the transition between coal seam and overburden. For the −5% reactor pressure assumption, the horizontal steam jacket extent in the 100-mD permeability scenario is smaller than that in the 10-mD one due to higher horizontal inflow rates at these depths (Figure 33).

However, in the overburden, the steam jacket extends farther in the 100-mD permeability scenario compared to the 10 mD one. This behavior is observed for all scenarios running at supra-hydrostatic reactor pressures. Hence, higher permeabilities in the coal seam as well as slightly supra-hydrostatic pressures at the reactor top result in a greater steam jacket extent in the vertical than in the horizontal direction for all sub-hydrostatic scenario. The maximum vertical extent of the steam jacket above the reactor reaches about 1.1 m for the −5% and 2 m for the −1% scenarios. As expected, the simulation results on water in- and outflow, scaled to 1-m reactor length show relatively constant water flows in all investigated scenarios (Figure 33). The maximum steam jacket extent is reached (see Figure 32) with a highest outflow rate of up to about 1 m^3/day and about 0.8 m^3/day in average in the +5% scenario with 100 mD permeability. For all the scenarios with +5% reactor pressure, the outflow is limited to a maximum rate of about 0.4 m^3/day due to the low coal seam permeability. If any, only low flow rates are observed in the +1% pressure scenarios. Almost reverse flow rates are observed in the sub-hydrostatic scenarios, with a maximum inflow rate of about 1.2 m^3/day and an average inflow of about 0.8 m^3/day in the 100 mD permeability and −5% reactor pressure scenario. Due to the steam jacket formation at the top of the reactor and the permeability anisotropy, the calculated inflow mainly occurs horizontally from the coal seam (not shown here).

A decrease in water outflow and increase in water inflow are observed as negative peaks at simulation times between 0.3 and 0.9 days (Figure 33, bottom). Although different in amplitude, the peak is observed in all calculated water flow rates, indicating the time of steam jacket formation above the reactor. At the time of steam jacket formation, decreasing relative permeabilities of the wetting phase at the reactor top induce a change in the hydraulic flow regime, changing from radial to mainly horizontal wetting-phase flow behavior, while the non-wetting phase (vapor) flow is generally radial, depending on the respective pressure, temperature and permeability regime.

4.4.3 PRESSURE AND TEMPERATURE VARIATION IN THE OVERBURDEN AQUIFER

Figure 34 shows the gas saturations, pressures, and temperatures calculated for the twelve investigated scenarios along the vertical profile given in Figure 31 at the end of the simulation time (30 days). Since overburden permeability was maintained at a constant value (50 mD), the variation of coal seam permeability has a negligible impact on gas saturation, pressure and temperature in the overburden. The thermal front (temperatures ≥ 200°C) moves upward with the steam jacket, whereby its extent above the reactor depends on the reactor pressure as presented in Figure 32. The higher the reactor pressure, the further the steam jacket extent and associated migration of the thermal front (about 1.1 to 3.5 m). A relatively linear thermal gradient between 600 and 200 °C develops where the vapor phase (steam jacket) occurs. The discontinuity

in the temperature profiles indicates the transition from the gas-rich water (vapor) to the liquid water-saturated zone, in which an exponential decrease in temperature with decreasing depth is observed due to its higher specific heat capacity and conductivity.

The reactor pressure also influences the initially hydrostatic pressure regime in the reactor's vicinity. Figure 34 shows that in the gas-rich zone (steam jacket) and in the liquid water-saturated zone, the pressure gradient is shifted to higher values with increasing reactor pressures. Sub-hydrostatic pressure gradients develop below the liquid water-saturated zone above the reactor in the −1% and −5% scenarios, explaining the observed preferential inflow into the reactor at these depths.

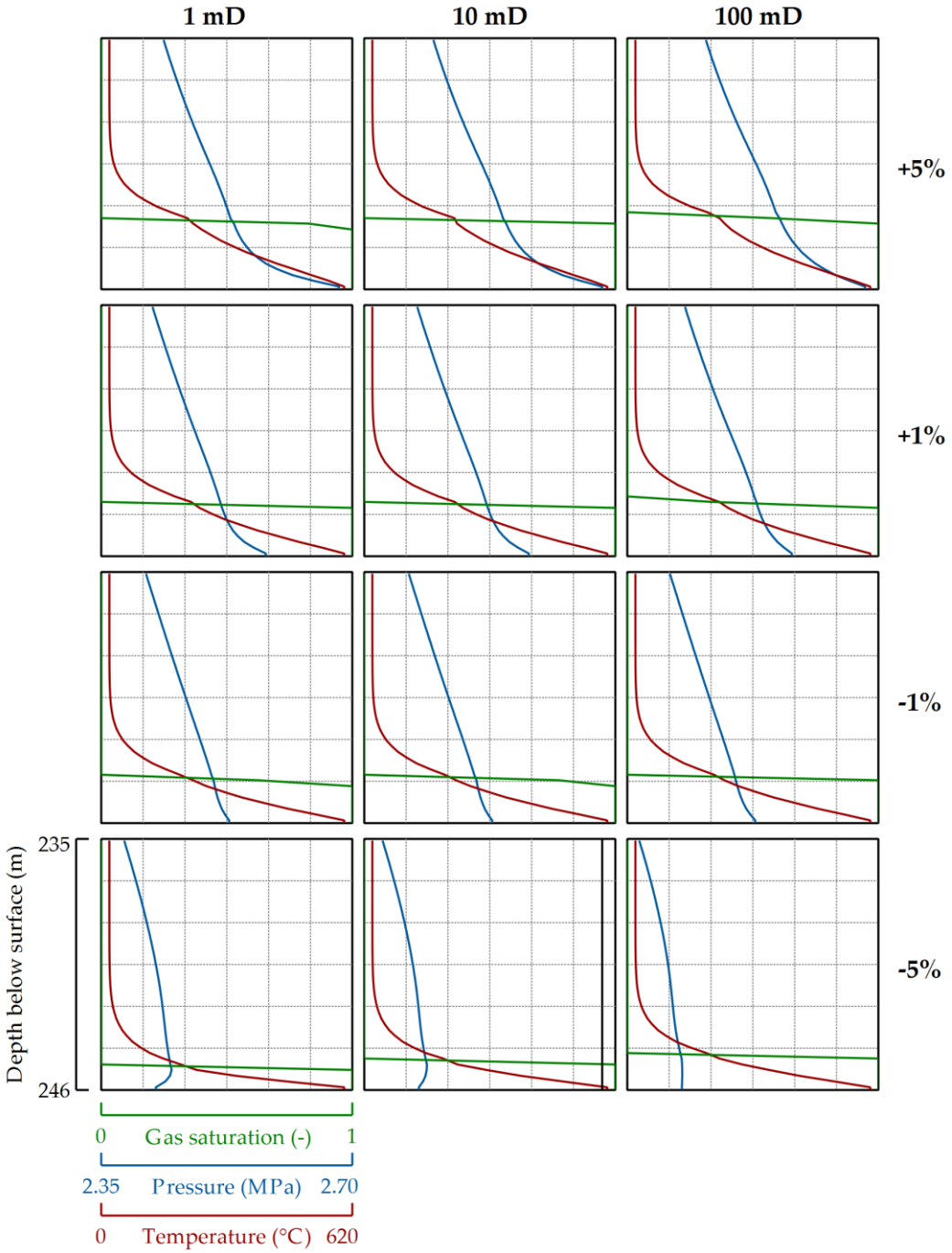

Figure 34: Simulated gas saturations (green), pressures (blue), and temperatures (red) along the vertical profile shown in Figure 31 for all investigated scenarios at the end of simulation time (30 days).

4.5 DISCUSSION AND CONCLUSIONS

In the present study, we introduced a new modeling approach to quantify and predict steam jacket dynamics as well as water flows into and out of a UCG reactor. These processes are highly variable phenomena in time and space, depending mainly on thermal and hydrogeological coal seam and overburden properties as well as UCG operation conditions. The very good agreement between our simulation results and the U.S. field trial data indicates that the relevant physics related to non-isothermal multiphase flow processes are sufficiently reproduced by our modeling approach, validating it at the same time.

The mathematical model developed by Camp (1980) to assess water balances under consideration of reactor growth is limited to the special case of uniform isotropic permeability and isothermal single-phase flow. Nevertheless, that model reproduces the water flow observed at both U.S. field tests reasonably well (Gunn and Krantz, 1987), using data on time-dependent reactor pressure and coal consumption in the semi-analytical modeling approach for the spalling-enhanced drying of coal and overburden rock as well as water balance calculations. Compared to water production from coal and rock drying, water in- and outflows are relatively low for the Hanna trial (Gunn and Krantz, 1987). This is mainly due to the low Hanna coal seam permeability (approximately 3 to 15 mD) and the moderate pressure gradients between the reactor and the overburden aquifer. For that reason, we decided to also validate our modeling approach against the Hoe Creek field test, exhibiting significantly higher permeabilities as well as water in- and outflows. Also for this field test, our simulation results are in a very good agreement with the data from the literature, emphasizing that the modeling approach is generally applicable to describe the thermo-hydraulic processes occurring in the UCG reactor vicinity. The difference between our best-fit coal seam permeability (100 mD) and Camp's model (350 mD) is expected to arise from neglecting a hydraulically permeable overburden and isothermal flow. Deviations from to the permeability documented for the Hoe Creek field site (coal permeability between 225-408 mD (Stone and Snoeberger, 1976) are likely to result from the generally high permeability heterogeneity of the target coal seam.

According to Camp and White (2015), low coal and overburden permeabilities are preferable in view of limiting water flow into the UCG reactor, since spalling-enhanced drying of coal and roof rocks generally supplies sufficient water to feed an efficient gasification process. In this context, our modeling approach supports UCG operators to adjust reactor operating pressures to maintain the required water inflow and minimize potential fluid leakages out of the reactor. Further, we demonstrated that low permeability strata and low to moderate reactor pressures mitigate the spatial steam jacket extent; hence, limiting upward and lateral migration distances of UCG by-products. A lower water inflow will also reduce the water amount produced from the gasifier to the surface, minimizing the costs of synthesis gas dehydration. Our simulation results further demonstrate that the steam jacket will evolve in the lateral direction by multiple times the coal seam thickness if the reactor is operated at supra-hydrostatic pressures.

Camp and White (2015) discuss that a fingering phenomena being related to upward vapor migration is rather more likely than a continuous steam jacket front advancement in highly heterogeneous coals. However, this was not observed in our simulation results due to the applied directional homogeneous permeability distribution. Modeling the development of gas fingering

requires detailed knowledge on a potential spatial distribution of the coal's dual porosity and permeability characteristics to consider the coal cleat system and potential fractures in addition to the coal matrix in our non-isothermal multiphase flow simulations. Furthermore, phase transitions occur abruptly, effectively representing a jump from fully liquid- to gas-saturated grid elements, which is in good agreement with existing publications on evaporation front movements in porous media (Plumb and Klimenko, 2010; Saulov et al., 2010). A comparison of isothermal simulations without any phase transition with non-isothermal ones with phase transitions shows that neglecting non-isothermal effects results in deviations in the calculated spatial flow regimes and water balances. This is not discussed in detail here, since it is out of the scope of the present study and of limited scientific relevance for the presented results.

The prediction of steam jacket dynamics and the accompanying optimization of water balances is of substantial importance in view of optimizing the calorific synthesis gas value and designing an optimum UCG operation by balancing the steam-char reaction and heat losses due to water evaporation to achieve a maximum coal-to-synthesis gas conversion efficiency. Synthesis gas and UCG by-products will be contained within the reactor and the area of maximum steam jacket extent if operators maintain sub-hydrostatic reactor pressures. For that purpose, our thermo-hydraulic modeling approach provides an efficient method to support the design and operation of pressure monitoring in pilot- to commercial-scale UCG operations, and thus an efficient tool to tackle geological and operational uncertainties.

In summary, our modeling approach allows for a detailed quantification and prediction of steam jacket dynamics and non-isothermal multiphase flow processes in the UCG reactor vicinity, especially in view of water balances, avoiding aquifer contamination during the entire UCG operation lifecycle.

Future work aims at the integration of the coal cleat system in addition to its matrix to investigate preferential migration pathways and potential gas fingering processes, since effective coal permeability is controlled by fractures that encompass its natural cleat system and any other present fractures (Perkins and Love, 2010). Moreover, thermo-mechanically-induced permeability changes in the close vicinity of the reactor will be considered in our future research activities to investigate the formation of potential leakage pathways for gas losses. In this context, the presence of high-permeable faults and their potential reactivation have also to be assessed in view of preferential leakage pathways for UCG gases.

5 DISCUSSION AND CONCLUSION

Coal deposits are abundant in many regions of the world and large reserves and resources of hard coal and lignite are available in sufficient quantities to meet expected increasing demands for many decades from a geological point of view (BGR, 2015). The classification as resources and not yet as reserves is important as it reflects the likelihood that the fossil fuels will be brought to the market. With their share of around 55% of the reserves, and around 89% of the resources (BGR, 2015), coal has the largest potential to provide security of future energy supply of all non-renewable energy resources. Around 500 coal-fired plants were built worldwide in the years between 2010 and 2015, whereby specially China and India greatly increased their stock (González-Eguino et al., 2017). However, it is known that both, conventional mining extractions of coal reserves (underground and open pit) are problematic, since these leave a massive environmental footprint due to potential land subsidence, localized flooding, water pollution and the high amount of carbon and methane releases (Eftekhari et al., 2012; Self et al., 2012). Additionally, it has other issues including high machinery costs, coal processing requirements and more important it needs the presence of coal miners underground in a hazardous work environments (Burton et al., 2006; Self et al., 2012).

Underground coal gasification (UCG) aims at in-situ conversion of coal to synthesis gas. Thereby, UCG leaves most of ash underground, produces smaller volumes of pollutants such as mercury and tars, particulates and sulfur species, and thus has the possibility to provide a cleaner and convenient source of energy in the form of synthesis gas (mainly hydrogen, carbon monoxide, carbon dioxide and methane) from coal deposits that are currently not mineable by conventional methods. Additionally, UCG may provide the option of replacing conventional mining methods as far as specific boundary conditions (e.g., calorific value, coal seam thickness, coal seam depth, overburden strata, distance from abandoned mine workings) are met (DTI, 2004; Moorhouse et al., 2010). Apart from its high energetic and economic potential (Budzianowski, 2012; Eftekhari et al., 2012; Nakaten et al., 2014a, 2014b, 2014c), UCG may also cause environmental impacts such as ground subsidence above the reactor zone and groundwater pollution (Hettema et al., 1998; Kapusta and Stańczyk, 2011; Stańczyk et al., 2011; Tian, 2013; Tian et al., 2011, 2012, 2013, 2014, 2015; Wolf and Bruining, 2007). While UCG technology itself is a rather simple concept in theory, experience from major worldwide field trials over the last decades demonstrates that process control in practice is much more complicated (Couch, 2009; Klebingat et al., 2016). Various factors during in-situ reactor operation often hamper a continuously stable and efficient process performance (e.g., water inflow, heat losses, presence of faults), in consequence partially leading to lower synthesis gas qualities and undesired hazardous by-products (e.g., Bhutto et al., 2013; Burton et al., 2006; Couch, 2009; Sury et al., 2004). Pollutant-charged gas leakage from the UCG reactor due to roof rock failure as a thermo-mechanical response of in situ pressure and temperature conditions recently marks one of the most potential environmental impacts (Biezen, 1996; Buscheck et al., 2009; Klebingat et al., 2016; Wolf and Bruining, 2007). During the UCG process, temperatures of more than 1000 °C can be reached in the UCG reactor and its close

vicinity. This results in the build-up of a steam jacket around the reactor, and thus the temperature-dependent coal and rock behavior in the reactor vicinity is expected to be of the uttermost importance for assessment of UCG-driven changes in the rocks surrounding the UCG reactor. Coupled thermo-mechanical and thermo-hydraulic processes occurring in rocks adjacent to a UCG reactor are generally not well known, because of the difficulty to investigate and quantify the occurring reactions during deep UCG operations in the field and their effects on induced stress and hydraulic flow. Similar to conventional longwall mining, where roof support by coal pillars is required, dimensions of pillars are relevant in UCG operations when using the CRIP technology, where a protection pillar is left in the coal seam to mitigate the formation of stress peaks in the hanging wall during the gasification of each channel. Protection pillars especially avoid uncontrolled fluid cross-flow and isolates single channels during their operation, minimizing ground surface subsidence and allowing the channels to be flushed and/or cooled at the end of UCG operation (Najafi et al., 2014). However, a wider protection pillar results in a lower coal yield, and thus counteracts economic aspects of UCG operation. Major contributions to environmental impact mitigation can be achieved by improving the understanding of the involved coupled processes, but the current knowledge is mainly based on laboratory experiments (Stańczyk et al., 2010, 2011) and UCG field trials at shallow depths (Burton et al., 2006; Couch, 2009). Due to the high financial effort associated with UCG field trials, numerical modeling has become an important methodology to study the coupled processes influencing UCG performance.

The objectives of the accomplished research were to investigate: how thermo-mechanical rock behavior during UCG affects permeability changes and whether, when upscaling from 2D near-field to large-scale 3D models, temperature dependent rock parameters need to be implemented. This study further aims to determine what is the effect of the presence of a regional-scale fault on pillar width, and to quantify resulting ground surface subsidence by use of a coupled thermo-mechanical 3D model with real site-specific data of a hypothetical UCG site. Furthermore, coupled thermo-hydraulic simulations were employed to improve the understanding of the hitherto neglected steam jacket dynamics in the UCG reactor vicinity and to validate the new model approach by operational data. With respect to the formulated objectives of this thesis, thermo-mechanical and thermo-hydraulic impacts of UCG operation were assessed by application of coupled 2D and 3D numerical simulations to elaborate reliable predictions of near-field and site-specific UCG impacts. In particular, qualitative and quantitative analyses of coupled thermo-mechanical and thermo-hydraulic near-field processes in the close reactor vicinity may provide an important basis for future research.

In the first part, the coupled thermo-mechanical impact of temperature-dependent and temperature-independent parameters on permeability changes was investigated in a synthetic underground coal gasification reactor vicinity. For that purpose, a 2D thermo-mechanical numerical model was implemented, comprising three geological units and thermo-mechanical parameters determined in recently published data on high-temperature experiments. A parameter sensitivity analysis identified the parameters most sensitive to temperature as described hereinafter. Simulation results demonstrate that the temperature-dependent thermo-mechanical properties elastic modulus, tensile strength and linear thermal expansion coefficient have a notable direct influence on stress and deformation (Figure 8), while thermal conductivity mainly influences the spatial temperature distribution around the UCG reactor (Figure 9), and thus indirectly affects stress changes and displacements. Especially the temperature distribution in the

reactor vicinity is controlled by the thermal conductivity and may result in overestimating the size of areas with high permeability changes unless temperature-dependent properties are considered. Hence, the thermo-mechanical rock behavior is mainly influenced by the parameters thermal expansion coefficient, tensile strength and elastic modulus. In the close reactor vicinity, the high temperatures induce positive volumetric strains. However, permeability changes calculated based on volumetric strain show only negligible differences between simulations using temperature-dependent and temperature-independent parameters. A similar impact of elevated temperature on permeability was also discussed in Akbarzadeh and Chalaturnyk (2014a); however, without temperature-dependent rock properties. Hence, near-field models (meter scale) employed for the assessment of reactor growth, induced by the thermodynamic gasification processes require temperature-dependent parameters for simulations, whereas far-field models (reservoir to regional scale) can benefit from neglecting temperature dependence, which in turn increases the computational efficiency significantly by avoiding dynamic thermo-mechanical parameters.

Several studies discussed the spalling and collapse of the overburden and its extent in the surrounding rock strata due to the increase in stresses as a result of the gasification process (Suchowerska et al., 2012; Sury et al., 2004; Vorobiev et al., 2008; Yang et al., 2014). The authors showed that the dramatic stress increase is limited to reactor vicinity, whereby the reactor roof stability mechanism benefits from the stress-arching effect (Elahi and Chen, 2016; Yang et al., 2014). For some clay-rich strata, even a self-sealing capability was observed, which means that fractures will be repaired as the clay naturally swells (Camp and White, 2015; Wolf et al., 1992). Simulation results of the stress increase around the reactor show that shear and tensile failure occur at multiple locations in the reactor near-field under the given stress-regime, but also with limited extent in the surrounding rock (Figure 13 and Figure 14). A significant temperature increase (≥ 200 °C), which results in high decrease of rock strength is only induced in the close reactor vicinity. In the considered scenarios, the region of failure in lateral direction is about three times the coal seam thickness (4 m), since a stress-arching effect develops with time. At the reactor top, a field of pure tensile failure is observed in the sandstone for the temperature-dependent simulation results (Figure 14). However, to study the shear and tensile rock failure extent in detail, different initial stress states should have been investigated, which was not the focus of the considered simulations.

Nowadays, it is possible to develop and apply 3D models of varying complexity due to the significantly lower demand in computing time with the availability and advancement of innovative modeling and coupling techniques as well as parallel computations. There are few 3D models developed so far in the context of UCG with varying levels of complexity (Biezen, 1996; Daggupati et al., 2011; Nitao et al., 2011; Nourozieh et al., 2010; Seifi et al., 2011; Shirazi et al., 2013; Yang et al., 2014). They used computational fluid dynamics (CFD) software tools to obtain time-dependent reactor growth. However, applicability of these models is limited to specific and isolated cases and the models can hardly be used to predict the performance of UCG trials (Khan et al., 2015). The model for reactor growth developed by Biezen (1996), which appears to be the first 3D UCG model, was limited due to the absence of heat transfer. Nourozieh et al. (2010) developed a multilayer 3D model to study CRIP-based UCG operation in deep coal seams, including the corresponding chemical processes and heat transfer, but without considering thermo-mechanical failure. Validation or comparison with experiments was not reported for Biezen (1996)

and Nourozieh et al. (2010). Shirazi et al. (2013) developed a small-scale 3D packed-bed model, which revealed the effect of different parameters on reactor growth as well as reactor shape and size. According to Shirazi et al. (2013) led a higher coal seam permeability to faster growth of the reactor and resulted in a much wider reactor, which was in good agreement with experimental results from Cui et al. (2014). However, all models compromised between model complexity and simplicity in order to get faster computation runtimes (Khan et al., 2015). Regardless of the approach of the models, there is so far not a single model that includes all the important physical and chemical models for the successful prediction of UCG. Although thermo-mechanical failure is documented by field trials, there are only very few models that consider this phenomenon with unrealistic and simple assumptions (Khan et al., 2015).

In order to enhance the features of a 3D model and to apply the model for the assessment and prediction of UCG performance considering thermo-mechanical impacts, it is imperative to incorporate coal seam properties and geology of the target site into the model. Hereby, the previous findings from the 2D model emphasize that model simplifications with regard to the consideration of thermo-mechanical parameters in far-field numerical models can significantly reduce the computational time, while preserving the validity of the numerical results. Taking into account these findings, 3D modeling was applied to assess complex site-scale geological models with regard to potential environmental UCG impacts. Detailed knowledge on site geology as well as permeability of potentially existing discontinuities is generally not available (Burton et al., 2006). Hence, coupled numerical models allow for the assessment of potential permeability changes and mechanical integrity of UCG reactors, which is of uttermost importance for an efficient and more environmental-friendly UCG operation.

The first 3D UCG model based on real structural geological data was developed to investigate a hypothetical UCG operation at the Polish Wieczorek mine. This complex 3D regional-scale model was employed to assess the impacts of using isothermal and non-isothermal simulations, different pillar widths and varying regional stress regimes on the spatial changes in temperature and permeability, ground surface subsidence and the potential formation of hydraulic short circuits between single UCG channels. Simulations further show the impact of high temperatures on failure at a fault plane, comparing isothermal and non-isothermal scenarios (Figure 24 and Figure 25). In addition, stress states at fault elements, permeability changes in UCG channel vicinity and fault integrity in terms of hydraulic short circuit formation were considered. Since sedimentary rocks have generally low values of heat conductivity and heat capacity compared to igneous rocks, a significant temperature increase is induced in the close reactor vicinity only. Further, the reliable prediction and management of mining-induced surface subsidence is one of the environmentally challenging issues in the context of coal mining. Luo et al. (2009) developed a UCG subsidence prediction methodology and showed that overlying strata and ground surface subsidence behavior in UCG operation is relatively similar to that in conventional longwall coal mining. Depending on UCG panel design, channel dimensions and coal seam depth, the maximum surface subsidence determined in the literature (Li et al., 2015; Sirdesai et al., 2015) is in the same range of the simulation results in this study. Even if the strength of overlying strata above a gasified coal seam can increase under the influence of temperature as suggested by Li et al. (2015) and observed in experiments by Liu et al. (2016b) at temperatures between 100 and 450 °C due to cementation reactions effecting weakening, increasing temperature induces a general decrease in rock strength (Evans and Kohlstedt, 1995; Feng et al., 2017; Liu et al., 2016a; Tian et al., 2015).

However, microstructural changes in mineralogy and the associated variation in strength are not considered in the simulations. In fact, vertical displacements at the ground surface calculated in the simulations are about 50% higher in the isothermal scenario and notably less homogeneous compared to those in the non-isothermal one at the end of the operational time. At that moment, the non-isothermal simulation has not achieved a thermo-mechanical equilibrium state due to sustained thermally-induced stresses, whereby the high temperatures effect a thermal expansion of the heated surrounding rocks in the affected strata. Considering the development of high vertical displacements in the UCG channel vicinity, it becomes obvious that the simulated displacements are related to thermally-induced stresses.

Thermo-mechanical stresses due to coal extraction and thermal loading induce permeability changes. These permeability changes show significant deviations in the close UCG channel vicinity, comparing the isothermal and non-isothermal simulations, due to the absence of temperature-induced stress effects. Permeability, in consideration of the difference between hydrostatic and UCG reactor pressure, controls fluid in- and outflow into and out of the reactor, respectively (Blinderman and Anderson, 2004; Otto and Kempka, 2015a). Here, fluid flow is likely to be affected by the local permeability increase, which is of relevance in the determination of the temporal and spatial steam jacket extent, emerging due to water evaporation in the close UCG reactor vicinity (Blinderman and Anderson, 2004; Blinderman and Jones, 2002). Nevertheless, both simulated 60-m pillar width scenarios show that permeability changes only occur in close UCG channel vicinity, whereby hydraulic short circuit formation between single channels is not observed in the absence of geologic faults. Therefore, the increase in local permeability due to mechanical and thermal stresses (Figure 21) does not compromise UCG operation for a pillar width of 60 m. Simulation results rather suggest that pillar widths of 30 m (equals a coal-seam-thickness-to-pillar-width-ratio of about 1:3) would suffice to avoid hydraulic short circuit formation between single UCG channels for the investigated study area. Najafi et al. (2014) presented an approach to estimate the required protection pillar width in CRIP-based UCG operation and compared purely mechanical with thermo-mechanical simulations. They show that temperature induces thermal stresses and reduces pillar strength, what is also demonstrated in the present thesis (Figure 24). However, Najafi et al. (2014) focused on side abutment stresses occurring around the pillars, whereby a maximum lateral failure zone of about 3.25 m in a 3.5 m thick coal seam was observed. The authors did not consider fault planes as regions of mechanical weakness and potential fluid migration pathways in their model. From the UCG process performance perspective it is obvious, that an ideal UCG region would have no minor and major faults (Camp and White, 2015). However, the absence of faults and fault segments in a geologically complex area of coal-bearing formations is very unlikely (Ligtenberg, 2005). Therefore, the presence of faults complicates UCG projects, because faults may act as UCG fluid migration pathways (Camp and White, 2015; Ligtenberg, 2005).

Simulations on fault integrity show that shear and tensile failure significantly increase due to thermal stress propagation, what may result in a coalescence of shear failure. If distances between UCG channels are not sufficiently high, this behavior can trigger fault reactivation, and therefore form potential hydraulic short circuits between single UCG channels but also generate mining-induced seismicity (Hasegawa et al., 1989; Sen et al., 2013).

In addition to variation in pillar width, different stress regimes were considered in the coupled thermo-mechanical simulations to assess their impact on fault integrity in terms of hydraulic short circuit formation. The results show a significant influence of the stress field and S_{Hmax} orientation on fault integrity. Even for a pillar width of 140 m, a coalescence of reactivated fault areas is feasible as shown for the scenario based on a strike-slip stress regime with the S_{Hmax} orientation parallel to the fault plane (Figure 27). Simulation results exhibit a high uncertainty if only limited data on the local stress regime is available. Additionally, non-detectable sub-seismic faults of various orientations can create hydraulic conduits between UCG reactors and shallower strata, and thus generate environmental hazards related to UCG operation, such as migration of UCG pollutants into shallow freshwater aquifers. In this context, thermo-mechanical processes are the key for quantification of potential leakage pathway formation (Vorobiev et al., 2008). A large regional fault, as implemented in this 3D model, would be highly undesirable and can impede UCG in practice. As a result, a higher resolution mapping effort may be needed for UCG site evaluation. For a large-scale UCG project operating for decades, mine-plan layouts may need to be adjusted accordingly. Thereby, large seismic surveys but also information on one or more of the in-situ stress magnitudes (S_V, S_{Hmax}, S_{hmin}) for a certain depth range, e.g., by use of hydraulic fracturing, leak-off tests, overcoring, undercoring, core-based methods and source mechanisms of earthquakes (Zang et al., 2013), are crucial for a candidate UCG area. The risks include gas losses, contaminant migration and uncontrolled water inflow (Burton et al., 2006). However, recent numerical simulations on fault reactivation are mainly associated to hydraulic fracturing (Rutqvist et al., 2013), CO_2 storage (Cappa and Rutqvist, 2011; Tillner et al., 2016) and geothermal heat recovery (Jacquey et al., 2015), whereas the process of fault reactivation has not been adequately represented in the field of UCG (Khan et al., 2015).

As stated in advance of the present study, water in- and outflow in the reactor vicinity is a highly variable phenomenon that depends on thermal and hydraulic coal seam and overburden properties as well as UCG operation conditions. In order to prevent or significantly minimize environmental impacts such as groundwater pollution, UCG reactors are generally operated below hydrostatic pressure to limit the outflow of fluids from the reactor and to avoid overburden aquifer contamination (Burton et al., 2006). Evolving high reactor temperatures result in the build-up of a steam jacket in the close reactor vicinity. Prediction of steam jacket dynamics and accompanying optimization of UCG water balances is of substantial importance to achieve a maximum coal-to-synthesis gas conversion efficiency (Blinderman and Jones, 2002). Progress on understanding the complex and strongly coupled thermal-hydraulic processes in UCG has been achieved by several studies. Those focused either on the time dependent pure temperature distribution (Sarhosis et al., 2013) or additionally on concentrations of different gas species after a UCG operation in the close reactor vicinity (Akbarzadeh and Chalaturnyk, 2013, 2014b; Buscheck et al., 2009; Nitao et al., 2011).

To improve the understanding of the role of the steam jacket in UCG operations, coupled thermo-hydraulic 2D and 3D models were developed to assess the occurring multiphase fluid flow processes. This newly developed modeling approach allows quantifying and predicting the steam jacket dynamics as well as water flows into and out of a UCG reactor. Therefore, it helps to optimize the calorific synthesis gas value by balancing the steam-char reaction and heat losses due to water evaporation, and enables the design of an optimum UCG operation. The employed multiphase flow numerical simulations presented in this thesis are suitable for high temperatures

to address the influence of reactor pressure dynamics as well as coal and overburden permeability on water inflow and steam jacket dynamics.

The U.S. field trials Hanna and Hoe Creek were applied for 3D model validation by comparing observed and simulated water inflow. The very good agreement between the model calculations and field tests observations (Figure 29 and Figure 30) show that the relevant physics and processes of non-isothermal multiphase flow can be reproduced with the presented modeling approach, validating it at the same time.

The model developed by Camp (1980) to assess water balances under consideration of reactor growth is limited to the special case of uniform, isotropic permeability and isothermal single-phase flow. Nevertheless, that model reproduces the water production observed in both U.S. field tests reasonably well (Gunn and Krantz, 1987), using data on time-dependent reactor pressure and coal consumption in the semi-analytical modeling approach for spalling-enhanced drying of coal and overburden rock as well as water balance calculations. Compared to water production from coal and rock drying, water in- and outflows are relatively low for the Hanna trial (Gunn and Krantz, 1987). This is mainly due to the low Hanna coal seam permeability and the moderate pressure gradients between the reactor and overburden aquifer. For that reason, my modeling approach was also validated against the Hoe Creek field test, exhibiting significantly higher permeabilities as well as water in- and outflows. Also for this field test, the simulation results are in a very good agreement with the data from the literature (Figure 30). In general, demonstrating model reliability by validation against published operational and/or experimental data is often neglected in literature on UCG modeling as discussed by Khan et al. (2015).

To discuss the effect of coal seam permeability and UCG reactor pressure on the dynamic multiphase flow processes in the reactor's vicinity, different simulation scenarios had to be analyzed. In this context, a 2D numerical model with a less complex geometry offers a sufficient accuracy to provide a quantitative analysis and description of the thermo-hydraulic processes (Khan et al., 2015; Kühn et al., 2005), while 3D effects were not relevant for this specific issue. The simulation results (Figure 32) show that from the UCG process performance perspective, low permeability in the coal and overburden rock as well as reactor pressure below the hydrostatic should be preferred because of reduced water inflow. Usual, excessive water enters into the reactor due to the combination of inflow through coal and adjacent strata as well as drying of surrounding rocks and of wet rock collapsing into the reactor (Camp and White, 2015).

These different water sources generally supply enough water for the gasification chemistry. From a contaminant transport perspective, low permeability and reactor pressures below the hydrostatic one are also preferred. Low permeability strata and avoiding overpressure in the reactor can limit the steam jacket extent, and thereby potential contaminants from migrating over large distances away from the reactor. Also, a lower inflow rate of water into the reactor will reduce the volume of water produced during gasification. The simulation results indicate that when the reactor is operated with overpressure, the steam jacket will expand many times beyond the coal seam thickness (Figure 32). Escaping fingers of gas are more likely than in a uniform outward flow and will tend to move preferentially up due to buoyancy and hydrostatics (Camp and White, 2015). However, this was not observed in the simulation results due to the isotropic and homogenous permeability distribution. Modeling of hypothetical gas finger flow would be

technically feasible; however, it requires detailed knowledge of permeability distribution, fracture networks of coal and/or implementation of potential faults with higher permeability for validation purposes.

Synthesis gas and UCG by-products will be contained within the reactor and area of maximum steam jacket extent, if operators maintain sub-hydrostatic reactor pressures. For that purpose, the thermo-hydraulic modeling approach provides an efficient method to support the design and operation of pressure and temperature monitoring in pilot- to commercial-scale UCG operation, and thus an efficient tool to tackle hydrogeological and operational uncertainties. Hence, the modeling approach allows for a thorough quantification and prediction of steam jacket dynamics and non-isothermal multiphase flow processes in the UCG reactor vicinity, and thereby enables especially in view of water balances avoiding aquifer contamination during an entire UCG operation lifecycle. Sustainable and economic UCG site development requires the integration of numerical modeling.

In conclusion, application of numerical models led to specific new insights into thermo-mechanical rock behavior and fluid flow dynamics in UCG reactor vicinity. The proposed and newly developed 2D and 3D thermo-mechanical models as well as the employed multi-phase fluid flow modeling approach were proven appropriate for determining thermo-mechanical and thermo-hydraulic impacts at different scales. At the same time, the simulations are of great benefit to identify and reveal the factors, relevant to mitigate high negative environmental impacts, and thus to protect groundwater resources from contamination. With respect to the formulated objectives of this thesis and the findings gained thereof, it can be summarized that a more environmental-friendly, efficient and sustainable UCG operation is realizable in compliance with the following requirements:

- Sufficient pillar width between the UCG reactors, mainly depending on coal seam thickness and regional stress field. Here, the presence of (high permeable) faults and/or sub-seismic faults in the vicinity of a UCG panel is crucial and yet highly underestimated in all UCG publications.
- Reactor pressure below the hydrostatic pressure during the UCG operation is highly recommended to avoid a large extent of the steam jacket, and therefore the increase in probability of escape of synthesis gas as well as UCG by-products and contaminants. Low coal and overburden permeabilities are helpful in the light of controlling the subsurface water flow around as well as into and out of the UCG reactor. Steam jacket dynamics in UCG reactor vicinity were completely out of consideration in previous UCG literature.

These general findings are certainly site-specific, but will have a determining influence if UCG becomes economically feasible in the next decades as expected by several authors (Mostade, 2014; Sarhosis et al., 2016). However, since all the conclusions and findings of this thesis are based on numerical simulations and the corresponding input parameters, further field and laboratory tests are required to verify the accuracy of the present numerical results as well as implemented temperature-dependent rock properties.

In order to enable more precise predictions of UCG performance, future work should be directed towards implementing non-isotropic permeability into a multilayer model system as well as matrix and cleat permeabilities. Coal permeability is controlled by fractures that encompass natural

systems and any induced fractures (Thompson, 1978). In the presented MUFITS model approach, matrix permeability was used only. Fluid flow in porous media is often through conductive fractures surrounded by relatively stagnant porous volume into which contaminants can diffuse (Camp and White, 2015). Any oscillatory flow (e.g., various reactor pressure, barometric pumping) will spread contaminants. Once UCG fluids have diffused onto the dead pore volume and/or sorbed, it takes much longer contact with clean water to desorb them. Transport models that have dual permeability (fracture and matrix) are helpful in representing such transport (Camp and White, 2015).

Moreover, it is recommended to consider mechanically and thermally-induced permeability changes in the close reactor vicinity by a thermo-hydro-mechanical coupling in future investigations, to account for changes of groundwater flow behavior after potential UCG reactor collapses. In this context, also the effect of hydraulic short circuits and presence of high permeable faults including their potential reactivation, which may introduce preferential migration pathways for UCG fluids and contaminants, needs to be addressed. However, this coupled thermo-hydro-mechanical modeling approach was consciously not taken into account for the third part of the present study for the following reasons. Many of the published sequential hydro-mechanical coupling approaches are error-prone if inter-loop equilibration is not considered in the coupling (Akbarzadeh Kasani, 2016), since neglecting the undrained fluid-mechanical response effect introduces errors proportional to fluid diffusivity and inversely proportional to the rate of mechanical change (Taron and Elsworth, 2009). Consequently, a much more complex hydro-mechanical sequential coupling procedure than the so-called 'leapfrog coupling' as discussed by Kim et al. (2009; 2012; 2013), is required to produce reliable simulation results in presence of highly compressible fluids, e.g. the fixed-stress approach. Therefore, the high complexity of the coupled thermo-hydraulic processes requires a proper understanding of the heretofore largely neglected steam jacket dynamics and UCG water balances first, before considering thermo-hydro-mechanical coupled models.

Besides the application in the special context of UCG, the presented numerical modeling approach can be used to investigate and evaluate regions with potentially suitable host rock formations for geologic nuclear waste repositories in the near- and far-field (Alexander et al., 2015; Gomez et al., 2016; Min et al., 2005; Stephansson and Min, 2004; Zang et al., 2012, 2013). The requirements of the modeling approaches as well as the implementation of boundary conditions and rock properties are highly similar. Compared to UCG, these may differ in the time scales of the relevant processes, but need to consider lower temperatures at the same time. Here, numerical simulations with temperature-dependent rock properties could improve quantification and predictions of deformations, damage and healing behavior of rock as well as safety margins against failure. Due to the high safety requirements, the search for a repository is still an ongoing process. Additionally, sinkhole formation in the context of *in situ* leaching (Kinscher et al., 2015), resulting from dissolution and mechanical erosion of rocks and sediments in the subsurface is a geological phenomenon, which can be investigated with similar modeling approaches (Al-Halbouni et al., 2017; Holohan et al., 2011). Due to the growing global energy demand and increasingly limited availability of conventional or easy-to-produce crude oils, extensive attention is being paid to the exploitation of unconventional heavy and extra-heavy oils (Guo et al., 2016). The existing *in situ* heavy oil recovery techniques fall into three categories of thermal injection, chemical injection and gas injection (Guo et al., 2016). Within the framework of the thermal

injection research topic similar modeling approaches are used in order to improve the pressure-volume-temperature performance of heavy crude oil (Dong et al., 2015), to study the influence of injection parameters on the profiles of superheated steam in the wellbore (Sun et al., 2017) and to optimize the injection temperature for enhanced oil recovery (Bordeaux Rego et al., 2017).

REFERENCES

Adhikary D, Khanal M, Jayasundara C, Balusu R. (2016). Deficiencies in 2D Simulation: A Comparative Study of 2D Versus 3D Simulation of Multi-seam Longwall Mining. Rock Mechanics and Rock Engineering 49(6): 2181–2185. DOI: 10.1007/s00603-015-0842-7.

Afanasyev A. (2015a). MUFITS Reference Manual. http://www.mufits.imec.msu.ru/.

Afanasyev AA. (2012). Simulation of the properties of a binary carbon dioxide-water mixture under sub- and supercritical conditions. High Temperature 50(3): 340–347. DOI: 10.1134/S0018151X12030017.

Afanasyev AA. (2013a). Application of the reservoir simulator MUFITS for 3D modlling of CO_2 Storage in geological formations. Energy Procedia 40: 365–374. DOI: 10.1016/j.egypro.2013.08.042.

Afanasyev AA. (2013b). Multiphase compositional modelling of CO_2 injection under subcritical conditions: The impact of dissolution and phase transitions between liquid and gaseous CO_2 on reservoir temperature. International Journal of Greenhouse Gas Control 19: 731–742. DOI: 10.1016/j.ijggc.2013.01.042.

Afanasyev AA. (2015b). Hydrodynamic Modelling of Petroleum Reservoirs using Simulator MUFITS. Energy Procedia 76: 427–435. DOI: 10.1016/j.egypro.2015.07.861.

Afanasyev A, Costa A, Chiodini G. (2015). Investigation of hydrothermal activity at Campi Flegrei caldera using 3D numerical simulations: Extension to high temperature processes. Journal of Volcanology and Geothermal Research 299: 68–77. DOI: 10.1016/j.jvolgeores.2015.04.004.

Afanasyev A, Kempka T, Kühn M, Melnik O. (2016). Validation of the MUFITS Reservoir Simulator Against Standard CO_2 Storage Benchmarks and History-matched Models of the Ketzin Pilot Site. Energy Procedia 97: 395–402. DOI: 10.1016/j.egypro.2016.10.032.

Aiman WR, Thorsness CB, Hill RW, Rozsa RB, Cena R, Gregg DW, Stephens DR. (1978). The Hoe Creek II Field Experiment On Underground Coal Gasification, Preliminary Results. Combustion Institute/Western States Section, Spring Meeting, 17-18 April, Boulder, Colorado, 7 pp.

Akbarzadeh H, Chalaturnyk RJ. (2013). Coupled Fluid-Thermal-Mechanical Analyses of a Deep Underground Coal Gasification Cavity. Quest Journals Journal of Architecture and Civil Engineering 1(1): 1–14.

Akbarzadeh H, Chalaturnyk RJ. (2014a). Structural changes in coal at elevated temperature pertinent to underground coal gasification: A review. International Journal of Coal Geology 131: 126–146. DOI: 10.1016/j.coal.2014.06.009.

Akbarzadeh H, Chalaturnyk RJ. (2014b). Sequentially coupled flow-geomechanical modeling of underground coal gasification for a three-dimensional problem. Mitigation and Adaptation Strategies for Global Change 21: 577–594. DOI: 10.1007/s11027-014-9583-2.

Akbarzadeh Kasani H. (2016). Reservoir-Geomechanics of Underground Coal Gasification (UCG). Ph.D. Thesis, University of Alberta, Edmonton, Alberta, Canada. DOI: 10.7939/R3SB3X40J.

Akbarzadeh Kasani H, Chalaturnyk RJ. (2017). Coupled reservoir and geomechanical simulation for a deep underground coal gasification project. Journal of Natural Gas Science and Engineering. 37: 487–501. DOI: 10.1016/j.jngse.2016.12.002.

Al-Halbouni D, Holohan EP, Saberi L, Alrshdan H, Sawarieh A, Closson D, Walter TR, Dahm T. (2017). Sinkholes, subsidence and subrosion on the eastern shore of the Dead Sea as revealed by a close-range photogrammetric survey. Geomorphology 285: 305–324. DOI: 10.1016/j.geomorph.2017.02.006.

Alexander WR, Reijonen HM, McKinley IG. (2015). Natural analogues: studies of geological processes relevant to radioactive waste disposal in deep geological repositories. Swiss Journal of Geosciences (108): 75–100. DOI: 10.1007/s00015-015-0187-y.

Badzioch S, Gregory DR, Field MA. (1964). Investigation of the temperature variation of thermal conductivity and thermal diffusivity of coal. Fuel 43: 267–280.

Balley AC, Bartlett F, Boswinkel HH, Bruining J, Chandelle V, Del Amor G, Garstang JH, Hewel-Bundermann H, Hewing G, Krablell K, Ledent P, Li T k:, Mostade M, Olivier JGJ, Patigny J, Pottler J, Witte P. (1989). The Future Development of Underground Coal Gasification in Europe - A Comprehensive Report to CEC. Work performed under Amendment No 2a of contract LG 02-1-78 for CEC. European Working Group on UCG.

Barbour FA, Covell JR. (1988). Trace Gas, Product Water, and Particulate Characterization for Rocky Mountain 1 UCG Project. Underground Coal Gasification Test Hanna, Wyoming. Western Research Institute, University of Wyoming Research Corporation: Laramie, Wyoming, USA, 105 pp.

Barr-Howell BD, Howell JM, Peppas NA. (1985). Thermoplastic and Viscoelastic Properties of Coal. Abstract of Papers of the American Chemical Society 189: 64–70.

Bartke TC, Fischer DD, King SB, Boyd RM, Humphrey AE. (1985a). Volume 3: The Hanna II, Phase I Field Test. Hanna, Wyoming Underground Coal Gasification Data Base, 52 pp.

Bartke TC, Fischer DD, King SB, Boyd RM, Humphrey AE. (1985b). Volume 4: The Hanna II, Phase II and III Field Test. Hanna, Wyoming Underground Coal Gasification Data Base, 62 pp.

Bauer SJ, Johnson B. (1979). Effects of Slow Uniform Heating on the Physical Properties of the Westerly and Charcoal Granites. 20th U.S. Symposium on Rock Mechanics (USRMS). American Rock Mechanics Association, 7–18.

Bernabe Y. (1987). The effective pressure law for permeability during pore pressure and confining pressure cycling of several crystalline rocks. Journal of Geophysical Research 92(B1): 649. DOI: 10.1029/JB092iB01p00649.

BGR. (2015). Reserves, Resources and Availability of Energy Resources. Federal Institute for Geosciences and Natural Resources (BGR), Energy study 2015, https://www.bgr.bund.de/EN/Themen/Energie/Downloads/energiestudie_2015_en.html.

Bhutto AW, Bazmi AA, Zahedi G. (2013). Underground coal gasification: From fundamentals to applications. Progress in Energy and Combustion Science 39(1): 189–214. DOI: http://dx.doi.org/10.1016/j.pecs.2012.09.004.

Biezen ENJ. (1996). Modeling Underground Coal Gasification. Ph.D. Thesis, Delft University of Technology, Delft, The Netherlands. uuid:6c2d9563-a8f5-4514-8bd9-f72c66ce1e83.

Blinderman MS. (2016). Ergo Exergy Technologies Inc., Montreal, QC, Canada. Personal communication.

Blinderman MS, Anderson B. (2004). Underground Coal Gasification for Power Generation: High Efficiency and CO_2-Emissions. ASME 2004 Power Conference. ASME, 473–479. DOI: 10.1115/POWER2004-52036.

Blinderman MS, Jones RM. (2002). The Chinchilla IGCC Project to Date: Underground Coal Gasification and Environment. Gasification Technologies Conference, San Francisco, USA, October 27-30, 14 pp.

Blinderman MS, Saulov DN, Klimenko AY. (2008). Forward and reverse combustion linking in underground coal gasification. Energy 33(3): 446–454. DOI: DOI: 10.1016/j.energy.2007.10.004.

Boger C, Marshall JS, Pilcher RC. (2014). Chapter 18 – Worldwide Coal Mine Methane and Coalbed Methane Activities. Coal Bed Methane, 351–407. DOI: 10.1016/B978-0-12-800880-5.00018-8.

Bordeaux Rego F, Botechia VE, Schiozer DJ. (2017). Heavy oil recovery by polymer flooding and hot water injection using numerical simulation. Journal of Petroleum Science and Engineering. 153(February): 187–196. DOI: 10.1016/j.petrol.2017.03.033.

Boysen JE. (1978). Daily Material and Energy Balances for the Hanna Field Tests. Report: LETC Internal Document; Department of Energy Laramie Energy Technology Center: Laramie,WY, USA.

Brandenburg CF, Fischer DD, Boyd RM, King SB, Humphrey AE. (1977). A review of LERC's in situ coal gasification project. Proceeding 3rd Annual UCC Symposium; Fallen Leaf Lake, CA, USA 6-9 June. South Lake Tahoe, 66–76.

Britten J., Thorsness CB. (1989). A model for cavity growth and resource recovery during UCG. In Situ 13(1&2): 1–53.

Brown SR, Bruhn RL. (1998). Fluid permeability of deformable fracture networks. Journal of Geophysical Research 103(B2): 2489-2500. DOI: 10.1029/97JB03113.

Budzianowski WM. (2012). Value-added carbon management technologies for low CO_2 intensive carbon-based energy vectors. Energy 41(14): 280–297.

Burton E, Friedmann J, Upadhye R. (2006). Best Practices in Underground Coal Gasification. Contract No. W-7405-Eng-48, Lawrence Livermore National Laboratory: Livermore, CA, USA.

Buscheck T, Hao Y, Morris JP, Burton E. (2009). Thermal-Hydrological Sensitivity Analysis of Underground Coal Gasification. Proceedings of the 2009 International Pittsburgh Coal Conference, Pittsburgh PA, USA, 8 pp.

Byerlee J. (1978). Friction of Rocks. Pure & Applied Geophysics 116: 615–626. DOI: 10.1007/BF00876528.

Cała M, Stopkowicz A, Kowalska M, Blajer M. (2014). Modelling of thermal phenomena in the rock mass in the vicinity of a georeactor. Przegląd Górniczy 11(82): 76–85.

Camp D, White J. (2015). Underground Coal Gasification: An Overview of Groundwater Contamination Hazards and Mitigation Strategies. Report No.: LLNL-TR-668633; Lawrence Livermore National Laboratory: Livermore, CA, USA, 134 pp.

Camp DW. (1980). A model of water influx for underground coal gasification. MS Thesis, University of Colorado, Boulder, CO, USA.

Camp DW, Krantz WB, Gunn RD. (1980). A Water-Influx Model for UCG with Spalling-Enhanced Drying. 15th Intersociety Energy Conversion Engineering Conference. Western Research Institute (WRI), 8 pp.

Campbell GG, Brandenburg CF, Boyd RM, Sterner TE. (1975). Underground Coal Gasification at Hanna, Wyoming. Proceedings of Thermal Power Conference, Washington State University, Pullman, WA, USA. Laramie Aramie Energy Research Center Laramie, 22 pp.

Campbell JH, Wang FT, Mead SW, Busby JF. (1979). Groundwater quality near an underground coal gasification experiment. Journal of Hydrology 44(3–4): 241–266. DOI: 10.1016/0022-1694(79)90134-3.

Cappa F, Rutqvist J. (2011). Modeling of coupled deformation and permeability evolution during fault reactivation induced by deep underground injection of CO_2. International Journal of Greenhouse Gas Control 5: 336–346. DOI: 10.1016/j.ijggc.2010.08.005.

Catton H, Lee S. (1987). Two-Phase Flow in Porous Medium. ASME/JSME Thermal Engineering Joint Conference Proceedings, ed. Marto and I. Tanasawa, Vol. 2, NY, USA, 333–341.

Chandelle V, Jacquemin C, Létolle R, Mostade M, Pirard J-P, Somers Y. (1993). Underground coal gasification on the Thulin site: results of analysis from post-burn drillings. Fuel 72(7): 949–963. DOI: Doi: 10.1016/0016-2361(93)90292-a.

Chećko J. (2013). Analysis of geological, hydrogeological and mining conditions in the area of the developed georeactor located in KWK "Wieczorek" mine. Przegląd Górniczy 69/2: 37–45.

Chin LY, Rajagopal R, Thomas LK. (2000). Fully Coupled Geomechanics and Fluid-Flow Analysis of Wells With Stress-Dependent Permeability. SPE Journal 5(1): 2–6. DOI: 10.2118/58968-PA.

Clauser C, Huenges E. (1995). Rock Physics & Phase Relations: A Handbook of Physical Constants. In: Ahrens TJ (ed) Rock Physics & Phase Relations: A Handbook of Physical Constants. American Geophysical Union: Washington, D.C., USA, 105–126. DOI: 10.1029/RF003.

Corkum AG, Board MP. (2016). Numerical analysis of longwall mining layout at Solvay Mine, Wyoming. International Journal of Rock Mechanics & Mining Sciences 89: 94–108. DOI: 10.1016/j.ijrmms.2016.09.001.

Couch G. (2009). Underground coal gasification. CCC/151, IEA Clean Coal Centre. CCC/151, IEA Clean Coal Centre: London.

Cui Y, Liang J, Wang Z, Zhang X, Fan C, Liang D, Wang X. (2014). Forward and reverse combustion gasification of coal with production of high-quality syngas in a simulated pilot system for in situ gasification. Applied Energy 131: 9–19.

Daggupati S, Mandapati RN, Mahajani SM, Ganesh A, Mathur DK, Sharma RK, Aghalayam P. (2010). Laboratory studies on combustion cavity growth in lignite coal blocks in the context of underground coal gasification. Energy 35(6): 2374–2386. DOI: 10.1016/j.energy.2010.02.015.

Daggupati S, Mandapati RN, Mahajani SM, Ganesh A, Pal AK, Sharma RK, Aghalayam P. (2011). Compartment Modeling for Flow Characterization of Underground Coal Gasification Cavity. Industrial & Engineering Chemistry Research 50(1): 277–290. DOI: 10.1021/ie101307k.

David C, Menendez B, Darot M. (1999). Influence of stress-induced and thermal cracking on physical properties and microstructure of La Peyratte granite. International Journal of Rock Mechanics and Mining Sciences 36(4): 433–448. DOI: 10.1016/S0148-9062(99)00010-8.

David C, Wong TF, Zhu W, Zhang J. (1994). Laboratory measurement of compaction-induced permeability change in porous rocks: Implications for the generation and maintenance of pore pressure excess in the crust. Pure and Applied Geophysics 143(1–3): 425–456. DOI: 10.1007/BF00874337.

Dong X, Liu H, Hou J, Zhang Z, Chen Z. (2015). Multi-thermal fluid assisted gravity drainage process: A new improved-oil-recovery technique for thick heavy oil reservoir. Journal of Petroleum Science and Engineering 133: 1–11. DOI: 10.1016/j.petrol.2015.05.001.

DTI. (2004). Review of the feasibility of underground coal gasification in the UK. Department of Trade and Industry Report (September): 64 pp. http://www.cluffnaturalresources.com/wp-content/uploads/2016/01/2004-Review-of-Feasibility-of-UCG-in-the-UK.pdf.

Durucan S, Korre A, Shi J-Q, Idiens M, Stańczyk K, Kapusta K, Rogut-Dabrowska A, Kempka T, Wolf K-H, Younger P, Zavsek S, Poulsen NE, Bojda D, Franzsen S, Muresan M, Gao J, Beath A, Mastalerz M. (2014). TOPS: Technology Options for Coupled Underground Coal Gasification and CO_2 Capture and Storage. Energy Procedia 63: 5827–5835. DOI: 10.1016/j.egypro.2014.11.616.

Edenhofer O, Pichs-Madruga R, Sokona Y, Seyboth K, Eickemeier P, Matschoss P, Hansen G, Kadner S, Schlömer S, Zwickel T, Stechow C Von. (2011). IPCC, 2011: Summary for Policymakers. In: IPCC Special Report on Renewable Energy Sources and Climate Change Mitigation. Cambridge University Press, 246 pp. DOI: 10.5860/CHOICE.49-6309.

Eftekhari AA, Van Der Kooi H, Bruining H. (2012). Exergy analysis of underground coal gasification with simultaneous storage of carbon dioxide. Energy 45(1): 729–745. DOI: 10.1016/j.energy.2012.07.019.

Eftekhari AA, Wolf KH, Rogut J, Bruining H. (2015). Mathematical modeling of alternating injection of oxygen and steam in underground coal gasification. International Journal of Coal Geology 150–151: 154–165. DOI: 10.1016/j.coal.2015.08.008.

Elahi SM, Chen Z. (2016). Geomechanical Simulation of Underground Coal Gasification. American Rock Mechanics Association 16(880): 1-13.

Evans BW, Kohlstedt DL. (1995). Rheology of rocks. Rock Physics and Phase Relations: A Handbook of Physical Constants. 148–165. DOI: 10.1029/RF003p0148.

Feng Z, Zhao Y, Wan Z. (2017). Effect of Temperature on Deformation of Triaxially Stressed Anthracite. Rock Mechanics and Rock Engineering 50(4): 1073–1078. DOI: 10.1007/s00603-016-1135-5.

Fischer DD, King SB, Humphrey AE. (1975). A report on the successful development of Underground Coal Gasification at Hanna, Wyoming. Energy Research and Development Administration, Laramie Energy Research Center, Wyoming: Laramie, Wyoming, USA. DOI: 10.2307/25303439.

Friedmann SJ, Upadhye R, Kong FM. (2009). Prospects for underground coal gasification in carbon-constrained world. Energy Procedia 1: 4551–4557.

Gercek H. (2007). Poisson's ratio values for rocks. International Journal of Rock Mechanics and Mining Sciences 44(1): 1–13. DOI: 10.1016/j.ijrmms.2006.04.011.

Geuzaine C, Remacle J-F. (2009). Gmsh: a three-dimensional finite element mesh generator with built-in pre- and post-processing facilities. International Journal for Numerical Methods in Engineering 79: 1309-1331.

Gomez P, Detournay C, Hart R, Nelson M. (2016). Applied Numerical Modeling in Geomechanics – 2016 - FLAC3D. Proceedings of the 4th Itasca Symposium on Applied Numerical Modeling in Geomechaniccs.

González-Eguino M, Olabe A, Ribera T. (2017). New Coal-Fired Plants Jeopardise Paris Agreement. Sustainability 9(2): 168. DOI: 10.3390/su9020168.

Gunn RD. (1979). Material Balance: Its Applications and Mis-applications in Underground Coal Gasification. Laramie Energy Technology Center, Report, LETC/RI- 79105.

Gunn RD, Krantz WB. (1987). Underground Coal Gasification: Development of Theory, Laboratory Experimentation, Interpretation & Correlation With the Hanna Field Tests. Department of Energy Office of Fossil Energy Morgantown Energy Technology Center, Final Report: DE-AS20-80LC 10442.

Guo K, Li H, Yu Z. (2016). In-situ heavy and extra-heavy oil recovery: A review. Fuel 185: 886–902. DOI: 10.1016/j.fuel.2016.08.047.

Haifeng W, Yuanping C, Lei W. (2012). Regional gas drainage techniques in Chinese coal mines. International Journal of Mining Science and Technology 22(6): 873–878. DOI: 10.1016/j.ijmst.2012.11.002.

Hajpál M, Török Á. (1998). Petrophysical and Mineralogical Studies of Burnt Sandstones. 2nd International PhD Symposium in Civil Engineering, Budapest, Hungary, 6–8 August 1998, 1–9.

Hasegawa HS, Wetmiller RJ, Gendzwill DJ. (1989). Induced seismicity in mines in Canada-An overview. Pure and Applied Geophysics. 129(3–4): 423–453. DOI: 10.1007/BF00874518.

Hettema MHH, De Pater CJ, Wolf K-H. (1992). High temperature properties of roof rock of coal. Proceedings of the ISRM Symposium, Eurock'92, Chester, UK, 93–98.

Hettema MHH, Wolf K-H, De Pater CJ. (1998). The influence of steam pressure on thermal spalling of sedimentary rock: Theory and experiments. International Journal of Rock Mechanics and Mining Sciences 35(1): 3–15. DOI: 10.1016/S0148-9062(97)00318-5.

Hettema MHH, Wolf K-H, Pater CJ De. (1993). Thermo-mechanical properties of roof rock of coal for underground gasification. Topics in Applied Mechanics. Springer: Berlin, Germany.

Hewing G, Hewel-Bundermann H, Krabiell K, Witte P. (1978). Post-1987 R & D Studies of Underground Coal Gasification. Research Association for Second-Generation Coal Extraction: Essen, Germany.

Holohan EP, Schöpfer MPJ, Walsh JJ. (2011). Mechanical and geometric controls on the structural evolution of pit crater and caldera subsidence. Journal of Geophysical Research 116(7): 1–23. DOI: 10.1029/2010JB008032.

Hudson JA, Backstrom A, Rutqvist J, Jing L, Backers T, Chijimatsu M, Rinne M, Neretnieks I, Pan PZ, Lee H-S, Koyama T, Feng X-T, Christiansson R, Kobayashi A, Shen B-T. (2008). Characterising and modelling the excavation damaged zone (EDZ) in crystalline rock in the context of radioactive waste disposal. Environmental Geology 57: 1275–1297.

Humenick M. (1978). Groundwater pollutants from underground coal gasification. Water Research 12(7): 463–469. DOI: 10.1016/0043-1354(78)90153-7.

IEA. (2015). Key Coal Trends. International Energy Agency Report, 22 pp. http://www.iea.org/publications/freepublications/publication/KeyCoalTrends.pdf.

IEA. (2016). World Energy Outlook 2016. International Energy Agency: Paris, France, 28 pp. https://www.eia.gov/forecasts/aeo/data/browser/#/?id=8-AEO2016&cases=ref2016~ref_no_cpp&-sourcekey=0.

Imran M, Kumar D, Kumar N, Qayyum A, Saeed A, Shamim M. (2014). Environmental concerns of underground coal gasification. Renewable and Sustainable Energy Reviews 31: 600–610. DOI: 10.1016/j.rser.2013.12.024.

Itasca Consulting Group. (2014). Inc. Advanced Three-Dimensional Continuum Modelling for Geotechnical Analysis of Rock, Soil and Structural Support. Itasca Consulting Group, Inc.: Minneapolis, MN, USA.

Jacquey AB, Cacace M, Blöcher G, Scheck-Wenderoth M. (2015). Numerical Investigation of Thermoelastic Effects on Fault Slip Tendency during Injection and Production of Geothermal Fluids. Energy Procedia 76: 311–320. DOI: 10.1016/j.egypro.2015.07.868.

Jarosinski M. (2005a). Recent tectonic stress regime in Poland based on analyses of hydraulic fracturing of borehole walls. Przeglad Geologiczny 53(10/I): 863–872.

Jarosinski M. (2005b). Ongoing tectonic reactivation of the Outer Carpathians and its impact on the foreland: Results of borehole breakout measurements in Poland. Tectonophysics 410(1–4): 189–216. DOI: 10.1016/j.tecto.2004.12.040.

Jarosinski M. (2006). Recent tectonic stress field investigations in Poland: a state of the art. Geological Quarterly 50(3): 303–321.

Kapusta K, Stańczyk K. (2011). Pollution of water during underground coal gasification of hard coal and lignite. Fuel 90(5): 1927–1934. DOI: 10.1016/j.fuel.2010.11.025.

Kapusta K, Stańczyk K, Wiatowski M, Chećko J. (2013). Environmental aspects of a field-scale underground coal gasification trial in a shallow coal seam at the Experimental Mine Barbara in Poland. Fuel 113: 196–208. DOI: https://doi.org/10.1016/j.fuel.2013.05.015.

Karacan CÖ, Ruiz FA, Cotè M, Phipps S. (2011). Coal mine methane: A review of capture and utilization practices with benefits to mining safety and to greenhouse gas reduction. International Journal of Coal Geology 86(2–3): 121–156. DOI: 10.1016/j.coal.2011.02.009.

Kempka T, Fernández-Steeger T, Li DY, Schulten M, Schlüter R, Krooss BM. (2011a). Carbon dioxide sorption capacities of coal gasification residues. Environmental Science and Technology 45(4): 1719–1723. DOI: 10.1021/es102839x.

Kempka T, Nakaten N, Schlüter N, Azzam R. (2009). Economic viability of in-situ coal gasification with downstream CO_2 storage. Glückauf Mining Reporter 1: 43–50.

Kempka T, Plötz M-L, Schlüter R, Hamann J, Deowan SA, Azzam R. (2011b). Carbon dioxide utilisation for carbamide production by application of the coupled UCG-urea process. Energy Procedia 4: 2200–2205. DOI: 10.1016/j.egypro.2011.02.107.

Khadse A, Qayyumi M, Mahajani S, Aghalayam P. (2007). Underground coal gasification: A new clean coal utilization technique for India. Energy 32(11): 2061–2071. DOI: 10.1016/j.energy.2007.04.012.

Khan M, Mmbaga J, Shirazi A, Trivedi J, Liu Q, Gupta R. (2015). Modelling Underground Coal Gasification—A Review. Energies 8(11): 12603–12668. DOI: 10.3390/en81112331.

Kim J, Moridis G, Yang D, Rutqvist J. (2012). Numerical Studies on Two-Way Coupled Fluid Flow and Geomechanics in Hydrate Deposits. SPE Journal 17(2): 485–501. DOI: 10.2118/141304-PA.

Kim J, Tchelepi H a, Stanford U, Juanes R. (2009). Stability, Accuracy and Efficiency of Sequential Methods for Coupled Flow and Geomechanics. Society of Petroleum Engineers (November 2008): 1–20. DOI: 10.2118/119084-PA.

Kim J, Tchelepi HA, Juanes R. (2013). Rigorous Coupling of Geomechanics and Multiphase Flow With Strong Capillarity. SPE Journal (December): 1123–1139. DOI: 10.2118/141268-PA.

Kinscher J, Bernard P, Contrucci I, Mangeney A, Piguet JP, Bigarre P. (2015). Location of microseismic swarms induced by salt solution mining. Geophysical Journal International 200(1): 337–362. DOI: 10.1093/gji/ggu396.

Klebingat S, Kempka T, Schulten M, Azzam R, Fernandez-Steeger TM. (2016). Innovative thermodynamic underground coal gasification model for coupled synthesis gas quality and tar production analyses. Fuel 183: 680–686. DOI: 10.1016/S1532-0464(03)00032-7.

Klimenko AY. (2009). Early Ideas in Underground Coal Gasification and Their Evolution. Energies 2(2): 456–476. DOI: 10.3390/en20200456.

Koledoye BA, Aydin A, May E. (2003). A new process-based methodology for the analysis of shale smear along normal faults in the Niger Delta. AAPG Bulletin 87(3): 445–463.

Krantz WB, Camp DW, Gunn RD. (1980). A Water-Influx Model for UCG. Proceedings of the Sixth Underground Coal Conversion Symposium, Shangri-La, Oklahoma, July 13 - 17, USA, 21–31.

Kühn M, Zeeb C, Gessner K. (2005). 2D or not 2D: Are two dimensions enough to accurately model convective fluid flow through faults and surrounding host rocks? Geophysical Research Abstracts 7(1): 1-8.

LaFleur DW, Grisak GE, Stetzenbach KJ, Thompson GM. (1984). Evaluation of the Porosity of the Hanna No. 1 Coal Seam. Department of Energy Laramie Energy Technology Center, Final Report: DE-AS2D-83LC10987.

Lee SC. (1984). Computational method for thermoviscoelasticity with application to rock mechanics. Ph.D. Thesis, Ohio State University, Columbus, USA. http://adsabs.harvard.edu/abs/1984PhDT.....9L.

Levie BE, Krantz WB, Camp DW, Gunn RD. (1980). Application of the Spalling-Enhanced-Drying Model in Predicting Cavity Geometry and Operating Strategy for the Hanna 2, Phase 2 UCG Field Test. 1–10.

Li H, Guo G, Zha J, Yuan Y, Zhao B. (2015). Research on the surface movement rules and prediction method of underground coal gasification. Bulletin of Engineering Geology and the Environment 75(3): 1133-1142. DOI: 10.1007/s10064-015-0809-7.

Liberatore AJ, Wilson MW. (1983). Field Scale Experiment in UCG of coal at pricetown, Morgantown Energy Technology Center Report: DE83011052, West Virginia, USA.

Ligtenberg JH. (2005). Detection of Fluid migration pathways in seismic data: Implications for fault seal analysis. Basin Research 17(1): 141–153. DOI: 10.1111/j.1365-2117.2005.00258.x.

Liu S, Li J, Mei M, Dong D. (2007). Groundwater Pollution from Underground Coal Gasification. Journal of China University of Mining and Technology 17(4): 467–472. DOI: 10.1016/S1006-

1266(07)60127-8.

Liu X, Yuan S, Sieffert Y, Fityus S, Buzzi O. (2016a). Changes in Mineralogy, Microstructure, Compressive Strength and Intrinsic Permeability of Two Sedimentary Rocks Subjected to High-Temperature Heating. Rock Mechanics and Rock Engineering 49(8): 1–14. DOI: 10.1007/s00603-016-0950-z.

Liu X, Zhang C, Yuan S, Fityus S, Sloan SW, Buzzi O. (2016b). Effect of High Temperature on Mineralogy, Microstructure, Shear Stiffness and Tensile Strength of Two Australian Mudstones. Rock Mechanics and Rock Engineering 49(9): 3513-3524. DOI: 10.1007/s00603-016-1024-y.

Luo Y, Coertzen M, Dumble S. (2009). Comparison of UCG Cavity Growth With CFD Model Predictions. Proceedings of the Seventh International Conference on CFD in the Minerals and Process Industries CSIRO. Melbourne, 1–5.

Małkowski P, Niedbalski Z, Hydzik-Wiśniewska J. (2013). The Change of Structural and Thermal Properties of Rocks Exposed to High Temperatures in the Vicinity of Designed Geo-Reactor. Archives of Mining Sciences 58(2): 465–480. DOI: 10.2478/amsc-2013-0031.

McKee CR, Santoro RD. (1980). Gas leakage and water influx from in situ coal gasification. Department of Energy: Laramie Energy Technology Center, Contract No. DE-AP-20-80-LC00193. 18 pp. hdl.handle.net/10176/wyu:10455.

Min K-B, Lee J, Stephansson O. (2013). Implications of thermally-induced fracture slip and permeability change on the long-term performance of a deep geological repository. International Journal of Rock Mechanics and Mining Sciences 61: 275–288. DOI: 10.1016/j.ijrmms.2013.03.009.

Min K-B, Rutqvist J, Tsang C-F, Jing L. (2004). Stress-dependent permeability of fractured rock masses: a numerical study. International Journal of Rock Mechanics and Mining Sciences 41(7): 1191–1210. DOI: 10.1016/j.ijrmms.2004.05.005.

Min K-B, Rutqvist J, Tsang C-F, Jing L. (2005). Thermally induced mechanical and permeability changes around a nuclear waste repository—a far-field study based on equivalent properties determined by a discrete approach. International Journal of Rock Mechanics and Mining Sciences 42(5–6): 765–780. DOI: 10.1016/j.ijrmms.2005.03.014.

Min OK. (1983). Finite Element Modeling of Thermo-Mechanical Responses Associated with Underground Coal Conversion. Ph.D. Thesis, Ohio State University, Columbus, OH, USA. DOI: 10.1017/CBO9781107415324.004.

Moorhouse J, Huot M, McCulloch M. (2010). Underground Coal Gasification - Environmental Risks and Benefits. A Preliminary Review by the Pembina Institute. 41 pp. DOI: 10.1002/aic.690240502.

Morris J, Buscheck T, Hao Y. (2009). Coupled Geomechanical Simulations of UCG Cavity Evolution. Proceedings of the 2009 International Pittsburgh Coal Conference, Pittsburgh PA, USA, 11 pp.

Mortazavi HR. (1989). Rubbling and structural stability of underground coal gasification reactors. Ph.D. Thesis, University of Washington, Seattle, WA, USA. http://www.mdpi.com/1996-1073/8/6/5800/.

Mostade M. (2014). Underground Coal Gasification (UCG) - the Path to Commercialization. CPSI Journal 6(15): 18–37. http://www.academia.edu/25152766/Underground_Coal_Gasification_UCG_the_Path_to_Commercialization.

Najafi M, Jalali SME, KhaloKakaie R. (2014). Thermal–mechanical–numerical analysis of stress

distribution in the vicinity of underground coal gasification (UCG) panels. International Journal of Coal Geology 134–135: 1–16. DOI: 10.1016/j.coal.2014.09.014.

Najafi M, Jalali SME, KhaloKakaie R, Forouhandeh F. (2015). Prediction of cavity growth rate during underground coal gasification using multiple regression analysis. International Journal of Coal Science & Technology 2(4): 318–324. DOI: 10.1007/s40789-015-0095-9.

Nakaten N, Azzam R, Kempka T. (2014a). Sensitivity analysis on UCG–CCS economics. International Journal of Greenhouse Gas Control 26: 51–60. DOI: 10.1016/j.ijggc.2014.04.005.

Nakaten N, Islam R, Kempka T. (2014b). Underground Coal Gasification with Extended CO_2 Utilization - An Economic and Carbon Neutral Approach to Tackle Energy and Fertilizer Supply Shortages in Bangladesh. Energy Procedia 63: 8036–8043. DOI: 10.1016/j.egypro.2014.11.840.

Nakaten N, Kötting P, Azzam R, Kempka T. (2013). Underground Coal Gasification and CO_2 Storage Support Bulgaria's Low Carbon Energy Supply. Energy Procedia 40(0): 212–221. DOI: 10.1016/j.egypro.2013.08.025.

Nakaten N, Schlüter R, Azzam R, Kempka T. (2014c). Development of a techno-economic model for dynamic calculation of cost of electricity, energy demand and CO_2 emissions of an integrated UCG–CCS process. Energy 66: 779–790. DOI: 10.1016/j.energy.2014.01.014.

Neuzil CE. (2012). Hydromechanical effects of continental glaciation on groundwater systems. Geofluids 12(1): 22–37. DOI: 10.1111/j.1468-8123.2011.00347.x.

Nitao JJ, Camp DW, Buscheck TA, White JA, Burton GC, Wagoner JL, Chen M. (2011). Progress on a New Integrated 3-D UCG Simulator and its Initial Application. Proceedings of the International Pittsburgh Coal Conference, Pittsburgh, PA, USA, 12-15 September, 13 pp.

Nordin JS. (1992). Review of Information and Data Relevant to the Hoe Creek Underground Coal Gasification Site Restoration. Western Research Institute, The University of Wyoming Research Coporation, Report: WRI-92-R01. 68 pp.

Nourozieh H, Kariznovi M, Chen Z, Abedi J. (2010). Simulation Study of Underground Coal Gasification in Alberta Reservoirs: Geological Structure and Process Modeling. Energy & Fuels 24(6): 3540–3550. DOI: 10.1021/ef9013828.

Oliver RL, Mason GM, Spackman LK. (1989). Field and Laboratory Results From the Tono I (CRIP) Ucg Cavity Excavation Project, Widco Mine Site, Centralia, Washington. Fuel Science and Technology International 7(8): 1059–1120. DOI: 10.1080/08843758908962281.

Otto C, Kempka T. (2015a). Thermo-Mechanical Simulations of Rock Behavior in Underground Coal Gasification Show Negligible Impact of Temperature-Dependent Parameters on Permeability Changes. Energies 8(6): 5800–5827. DOI: 10.3390/en8065800.

Otto C, Kempka T. (2015b). Thermo-mechanical Simulations Confirm: Temperature-dependent Mudrock Properties are Nice to have in Far-field Environmental Assessments of Underground Coal Gasification. Energy Procedia 76: 582–591. DOI: 10.1016/j.egypro.2015.07.875.

Otto C, Kempka T. (2017). Prediction of Steam Jacket Dynamics and Water Balances in Underground Coal Gasification. Energies 10(739): 1–17. DOI: doi:10.3390/en10060739.

Otto C, Kempka T, Kapusta K, Stańczyk K. (2016). Fault Reactivation Can Generate Hydraulic Short Circuits in Underground Coal Gasification - New Insights from Regional-Scale Thermo-Mechanical 3D Modeling. Minerals 6(101): 1–23. DOI: 10.3390/www.mdpi.com/journal/minerals.

Pakala VKC. (2012). Evaporation Fronts in Porous Media. Department of Mechanical Engineering. Ph.D. Thesis, Department of Mechanical Engineering, University of Wyoming, Laramie, Wyoming, USA. DOI: 10.1017/CBO9781107415324.004.

Pana C. (2009). Review of Underground Coal Gasification with Reference to Alberta's Potential. ERCB/AGS Open File Report 2009-10, Energy Resources Conservation Board Alberta Geological Survey. 56 pp.

Perkins G, Love G. (2010). Commercialisation of Underground Coal Gasification. Chemeca 2010: Engineering at the Edge, 26-29 September, At Adelaide, USA. 12 pp.

Plumb OA, Klimenko AY. (2010). The Stability of Evaporating Fronts in Porous Media. Journal of Porous Media 13(2): 145–155.

Prabu V, Jayanti S. (2011). Simulation of cavity formation in underground coal gasification using bore hole combustion experiments. Energy. 36(10): 5854–5864. DOI: 10.1016/j.energy.2011.08.037.

Prabu V, Jayanti S. (2014). Heat-affected zone analysis of high ash coals during ex situ experimental simulation of underground coal gasification. Fuel 123: 167–174. DOI: 10.1016/j.fuel.2014.01.035.

Price NJ, Cosgrove JW. (1990). Analysis of Geological Structures. Cambridge University Press, 502 pp.

RAG Anthrazit Ibbenbüren GmbH. (2017). Kurzinformationen, Retrieved May 29, 2017, from https://www.rag.de/unter-tage/bergwerk-ibbenbueren/.

Ramasamy S, Sripada PP, Khan MM, Tian S, Trivedi J, Gupta R. (2014). Adsorption Behavior of CO_2 in Coal and Coal Char. Energy & Fuels 28(8): 5241–5251. DOI: 10.1021/ef500239b.

Roddy DJ, Younger PL. (2010). Underground coal gasification with CCS: A pathway to decarbonising industry. Energy & Environmental Science 400–407. DOI: 10.1039/b921197g.

Rutqvist J, Bäckström A, Chijimatsu M, Feng X-T, Pan P-Z, Hudson J, Jing L, Kobayashi A, Koyama T, Lee H-S, Huang X-H, Rinne M, Shen B. (2009). A multiple-code simulation study of the long-term EDZ evolution of geological nuclear waste repositories. Environmental Geology 57(6): 1313–1324. DOI: 10.1007/s00254-008-1536-1.

Rutqvist J, Rinaldi AP, Cappa F, Moridis GJ. (2013). Modeling of fault reactivation and induced seismicity during hydraulic fracturing of shale-gas reservoirs. Journal of Petroleum Science and Engineering 107: 31–44. DOI: 10.1016/j.petrol.2013.04.023.

Sajjad M, Rasul MG. (2014). Review on the Existing and Developing Underground Coal Gasification Techniques in Abandoned Coal Seam Gas Blocks : Australia and Global Context. Proceedings of 1st International e-Conference on Energies, 14–31 March, Basel, Switzerland, 16 pp. http://hdl.cqu.edu.au/10018/1029900

Sarhosis V, Lavis S, Mostade M, Thomas HR. (2016). Towards commercialising underground coal gasification in the EU. Environmental Geotechnics DOI: 10.1680/jenge.15.00044.

Sarhosis V, Yang D, Sheng Y, Kempka T. (2013). Coupled Hydro-thermal Analysis of Underground Coal Gasification Reactor Cool Down for Subsequent CO_2 Storage. Energy Procedia 40: 428–436. DOI: 10.1016/j.egypro.2013.08.049.

Sarraf A, Mmbaga JP, Gupta R, Hayes RE. (2011). Modeling cavity growth during Underground Coal

Gasification. Proceedings of the 2011 COMSOL Conference, Boston, MA, USA, 1–5.

Saulov DN, Plumb OA, Klimenko AY. (2010). Flame propagation in a gasification channel. Energy 35(3): 1264–1273. DOI: 10.1016/j.energy.2009.11.006.

Schiffer H-W, Thielemann T. (2012). Why there will be no peak coal in the foreseeable future. Open Journal of Geology 2(2): 57–64. DOI: 10.4236/ojg.2012.22006.

Seifi M, Abedi J, Chen Z. (2014). Application of porous medium approach to simulate UCG process. Fuel 116: 191–200. DOI: 10.1016/j.fuel.2013.07.091.

Seifi M, Chen Z, Abedi J. (2011). Numerical simulation of underground coal gasification using the CRIP method. The Canadian Journal of Chemical Engineering 89(6): 1528–1535. DOI: 10.1002/cjce.20496.

Self SJ, Reddy B V, Rosen M A. (2012). Review of underground coal gasification technologies and carbon capture. International Journal of Energy and Environmental Engineering 3(1): 16. DOI: 10.1186/2251-6832-3-16.

Sen AT, Cesca S, Bischoff M, Meier T, Dahm T. (2013). Automated full moment tensor inversion of coal mining-induced seismicity. Geophysical Journal International 195(2): 1267–1281. DOI: 10.1093/gji/ggt300.

Shafirovich E, Varma A. (2009). Underground Coal Gasification: A Brief Review of Current Status. Industrial & Engineering Chemistry Research 35(3): 7865–7875. DOI: 10.1021/ie801569r.

Shirazi AS, Karimipour S, Gupta R. (2013). Numerical Simulation and Evaluation of Cavity Growth in In Situ Coal Gasification. Industrial & Engineering Chemistry Research 52(33): 11712–11722. DOI: 10.1021/ie302866c.

Shoemaker HD, Shuck LZ, Haynes RR, Advani SH. (1977). The Mechanical Properties of the Pittsburgh Coal at Elevated Temperatures. Journal of Pressure Vessel Technology 99(1): 192–198. DOI: 10.1115/1.3454508.

Siemens CW. (1868). On the regenerative gas furnace as applied to the manufacture of cast steel. Journal of the Chemical Society 21: 279–310.

Singer JM, Tye RP. (1979). Thermal, mechanical, and physical properties of selected bituminous coals and cokes. U.S. Department of Interior, Bureau ofMines: Washington, DC, USA.

Sirdesai N, Singh R, Sing TN, Ranjith PG. (2015). Numerical and experimental study of strata behavior and land subsidence in an underground coal gasification project. International Association of Hydrological Sciences (November): 1–8. DOI: 10.5194/piahs-92-1-2015.

Somerton WH. (1973). Thermal Properties of Partially Liquid Saturated Rocks at Elevated Pressures and Temperatures. API Research Project 155 Final Report; University of California: Berkeley, CA, USA 36.

Somerton WH. (1992). Thermal properties and teemperature-related behavior of rock/fluid systems. Developments in Petroleum Science. Elsevier Science Publishers H.V.: Amsterdam, The Netherlands. DOI: 10.1017/CBO9781107415324.004.

Speight JG. (2005). Handbook on coal analysis. A Series on Analytical Chemistry and its Applications. John Wiley & Sons, Inc., Publication. 238 pp. DOI: 10.1002/0471718513.

Stańczyk K, Howaniec N, Smoliński A, Świądrowski J, Kapusta K, Wiatowski M, Grabowski J, Rogut

J. (2011). Gasification of lignite and hard coal with air and oxygen enriched air in a pilot scale ex situ reactor for underground gasification. Fuel 90(5): 1953–1962. DOI: 10.1016/j.fuel.2010.12.007.

Stańczyk K, Smoliński A, Kapusta K, Wiatowski M, Świądrowski J, Kotyrba A, Rogut J. (2010). Dynamic experimental simulation of hydrogen oriented underground gasification of lignite. Fuel 89(11): 3307–3314. DOI: 10.1016/j.fuel.2010.03.004.

Staúczyk K, Świądrowski J, Kapusta K, Howaniec N, Cybulski K, Rogut J, Smoliński A, Wiatowski M, Kotyrba A, Krause E, Tokarz A, Grabowski J, Ludwik-Pardała M, Bruining J, Eftekhari AA, Schuster A, Solcova O, Svoboda K, Soukup K, Landuyt P, Garot D, Śpiewak T, Szarafiński M, Niewiadomski M, Budynek P, Bednarczyk AJ, Marek A, Rzepa S, Rogosz B, Green M, Palarski J, Strozik G, Falshtynky V, Dychkowsky R, Publications R. (2012). Hydrogen-oriented underground coal gasification for Europe (HUGE). Research Fund for Coal and Steel series. DOI: 10.2777/9857.

Stephansson O, Min K. (2004). Thermo-Hydro-Mechanical (THM) Coupled Processes for Performance and Safety Assessments of Nuclear Waste Repository: Lessons Learnt from EC BENCHPAR Project. 6th European Commission Conference on Management and Disposal of Radioactive Waste (Luxemburg), 5 pp.

Stone R, Snoeberger DF. (1976). Evaluation of the Native Hydraulic Characteristics of the Felix Coal (Eocene, Wasatch Formation) and Associated Strata, Hoe Creek Site, Campbell County, Wyoming. Lawrence Livermore Laboratory, Report: UCRL-51992. 48 pp. http://uwdigital.uwyo.edu/islandora/object/wyu%3A11111

Su F, Nakanowataru T, Itakura K, Ohga K, Deguchi G. (2013). Evaluation of Structural Changes in the Coal Specimen Heating Process and UCG Model Experiments for Developing Efficient UCG Systems. Energies 6(5): 2386–2406. DOI: 10.3390/en6052386.

Suchowerska AM, Merifield RS, Carter JP, Clausen J. (2012). Prediction of underground cavity roof collapse using the Hoek–Brown failure criterion. Computers and Geotechnics 44: 93–103. DOI: 10.1016/j.compgeo.2012.03.014.

Sun F, Yao Y, Chen M, Li X, Zhao L, Meng Y, Sun Z, Zhang T, Feng D. (2017). Performance analysis of superheated steam injection for heavy oil recovery and modeling of wellbore heat efficiency. Energy 125: 795–804. DOI: 10.1016/j.energy.2017.02.114.

Sury M, White M, Kirton J, Carr P, Woodbridge R. (2004). Review of Environmental Issues of Underground Coal Gasification, DTI Cleaner Coal Programme, Report No. COAL R272 DTI/Pub URN 04/1880, http://large.stanford.edu/courses/2014/ph240/cui2/docs/file19154.pdf.

Tan Q, Luo X, Li S. (2008). Numerical modeling of thermal stress in a layered rock mass. The 42nd U.S. Rock Mechanics Symposium (USRMS). American Rock Mechanics Association.

Tang F, Wang L, Lu Y, Yang X. (2015). Thermophysical properties of coal measure strata under high temperature. Environmental Earth Sciences 73(10): 6009–6018. DOI: 10.1007/s12665-015-4364-0.

Taron J, Elsworth D. (2009). Thermal-hydrologic-mechanical-chemical processes in the evolution of engineered geothermal reservoirs. International Journal of Rock Mechanics and Mining Sciences 46(5): 855–864. DOI: 10.1016/j.ijrmms.2009.01.007.

Thompson PN. (1978). Gasifying coal underground. Endeavour 2(2): 93–97. DOI: 10.1016/0160-9327(78)90062-5.

Thompson TW, Menezes JJ, Gray KE. (1977). Roof Stability and Subsidence in In Situ Gasification of Coal. The 18th U.S. Symposium on Rock Mechanics (USRMS). American Rock Mechanics Association, 22-24 June, Golden, Colorado, USA. 5 pp.

Thorsness CB, Cena RJ. (1985). A UCG Process Data Base - Hoe Creek. Lawrence Livermore National Laboratory, Report No.: UCRL-84086: Berkeley, CA, USA.

Thorsness CB, Rozsa RB. (1978). In-Situ Coal Gasification: Model Calculations and Laboratory Experiments. Society of Petroleum Engineers Journal 18(2): 12. DOI: https://doi.org/10.2118/6182-PA.

Tian H. (2013). Development of a thermo-mechanical model for rocks exposed to high temperatures during underground coal gasification. Ph.D. Thesis, RWTH Aachen University. http://publications.rwth-aachen.de/record/209279.

Tian H, Kempka T, Xu N-X, Ziegler M. (2012). Physical Properties of Sandstones After High Temperature Treatment. Rock Mechanics and Rock Engineering 45(6): 1113–1117. DOI: 10.1007/s00603-012-0228-z.

Tian H, Kempka T, Xu N, Ziegler M. (2013). A Modified Mohr-Coulomb Failure Criterion for Intact Granites Exposed to High Temperatures. In: Hou MZ, Xie H and Were P (eds) Clean Energy Systems in the Subsurface: Production, Storage and Conversion. Springer Berlin Heidelberg: Berlin, Heidelberg, 379–393. DOI: 10.1007/978-3-642-37849-2.

Tian H, Kempka T, Yu S, Ziegler M. (2015). Mechanical Properties of Sandstones Exposed to High Temperature. Rock Mechanics and Rock Engineering 49: 321-327. DOI: 10.1007/s00603-015-0724-z.

Tian H, Ziegler M, Kempka T. (2011). Mechanical behavior of claystone exposed to high temperatures and its possible impacts on the stability of a deep nuclear waste repository. Rock mechanics: Achievements and ambitions; Cai, M., Ed.; Taylor & Francis: London, UK, 193–197.

Tian H, Ziegler M, Kempka T. (2014). Physical and mechanical behavior of claystone exposed to temperatures up to 1000 °C. International Journal of Rock Mechanics and Mining Sciences 70: 144–153. DOI: 10.1016/j.ijrmms.2014.04.014.

Tillner E, Langer M, Kempka T, Kühn M. (2016). Fault damage zone volume and initial salinity distribution determine intensity of shallow aquifer salinisation in subsurface storage. Hydrology and Earth System Sciences 20(3): 1049–1067. DOI: 10.5194/hess-20-1049-2016.

Tiwary RK. (2001). Environmental Impact of Coal Mining on Water Regime and its Management. Water, Air, and Soil Pollution (132): 185–199. DOI: 10.1023/A:1012083519667.

Tsang C-F, Bernier F, Davies C. (2005). Geohydromechanical processes in the Excavation Damaged Zone in crystalline rock, rock salt, and indurated and plastic clays—in the context of radioactive waste disposal. International Journal of Rock Mechanics and Mining Sciences 42(1): 109–125. DOI: 10.1016/j.ijrmms.2004.08.003.

UNFCCC. (2015). Adoption of the Paris Agreement. Proposal by the President. United Nations Framework Convention on Climate Change. Conference of the Parties (COP21). Paris - November 2015 21932(December): 32. DOI: FCCC/CP/2015/L.9/Rev.1.

van der Zee W. (2002). Dynamics of fault gouge development in layered sand clay sequences. Ph.D. Thesis, RWTH Aachen University, Shaker Verlag GmbH, Aachen, Germany. http://publications.rwth-aachen.de/record/57045.

Verbruggen A, Yurchenko Y. (2017). Positioning Nuclear Power in the Low-Carbon Electricity Transition. Sustainability 9(1): 163. DOI: 10.3390/su9010163.

Vorobiev O, Morris J, Antoun T, Friedmann SJ. (2008). Geomechanical Simulations Related to UCG Activities. Washington, D.C. : United States. Dept. of Energy. ; Oak Ridge, Tenn. : distributed by the Office of Scientific and Technical Information, U.S. Dept. of Energy, 2008: Pittsburgh, PA, United States, 9 pp.

Walters EA, Niemczyk TM. (1984). The Effect of Underground Coal Gasification on Ground Water. EPA-600/S2-84-123; Lawrence Livermore National Lab: Livermore, CA, USA.

Wolf K-H, Hettema MHH, de Pater CJ, Van Hooydonk R. (1992). Classification of overburden properties for underground coal gasification: laboratory studies under high temperature and in situ stress conditions. Rock Characterization: ISRM Symposium, Eurock '92, Chester, UK, 14–17 September, 99–104.

Wolf K-H, Bruining H. (2007). Modelling the interaction between underground coal fires and their roof rocks. Fuel 86(17–18): 2761–2777. DOI: 10.1016/j.fuel.2007.03.009.

Wolters F, Baille W, Emmerich K, Schmidt E, Wolters C, Königer F, Kunz J, Krase V, Schellhorn M. (2015). High-density bimodal bentonite blends for hydraulic sealings at the Ibbenbüren coalmine. Clay Minerals 50(3): 391–403. DOI: 10.1180/claymin.2015.050.3.11.

World Energy Council. (2007). 2007 Survey of Energy Resources. Survey of Energy Resources 1–600. DOI: 10.1016/j.matcom.2009.06.033.

World Energy Council. (2013). World Energy Resources: 2013 survey. World Energy Council for Sustainable Energy. 468 pp. http://www.worldenergy.org/wp-content/uploads/2013/09/Complete_WER_2013_-Survey.pdf.

Xi JF, Liang J, Wang ZQ, Zhu HQ, Duan YL, Bian XL. (2015). Effect of temperature field dynamic expansion of underground coal gasification on thermal stress field and stability of roof. Meitan Xuebao/Journal of the China Coal Society 40(8): 1949–1955. DOI: 10.13225/j.cnki.jccs.2015.0399.

Xin L, Wang Z, Huang W, Kang G, Lu X, Zhang P, Wang J. (2014). Temperature field distribution of burnt surrounding rock in UCG stope. International Journal of Mining Science and Technology 24(4): 573–580. DOI: 10.1016/j.ijmst.2014.06.001.

Yale DP. (1984). Network modelling of flow, storage and deformation in porous rocks. Ph.D. Thesis, Stanford University, California, CA, USA. https://pangea.stanford.edu/research/srb/docs/-theses/SRB_23_AUG84_YALE.pdf.

Yang D, Koukouzas N, Green M, Sheng Y. (2016). Recent development on underground coal gasification and subsequent CO_2 storage. Journal of the Energy Institute 89(4): 469–484. DOI: 10.1016/j.joei.2015.05.004.

Yang D, Sarhosis V, Sheng Y. (2014). Thermal–mechanical modelling around the cavities of underground coal gasification. Journal of the Energy Institute. 87(4): 321–329. DOI: 10.1016/j.joei.2014.03.029.

Yin T, Li X, Bin W, Yin Z, Jin J. (2011). Mechanical properties of sandstones after high temperature under dynamic loading. Chinese Journal of Geotechnical Engineering. 33(5): 777–784.

Younger PL. (2011). Hydrogeological and Geomechanical Aspects of Underground Coal Gasification and its Direct Coupling to Carbon Capture and Storage. Mine Water and the

Environment 30(2): 127–140. DOI: 10.1007/s10230-011-0145-5.

Zang A, Stephansson O, Heidbach O, Janouschkowetz S. (2012). World stress map database as a resource for rock mechanics and rock engineering. Geotechnical and Geological Engineering 30(3): 625–646. DOI: 10.1007/s10706-012-9505-6.

Zang A, Stephansson O, Heidbach O, Yoon JS, Ziegler M. (2013). Quantitative World Stress Map with three case studies: Geologic repository, gold mining and deep geothermal energy. 6th International Symposium on In Situ Rock Stress (RS2013), an ISRM Specialized Conference, 20-22 August, Sendai, Japan. 18 pp.

Zhang J, Feng Q, Zhang X, Wen S, Zhai Y. (2015). Relative Permeability of Coal: A Review. Transport in Porous Media 106(3): 563–594. DOI: 10.1007/s11242-014-0414-4.

Zhang J, Standifird WB, Roegiers J-C, Zhang Y. (2007). Stress-Dependent Fluid Flow and Permeability in Fractured Media: from Lab Experiments to Engineering Applications. Rock Mechanics and Rock Engineering 40(1): 3–21. DOI: 10.1007/s00603-006-0103-x.

Zhao X, Cai M, Cai M. (2010). Considerations of rock dilation on modeling failure and deformation of hard rocks — a case study of the mine-by test tunnel in Canada. Journal of Rock Mechanics and Geotechnical Engineering 2(4): 338–349. DOI: 10.3724/SP.J.1235.2010.00338.

Zoback MD. (2007). Reservoir Geomechanics. Cambridge University Press, Cambridge, UK. 449 pp. DOI: 10.1017/CBO9781107415324.004.

APPENDICES

A. Thermo-Mechanical Simulations Confirm: Temperature-Dependent Mudrock Properties are Nice to Have in Far-Field Environmental Assessments of Underground Coal Gasification

Abstract

Coupled thermo-mechanical simulations were carried out to quantify permeability changes in representative coal measure strata surrounding an underground coal gasification (UCG) reactor. Comparing temperature-dependent and -independent rock properties applied in our simulations, notable differences in rock failure behavior, but only insignificant differences in spatial permeability development are observed. Hence, temperature-dependent parameters are required for simulations of the close reactor vicinity, while far-field models can be sufficiently determined by temperature-independent parameters. Considering our findings in the large-scale assessment of potential environmental impacts of UCG, representative coupled simulations based on complex thermo-hydro-mechanical and regional-scale models become computationally feasible.

A. 1. INTRODUCTION

A.1.1 UNDERGROUND COAL GASIFICATION (UCG)

UCG can increase world-wide coal reserves by utilization of coal deposits not mineable by conventional methods and has a long history (Klimenko, 2009). The process of underground coal gasification is based on *in situ*, sub-stoichiometric coal combustion for production of a high-calorific synthesis gas, which can be applied for electricity generation or as chemical feedstock (Bhutto et al., 2013; Blinderman et al., 2008; Burton et al., 2006; Friedmann et al., 2009; Nakaten et al., 2013, 2014c). Figure 35 presents a schematic view of the in-situ coal gasification principle using the Controlled Retracting and Injection Point (CRIP) configuration (Sarhosis et al., 2013). However, UCG can induce environmental impacts such as ground subsidence and groundwater pollution (Burton et al., 2006; Durucan et al., 2014; Hewing et al., 1978). Changes in the hydraulic conductivity of the hanging wall may generate potential pathways for UCG contaminant migration (Humenick, 1978; Kapusta and Stańczyk, 2011; Liu et al., 2007; Walters and Niemczyk, 1984). These changes are associated with mechanical stress changes resulting from the UCG reactor growth as well as thermal stresses (Wolf and Bruining, 2007). Permeability controls fluid in- and outflow into and out of the reactor, respectively, considering the pressure gradient between the hydrostatic fluid and UCG reactor operating pressure (Blinderman and Anderson, 2004; Seifi et al., 2011, 2014). Mitigation of potential environmental UCG impacts can be achieved by improving the understanding of coupled thermo-hydro-mechanical processes in the rocks surrounding the UCG reactor at different scales. Thereby, near-field models considering the close UCG reactor vicinity can be employed to represent temperature-dependent processes, while far-field models are required to assess environmental impacts at regional scale. However, far-field models become computationally expensive, if processes taking place in the close reactor vicinity are involved, especially in the assessment commercial-scale multi-channel UCG operations.

Hence, a coupled thermo-mechanical model has been developed in the scope of the present study to assess near-field temperature-dependent and -independent rock behavior and permeability changes in mudrocks as previously carried out for a sandstone based coal measure strata (Otto and Kempka, 2015a).

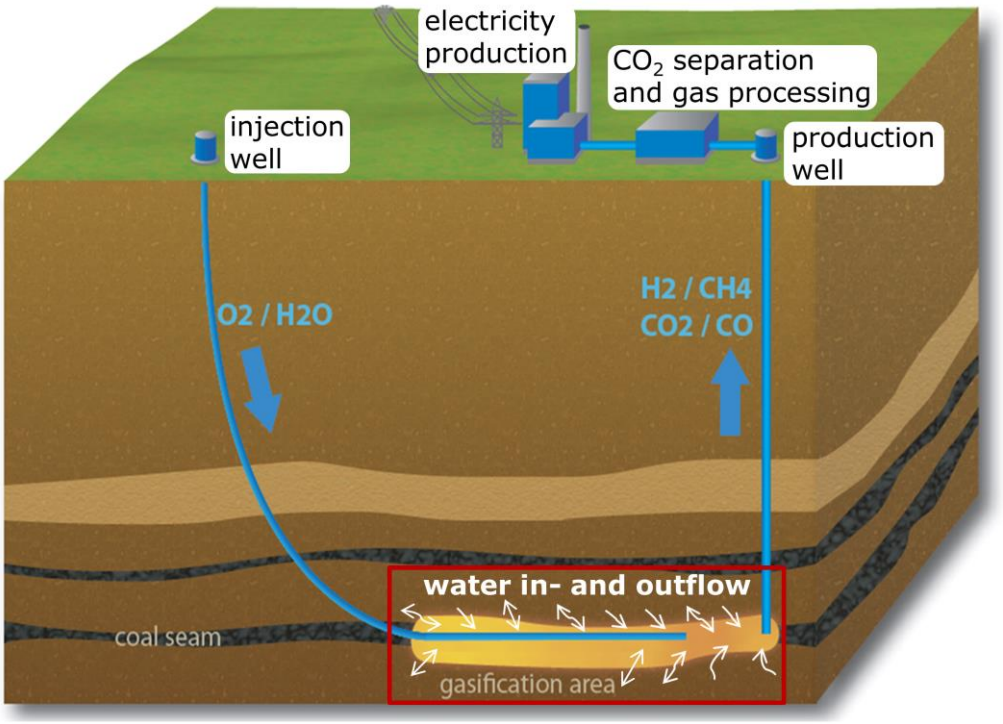

Figure 35: Principle of *in situ* coal gasification based on the CRIP method (modified after Sarhosis et al., 2013).

A. 2. METHODOLOGY

A.2.1 NUMERICAL MODEL GEOMETRY AND BOUNDARY CONDITIONS

The model used in the present study has been introduced by Otto and Kempka (2015a) for simulation of UCG processes considering, thermo-mechanical coal and sandstone properties. To assess these simulation results in view of a different host rock type, thermo-mechanical material properties of claystone and mudstone, hereafter called mudrock, were implemented into the given numerical model.

The size and grid discretization of the numerical model were adapted to calculation time and the impact of the chosen boundary conditions on the simulation results. The implemented numerical model uses the UCG reactor symmetry present along its vertical axis, assuming that a half-radial symmetric reactor develops along the UCG panel (Figure 36). The two-dimensional geometry of a coal seam of 4 m thickness was uniformly expanded towards the model boundaries, with the reactor bottom located at a depth of 250 m below the ground surface. The model size was set to 40 m × 110 m and discretized by about 3,000 elements, with sizes of 0.16 m to 5 m in all directions.

The finite-difference thermo-hydro-mechanical simulator FLAC^{3D} (Itasca, 2014) was employed to analyze thermo-mechanical stress changes, displacements and volumetric strain increments in the UCG reactor vicinity, using the unstructured grid presented in Figure 36.

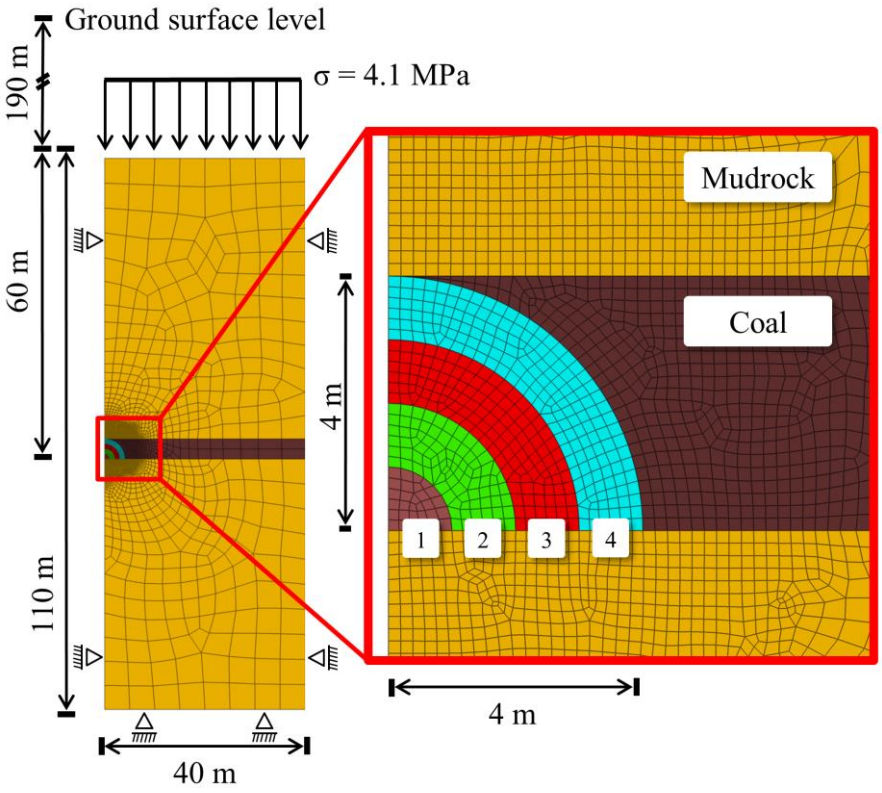

Figure 36: Geometry of the coupled thermal-mechanical UCG model. The model comprises two mudrock layers (colored in light brown) and one coal seam (colored in dark brown) with four geometric reactor growth steps considered in the simulations (light brown, green, red and turquois) (modified after Otto and Kempka, 2015a).

A.2.2 MODEL PARAMETERIZATION AND MATERIAL PROPERTIES

Thermo-mechanical data on claystone and mudstone specimens exposed to high temperatures were derived from literature (Tan et al., 2008; Tang et al., 2015; Tian, 2013; Tian et al., 2014). We incorporated both rock-type properties in one rock layer (mudrock), since the available data on thermo-mechanical properties of pure claystone and mudstone is limited. Temperature dependent thermo-mechanical properties of mudrock assigned to the present model include the elastic modulus (E), cohesion (c), friction angle (φ), linear thermal expansion coefficient (α), specific heat capacity (C_P) and thermal conductivity (λ) (Figure 37).

In contrast to sandstone, whose elastic modulus generally decreases with increasing temperature (Tian et al., 2012), Tian et al. (2014) found that the trend is slightly increasing for claystone (at 5 MPa confining pressure), what is in good agreement with the experimental results presented by Wolf et al. (1992). The normalized trends of friction angles and cohesion of the claystone specimens after high temperature treatment are always higher than those at room temperature, but also strongly alternating with increasing temperature (Tian, 2013).

Temperature-dependent thermal properties for the linear thermal expansion coefficient, specific heat capacity and thermal conductivity are not yet experimentally determined for claystone (Tian et al., 2014). In this study, the normalized trends of mudstone properties are used in the model instead. Tan et al. (2008) reported that the linear thermal expansion coefficient of mudstone increases in a continuous linear manner, until a temperature of 575 °C is reached. This is due to

the α–β quartz phase inversion as reported also for other sedimentary rocks (Somerton, 1992). Thereafter, the linear thermal expansion coefficient is slightly decreasing up to temperatures of 1000 °C. In accordance with other studies on sedimentary rocks (Clauser and Huenges, 1995), Tang et al. (2015) reported a generally decreasing trend in thermal conductivity with increasing temperature for mudstone. Furthermore, the test results of Tang et al. (2015) show that both, the specific heat capacity and the thermal conductivity, decrease with the increase in temperature when the testing temperature is below 400 °C. The specific heat capacity is almost constant and the thermal conductivity still continues to decrease for testing temperatures above 400 °C (Tang et al., 2015).

The claystone density (ρ) (Wolf et al., 1992) and the Poisson's ratio (ν) for mudstone (Tan et al., 2008) was maintained constant for both geological units (coal and mudrock). The tensile strength of claystone (0.19 MPa) was also taken from Wolf et al. (1992) and maintained constant with increasing temperature for the mudrock. Min (1983) reported a generally decreasing trend of the tensile strength of rock (oil shale and igneous rocks) with increasing temperature; however, no data for claystone or mudstone are yet available.

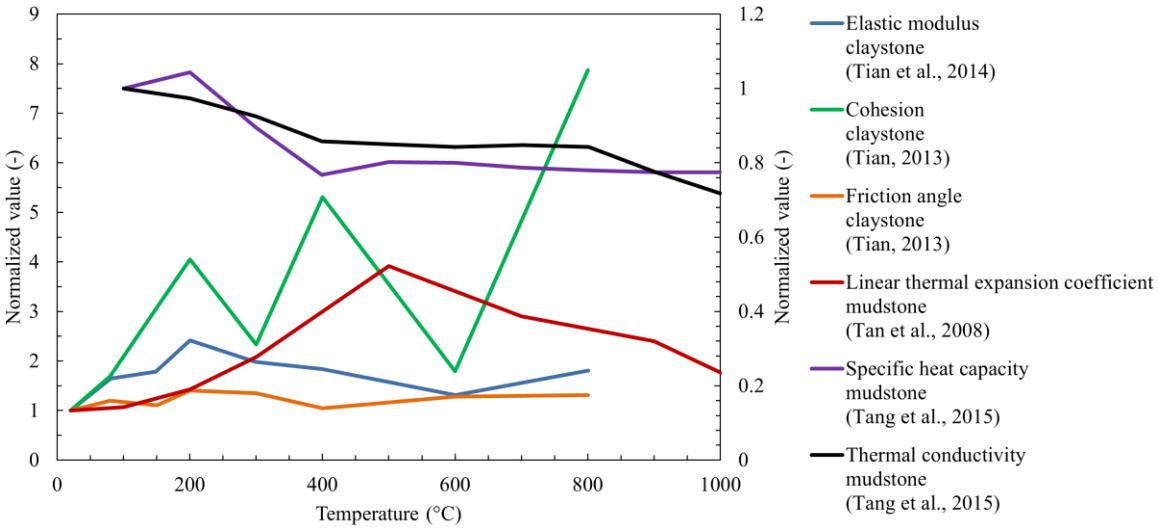

Figure 37: Trend of normalized thermo-mechanical properties of claystone and mudstone as a function of temperature. The normalized values of specific heat capacity and thermal conductivity are plotted on the secondary vertical axis. All data are normalized using the initial values presented in Table 8.

The normalized trends of thermo-mechanical coal properties after high temperature treatment are derived from literature (Badzioch et al., 1964; Min, 1983; Shoemaker et al., 1977; Singer and Tye, 1979) and discussed in Otto and Kempka (2015a). Changes in thermo-mechanical material properties affecting the coal behavior are mainly related to the various reactions in the different temperature zones (Couch, 2009): the drying zone (up to 200 °C), the drying and pyrolysis zone (200-900 °C), the reducing zone (550-900 °C) and oxidation zone (above 900 °C).

Temperatures above 1500 °C can be achieved in the UCG reactor and its close vicinity. However, the maximum testing temperature of the properties used in the present study is limited to 800 °C for the mechanical and 1000 °C for the thermal material properties. Hence, an overall temperature limit of 1000 °C is applied in the present simulations. The initial model parameters are presented in Table 8.

Table 8: Initial thermo-mechanical rock properties applied for model parameterization.

Input parameter		Unit	Mudrock	Coal
Mechanical parameters				
Young's modulus (E)	*f(T)*	GPa	2.1	2
Tensile strength (σ_t)	*Constant for rock, f(T) for coal*	MPa	0.19	0.275
Friction angle (φ)	*f(T)*	°	32.19	20
Cohesion (c)	*f(T)*	MPa	1.51	0.1
Poisson's coefficient (ν)	*Constant rock and coal*	-	0.23	0.44
Density (ρ)	*Constant rock and coal*	kg/m³	2300	1300
Thermal parameters				
Linear thermal expansion coefficient (α)	*f(T)*	K^{-1}	7.92×10^{-6}	5.0×10^{-6}
Specific heat capacity (C_P)	*f(T)*	J/(kg K)	1187	2000
Thermal conductivity (λ)	*f(T)*	W/m/K	1.19	0.23

A.2.3 DERIVING PERMEABILITY CHANGES FROM VOLUMETRIC STRAINS

In the present study, the approach discussed and introduced by Otto and Kempka (2015a) is applied, where deformation is associated with volume changes affecting the host rock and coal permeability. The rock compaction behavior in the UCG reactor vicinity was simulated using an isotropic elastoplastic constitutive law with the material properties shown in Table 9. For modeling thermal and mechanical stress-induced permeability changes, permeability is related to volumetric strain increments (Chin et al., 2000):

$$\phi = 1 - (1 - \phi_0) e^{-\Delta \varepsilon_v} \tag{13}$$

$$K = K_0 \left(\frac{\phi}{\phi_0} \right)^n \tag{14}$$

where ϕ is the porosity at a given volumetric strain ε_v, ϕ_0 the initial porosity, K the permeability at a given ε_v, K_0 the initial permeability, and n a power-law exponent (porosity sensitivity exponent) with a value range of 2 to 25 depending on stress and lithology (David et al., 1994).

A.2.4 SCENARIO ANALYSIS

Simulations of coupled thermo-mechanical processes for a UCG process duration of 50 days were carried out in two steps. First, the initial model is run to achieve a mechanical equilibrium and then applied as starting model for all further simulations. The UCG reactor is excavated stepwise, depending on the pre-defined coal consumption rate (0.654 t/day/m). A constant temperature of 1000 °C is applied at the reactor boundary, while the model is calculated to mechanical equilibrium after each reactor slice excavation. The temperature-dependent rock and coal properties are updated for each element during the entire simulation.

A. 3. SIMULATION RESULTS

A.3.1 PRINCIPAL STRESS DISTRIBUTION

During the UCG process, the experienced high temperatures generate a high thermal gradient of limited spatial extent for temperature-dependent as well as -independent material properties, and thus induce thermal stresses in the surrounding rock mass. Rock strength and behavior under high temperatures differ from those at initial conditions (Figure 37). In both simulations, the maximum distance of the 200 °C isotherm to the reactor boundary is almost identical (Figure 38). However, the temperature dependent simulation results exhibit a significantly larger spatial distribution of tensile stresses in the reactor vicinity.

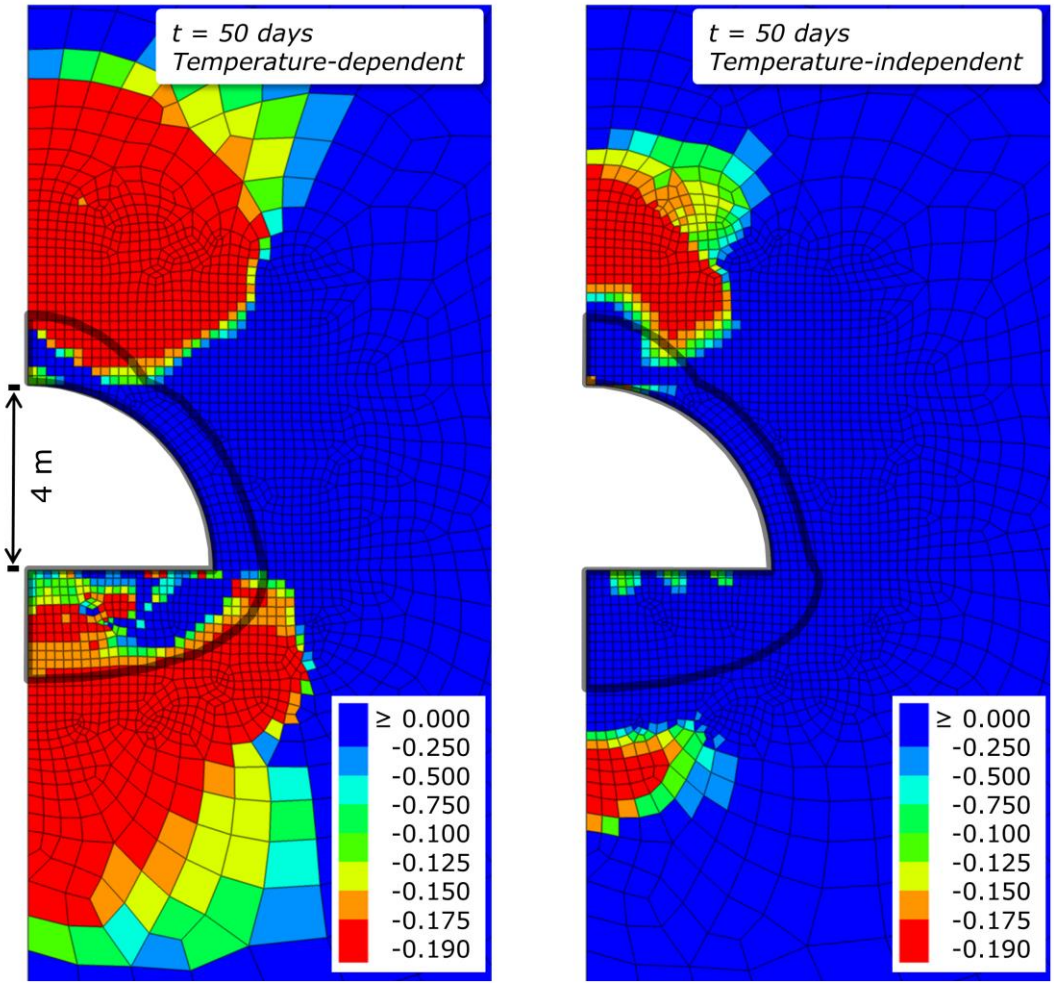

Figure 38: Tensile minimum principal stress (in MPa) with (a) temperature-dependent and (b) -independent properties after 50 days of simulation. The grey solid line represents the 200 °C isotherm. Blue colors indicate compressive stresses.

A.3.2 ELASTOPLASTIC ROCK BEHAVIOR

Shear and tensile failure determined by the Mohr-Coulomb failure criterion occur at multiple locations in the reactor vicinity considering temperature-dependent and -independent properties due to excavation effects and thermally-induced stresses (Figure 39). Shear and tensile failure (green) dominate at the reactor wall, followed by a region of pure tensile failure (blue) above and

below the reactor. The radius of tensile failure in the over- and underburden around the reactor is notably larger (up to 6 m) in the simulation using temperature-dependent parameters. The coal seam mainly experiences shear failure (red) in both models. The region of shear failure is determined by stress changes induced by excavation effects.

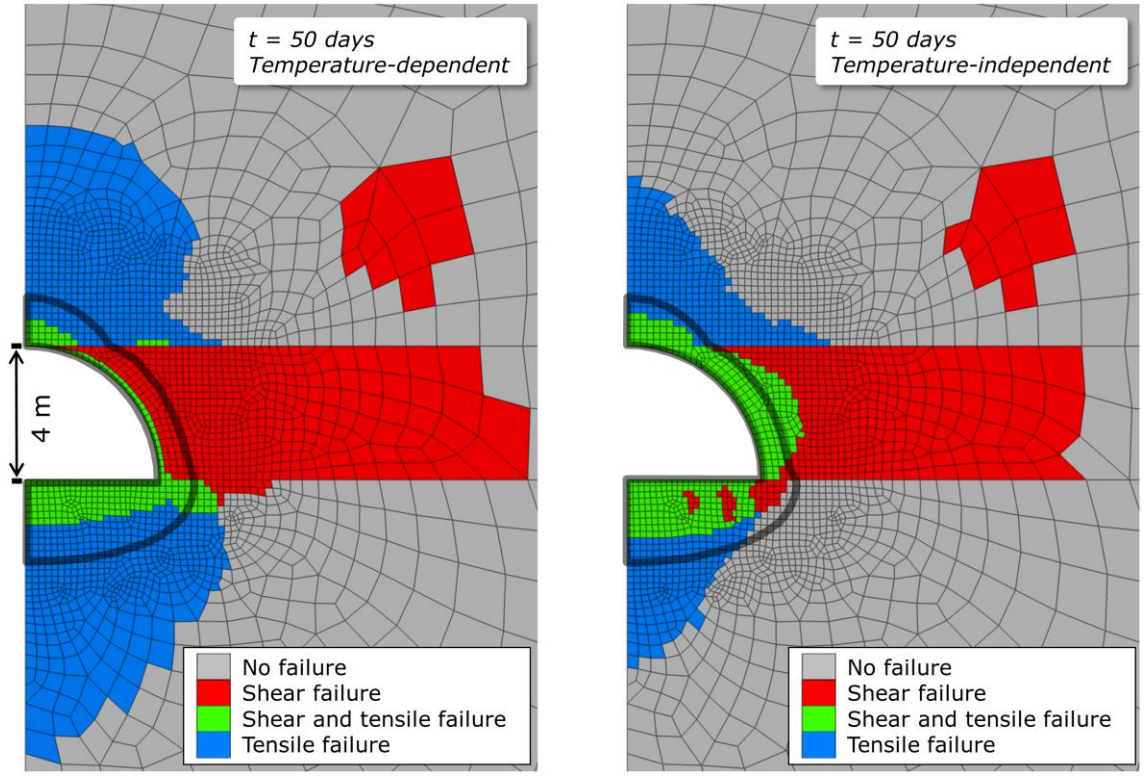

Figure 39: Distribution of shear and tensile rock failure experienced by rocks surrounding the UCG reactor after stepwise reactor zone excavation with (a) temperature-dependent and (b) -independent properties after 50 days of simulation. The grey solid line represents the 200 °C isotherm.

A.3.3 PERMEABILITY CHANGES

Equation 7 is applied for calculating permeability changes in the present models. For that purpose, normalized permeabilities with an initially uniform distribution and rock-specific porosity values derived from literature were applied (Table 9).

Table 9: Initial averaged data applied in the permeability change analysis (Min, 1983; Otto and Kempka, 2015a; Tian et al., 2014).

Initial Values	Coal	Mudrock
ϕ_0	0.02	0.0875
Normalized K_0	1	1
n	13	13

Simulation results indicate that the maximum permeability increase by more than one magnitude (red elements) is located around the UCG reactor at a distance of up to 2 m for the temperature-dependent and up to 0.8 m for the temperature-independent simulations (Figure 40). The area affected by increased permeability above the UCG reactor is notably larger for the temperature-dependent simulation; however, normalized permeability changes in that area in

comparison between both simulation cases do not exceed a factor of three. Permeability increases in the temperature-dependent simulation are mainly mechanically induced and in good agreement with the larger region of tensile failure plotted in Figure 39.

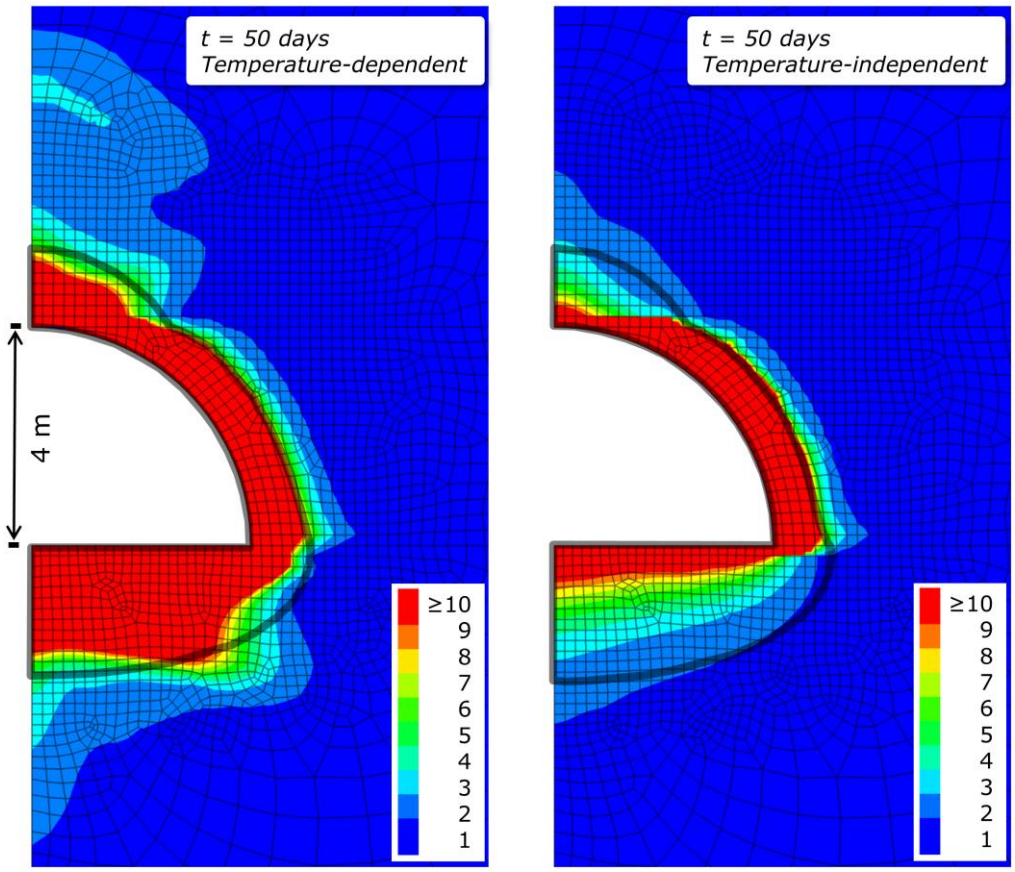

Figure 40: Permeability changes (-) show small differences for temperature-dependent (a) and temperature-independent parameters (b). The difference in regions of high permeability increase is only marginal. The grey solid line represents the 200 °C isotherm.

A. 4. DISCUSSION AND CONCLUSION

To investigate the impact of temperature-dependent parameters on rock behavior and permeability changes around a hypothetical UCG reactor, we compared coupled thermo-mechanical simulation results with temperature dependent and -independent claystone and mudstone parameters. For the thermo-mechanical numerical model, published data from high temperature experimental results was implemented, comprising three geological units as discussed in Otto and Kempka (2015a). The UCG reactor excavation was carried out stepwise, whereby a constant temperature of 1000 °C was permanently applied at the reactor wall to represent the heat flux generated by *in situ* coal combustion.

Tensile and shear failure in the rocks surrounding the UCG reactor occur in a radius of up to 6 m in the temperature dependent and -independent simulations. The associated volumetric strains result in significant permeability changes in the close reactor vicinity. For determination of permeability changes, we applied proven relationships between volumetric strain increments, porosity and permeability. Even though the formation of fractures is not considered in our simulations, the calculated volumetric strain increments achieve maximum values of up to 36%,

resulting in a permeability increase by more than three magnitudes in the high-temperature regions close to the UCG reactor (> 200 °C).

Tensile failure dominates in the rocks close to the reactor in the temperature-dependent simulation. Compared to the simulations results using sandstone properties (Otto and Kempka, 2015a), the radial extent of tensile failure is notably higher (up to about 6 m in the present study compared with about 2 m). The main reason for these deviations is the lower value of tensile strength of claystone (0.19 MPa) compared with sandstone (5 MPa) (Otto and Kempka, 2015a). Further, we expect the high alternations in the integrated temperature-dependent friction and cohesion data to contribute to this behavior.

A model verification against laboratory or field data on measured porosity and permeability changes is not yet feasible due to limited data availability. David et al. (1994) and Chin et al. (2000) developed the formulations applied here for the calculation of porosity and permeability changes for different porous and metamorphic rocks using laboratory experiments. However, we expect that the conceptual approach is applicable to the mudrock used in the present study, since a general increase in permeability due to baking, shrinking and fracturing effects is documented for rocks affected by high temperatures as experienced during *in situ* coal combustion (Wolf and Bruining, 2007). In general, any porosity and permeability relationship determined at laboratory or field scale can be easily implemented in the presented models.

Our simulation results demonstrate that the temperature-dependent thermo-mechanical properties have a notable influence on stress changes and deformation around the UCG reactor. In the close reactor vicinity, the deformations induce positive volumetric strains and zones of high permeability (up to three magnitudes increase). However, permeability changes calculated based on volumetric strain increments show only small differences between simulations using temperature-dependent and -independent parameters for the representative coal measure strata investigated here. Hence, our results support our previous findings (Otto and Kempka, 2015a), emphasizing that near-field thermo-mechanical UCG simulation models require temperature-dependent parameters, while far-field 3D models can benefit from neglecting temperature-dependency to increase computational efficiency.

A. 5. REFERENCES

Badzioch S, Gregory DR, Field MA. (1964). Investigation of the temperature variation of thermal conductivity and thermal diffusivity of coal. Fuel 43: 267–280.

Bhutto AW, Bazmi AA, Zahedi G. (2013). Underground coal gasification: From fundamentals to applications. Progress in Energy and Combustion Science 39(1): 189–214. DOI: http://dx.doi.org/10.1016/j.pecs.2012.09.004.

Blinderman MS, Anderson B. (2004). Underground Coal Gasification for Power Generation: High Efficiency and CO_2-Emissions. ASME 2004 Power Conference. ASME, 473–479. DOI: 10.1115/POWER2004-52036.

Blinderman MS, Saulov DN, Klimenko AY. (2008). Forward and reverse combustion linking in underground coal gasification. Energy 33(3): 446–454. DOI: DOI: 10.1016/j.energy.2007.10.004.

Burton E, Friedmann J, Upadhye R. (2006). Best Practices in Underground Coal Gasification. Contract No. W-7405-Eng-48, Lawrence Livermore National Laboratory: Livermore, CA, USA.

Chin LY, Rajagopal R, Thomas LK. (2000). Fully Coupled Geomechanics and Fluid-Flow Analysis of Wells with Stress-Dependent Permeability. SPE Journal 5(1): 2–6. DOI: 10.2118/58968-PA.

Clauser C, Huenges E. (1995). Rock Physics & Phase Relations: A Handbook of Physical Constants. In: Ahrens TJ (ed) Rock Physics & Phase Relations: A Handbook of Physical Constants. American Geophysical Union: Washington, D.C., USA. 105–126. DOI: 10.1029/RF003.

Couch G. (2009). Underground coal gasification. CCC/151, IEA Clean Coal Centre. CCC/151, IEA Clean Coal Centre: London.

David C, Wong TF, Zhu W, Zhang J. (1994). Laboratory measurement of compaction-induced permeability change in porous rocks: Implications for the generation and maintenance of pore pressure excess in the crust. Pure and Applied Geophysics 143(1–3): 425–456. DOI: 10.1007/BF00874337.

Durucan S, Korre A, Shi J-Q, Idiens M, Stańczyk K, Kapusta K, Rogut-Dabrowska A, Kempka T, Wolf K-H, Younger P, Zavsek S, Poulsen NE, Bojda D, Franzsen S, Muresan M, Gao J, Beath A, Mastalerz M. (2014). TOPS: Technology Options for Coupled Underground Coal Gasification and CO_2 Capture and Storage. Energy Procedia 63: 5827–5835. DOI: 10.1016/j.egypro.2014.11.616.

Friedmann SJ, Upadhye R, Kong FM. (2009). Prospects for underground coal gasification in carbon-constrained world. Energy Procedia 1: 4551–4557.

Hewing G, Hewel-Bundermann H, Krabiell K, Witte P. (1978). Post-1987 R & D Studies of Underground Coal Gasification. Research Association for Second-Generation Coal Extraction: Essen, Germany.

Humenick M. (1978). Groundwater pollutants from underground coal gasification. Water Research 12(7): 463–469. DOI: 10.1016/0043-1354(78)90153-7.

Itasca Consulting Group. (2014). Inc. Advanced Three-Dimensional Continuum Modelling for Geotechnical Analysis of Rock, Soil and Structural Support. Itasca Consulting Group, Inc.: Minneapolis, MN, USA.

Kapusta K, Stańczyk K. (2011). Pollution of water during underground coal gasification of hard coal and lignite. Fuel 90(5): 1927–1934. DOI: 10.1016/j.fuel.2010.11.025.

Klimenko AY. (2009). Early Ideas in Underground Coal Gasification and Their Evolution. Energies 2(2): 456–476. DOI: 10.3390/en20200456.

Liu S, Li J, Mei M, Dong D. (2007). Groundwater Pollution from Underground Coal Gasification. Journal of China University of Mining and Technology 17(4): 467–472. DOI: 10.1016/S1006-1266(07)60127-8.

Min OK. (1983). Finite Element Modeling of Thermo-Mechanical Responses Associated with Underground Coal Conversion. Ph.D. Thesis, Ohio State University, Columbus, OH, USA. DOI: 10.1017/CBO9781107415324.004.

Nakaten N, Kötting P, Azzam R, Kempka T. (2013). Underground Coal Gasification and CO_2 Storage Support Bulgaria's Low Carbon Energy Supply. Energy Procedia 40(0): 212–221. DOI: 10.1016/j.egypro.2013.08.025.

Nakaten N, Schlüter R, Azzam R, Kempka T. (2014). Development of a techno-economic model for dynamic calculation of cost of electricity, energy demand and CO_2 emissions of an integrated UCG–CCS process. Energy 66: 779–790. DOI: 10.1016/j.energy.2014.01.014.

Otto C, Kempka T. (2015). Thermo-Mechanical Simulations of Rock Behavior in Underground Coal Gasification Show Negligible Impact of Temperature-Dependent Parameters on Permeability Changes. Energies 8(6): 5800–5827. DOI: 10.3390/en8065800.

Sarhosis V, Yang D, Sheng Y, Kempka T. (2013). Coupled Hydro-thermal Analysis of Underground Coal Gasification Reactor Cool Down for Subsequent CO_2 Storage. Energy Procedia 40(0): 428–436. DOI: 10.1016/j.egypro.2013.08.049.

Seifi M, Abedi J, Chen Z. (2014). Application of porous medium approach to simulate UCG process. Fuel. Elsevier Ltd 116: 191–200. DOI: 10.1016/j.fuel.2013.07.091.

Seifi M, Chen Z, Abedi J. (2011). Numerical simulation of underground coal gasification using the CRIP method. The Canadian Journal of Chemical Engineering 89(6): 1528–1535. DOI: 10.1002/cjce.20496.

Shoemaker HD, Shuck LZ, Haynes RR, Advani SH. (1977). The Mechanical Properties of the Pittsburgh Coal at Elevated Temperatures. Journal of Pressure Vessel Technology 99(1): 192–198. DOI: 10.1115/1.3454508.

Singer JM, Tye RP. (1979). Thermal, mechanical, and physical properties of selected bituminous coals and cokes. U.S. Department of Interior, Bureau of Mines: Washington, DC, USA. 38 pp.

Somerton WH. (1992). Thermal properties and temperature-related behavior of rock/fluid systems. Developments in Petroleum Science. Elsevier Science Publishers H.V.: Amsterdam, The Netherlands. DOI: 10.1017/CBO9781107415324.004.

Tan Q, Luo X, Li S. (2008). Numerical modeling of thermal stress in a layered rock mass. The 42nd U.S. Rock Mechanics Symposium (USRMS). American Rock Mechanics Association.

Tang F, Wang L, Lu Y, Yang X. (2015). Thermophysical properties of coal measure strata under high temperature. Environmental Earth Sciences 73(10): 6009–6018. DOI: 10.1007/s12665-015-4364-0.

Tian H. (2013). Development of a thermo-mechanical model for rocks exposed to high temperatures during underground coal gasification. Ph.D. Thesis, RWTH Aachen University. http://publications.rwth-aachen.de/record/209279.

Tian H, Kempka T, Xu N-X, Ziegler M. (2012). Physical Properties of Sandstones after High Temperature Treatment. Rock Mechanics and Rock Engineering 45(6): 1113–1117. DOI: 10.1007/s00603-012-0228-z.

Tian H, Ziegler M, Kempka T. (2014). Physical and mechanical behavior of claystone exposed to temperatures up to 1000 °C. International Journal of Rock Mechanics and Mining Sciences 70: 144–153. DOI: 10.1016/j.ijrmms.2014.04.014.

Walters EA, Niemczyk TM. (1984). The Effect of Underground Coal Gasification on Ground Water. EPA-600/S2-84-123; Lawrence Livermore National Lab: Livermore, CA, USA.

Wolf K-H, Hettema MHH, de Pater CJ, Van Hooydonk R. (1992). Classification of overburden properties for underground coal gasification: laboratory studies under high temperature and in

situ stress conditions. Rock Characterization: ISRM Symposium, Eurock '92, Chester, UK, 14–17 September, 99–104.

Wolf K-H, Bruining H. (2007). Modelling the interaction between underground coal fires and their roof rocks. Fuel 86(17–18): 2761–2777. DOI: 10.1016/j.fuel.2007.03.009.

PUBLICATIONS OF THE AUTHOR

Otto, C.; Kempka, T. Prediction of Steam Jacket Dynamics and Water Balances in Underground Coal Gasification. *Energies* **2017,** *10*, 739, 1-17, doi: 10.3390/en10060739.

Kempka, T.; Nakaten, B.; De Lucia, Marco; Nakaten, N.; **Otto, C.**; Pohl, M.; Tillner, E.; Kühn, M. Flexible simulation framework to couple processes in complex 3D models for subsurface utilization assessment, *Energy Procedia* **2016**, *97*, 494–501, doi: 10.1016/j.egypro.2016.10.058.

Otto, C.; Kempka, T.; Kapusta, K.; Stańczyk, K. Fault Reactivation Can Generate Hydraulic Short Circuits in Underground Coal Gasification – New Insights from Regional-Scale Thermo-Mechanical 3D Modeling. *Minerals* **2016**, *6 (101)*, 1–23, doi: 10.3390/min6040101.

Otto, C.; Kempka, T. Thermo-mechanical Simulations Confirm: Temperature-dependent Mudrock Properties are Nice to have in Far-field Environmental Assessments of Underground Coal Gasification. *Energy Procedia* **2015**, *76*, 582–591, doi: 10.1016/j.egypro.2015.07.875.

Otto, C.; Kempka, T. Thermo-Mechanical Simulations of Rock Behavior in Underground Coal Gasification Show Negligible Impact of Temperature-Dependent Parameters on Permeability Changes. *Energies* **2015**, *8*, 5800–5827, doi: 10.3390/en8065800.

SELBSTSTÄNDIGKEITSERKLÄRUNG

Hiermit erkläre ich, Christopher Otto, dass ich als Autor der vorliegenden Dissertation mit dem Titel: *„Numerical Analysis of Thermal, Hydraulic and Mechanical Processes in the Near- and Far-Field of Underground Coal Gasification Reactors“*, die Arbeit selbstständig und ohne unerlaubte Hilfe angefertigt habe.

Ferner versichere ich, keine anderen als die angegebenen Quellen und Hilfsmittel benutzt zu haben. Alle Ausführungen, die anderen Schriften wörtlich oder inhaltlich entnommenen wurden, sind als solche kenntlich gemacht.

Die vorliegende Arbeit wurde in keinem anderen Promotionsverfahren angenommen oder abgelehnt.

_____

Ort, Datum

_____

Unterschrift